

Dynamics of a Grid-Connected Small-Scale Geared Wind Turbine with Slip-Synchronous Technology

by

Dillan Kyle Ockhuis

*Thesis presented in partial fulfilment of the requirements for the degree of
Master of Science in Engineering at Stellenbosch University*



UNIVERSITEIT
iYUNIVESITHI
STELLENBOSCH
UNIVERSITY

100
1918 · 2018

Supervisor: Prof. M.J. Kamper

March 2018

Declaration

By submitting this thesis electronically, I declare that the entirety of the work contained therein is my own, original work, that I am the sole author thereof (save to the extent explicitly otherwise stated), that reproduction and publication thereof by Stellenbosch University will not infringe any third party rights and that I have not previously in its entirety or in part submitted it for obtaining any qualification.

Date: March 2018

Copyright © 2018 Stellenbosch University
All rights reserved.

Abstract

Dynamics of a Grid-Connected Small-Scale Geared Wind Turbine with Slip-Synchronous Technology

D.K. Ockhuis

*Department of Electric and Electronic Engineering,
Stellenbosch University,
Private Bag X1, Matieland 7602, South Africa.*

Thesis: M.Eng (Elec)
March 2018

In this study, the dynamic behaviour of a 2.2 kW, fixed-speed downwind turbine is investigated. The downwind turbine drivetrain comprises of 1.9 m turbine blades, a gearbox with gear ratio of 1:3.78, a slip permanent magnet coupling and a permanent magnet synchronous generator (PMSG). The downwind turbine has a synchronous speed of 600 rpm (on the high-speed side of the gearbox) and is direct-grid connected by means of a grid connection controller (GCC). Each component of the downwind drivetrain was designed and developed by different persons however, the functionality of the drivetrain as a complete unit remains unknown.

The 2.2 kW downwind drivetrain was modelled using mathematical equations which then translated to a simulation model using MATLAB/Simulink. From this simulation model, a transfer function model of the downwind drivetrain was determined by simulating a dynamic step-test. The transfer function of the downwind turbine was then used to design a speed controller using the Internal Model Control (IMC) tuning rules. The speed controller in conjunction with the GCC allows the downwind turbine to synchronize with and connect to the grid without the need for a power converter.

The dynamics of connecting the simulated drivetrain to a grid is also evaluated using the developed simulation model. Furthermore, once grid connected, the on-grid dynamic performance of the downwind turbine was simulated and evaluated. Downwind turbines in particular are known to produce significant torque pulsations due to the tower shadow effect. The simulation model developed in this thesis is also used to simulate the effects of tower shadow and evaluates the effect on the resulting grid current. Furthermore, the simulation model also investigates and evaluates the dynamic behaviour of the grid-connected downwind turbine during various grid disturbances.

The physical downwind turbine drivetrain was tested and evaluated on a mechanical testbench in the electrical machines laboratory. The laboratory testing included:

- the implementation of the dynamic step-test on the physical downwind drivetrain,
- testing the speed controller's ability to control and maintain the downwind drivetrain's speed at synchronous speed prior to grid connection,
- autonomous grid connection using the grid connection controller,
- investigations regarding the downwind drivetrain's sensitivity to torque pulsations at different frequencies and,
- the overall functionality of the grid connection controller when the downwind drivetrain is subjected to above-rated conditions.

The laboratory test results closely resembled their respective simulated test results which served as validation of the accuracy of the developed simulation model.

The 2.2 kW downwind turbine was erected at the Stellenbosch University Mariendahl small wind turbine testing facility. However, due to unforeseen events and circumstances, no data could be collected with respect to the downwind turbine's on-site performance. However, the simulation model and laboratory tests suggests that the downwind turbine is on-grid stable and is unaffected by the torque pulsations caused by the tower shadow effect and could function on-site for future study.

Uittreksel

Dinamika van 'n Netwerk Gekoppelde Klein-Skaal Gerat Wind Turbine met Glip-Sinchroon Tegnologie

("Dynamics of a Grid-Connected Small-Scale Geared Wind Turbine with Slip-Synchronous Technology")

D.K. Ockhuis

*Departement Elektries en Elektroniese Ingenieurswese,
Stellenbosch Universiteit,
Privaatsak X1, Matieland 7602, Suid Afrika.*

Tesis: M.Ing (Elek)
Maart 2018

In hierdie studie word die dinamiese gedrag van 'n 2.2 kW, vaste-spoed afwind turbine ondersoek. Die afwind turbine aandrywingstelsel bestaan uit 1.9 m turbine lemme, 'n ratkas met ratverhouding van 1:3.78, 'n glip permanente magneet koppeling (S-PMC) en 'n permanente magneet sinchroon generator (PMSG). Die afwind-turbine het 'n sinchroon spoed van 600 rpm (op die hoëspoedkant van die ratkas) en is direk netwerk gekoppel deur 'n netwerkkoppelingsbeheerder (GCC). Elke komponent van die afwind turbine aandrywingstelsel was deur verskillende persone ontwerp en ontwikkel, maar die funksionaliteit van die aandrywingstelsel as 'n volledige eenheid bly onbekend.

Die 2.2 kW afwind dryfbaan is gemodelleer deur gebruik te maak van wiskundige vergelykings wat dan na 'n simulasiemodel vertaal is met MATLAB/Simulink. Uit hierdie simulasiemodel is 'n oordragfunksie model van die afwind aandrywingstelsel bepaal deur 'n dinamiese stap-toets te simuleer. Die oordragfunksie van die afwind turbine stelsel is dan gebruik om 'n spoedbeheerder te ontwerp met behulp van die Internal Model Control (IMC) reëls. Die spoedbeheerder in samewerking met die GCC laat die afwind turbine toe om met die kragnetwerk te sinchrooniseer en koppel sonder die behoefte aan 'n drywingsomsetter.

Die dinamika van die koppeling van die gesimuleerde aandrywingstelsel na 'n kragnetwerk word ook geëvalueer met behulp van die ontwikkelde simulasiemodel. Verder, sodra die aandrywingstelsel gekoppel is, is die dinamika van die gekoppelde aandrywingstelsel getoets en geëvalueer. Afwind turbines is bekend om wringkragspulsasies teweeg te bring as gevolg van die toring skaduwee effek. Die simulasiemodel wat in hierdie tesis ontwikkel is simuleer die effekte van toringskadu en evalueer die effek op die gevolglike aandrywingstelsel. Verder ondersoek die simulasiemodel ook die dinamiese gedrag van die kragnetwerk-gekoppelde turbine tydens verskeie kragnetwerk versteurings.

Die fisiese afwind turbine-aandrywingstelsel is getoets en geëvalueer op 'n meganiese toetsbank in die elektriese masjiene laboratorium. Laboratorium toetsing sluit in:

- die implementering van die dinamiese stap-toets op die fisiese aandrywingstelsel,
- die toets van die spoed beheerder se vermoë om die spoed van die aandrywingstelsel te bestuur en in stand te hou teen sinchroon spoed voor netwerkverbinding,
- outonome netwerkverbinding met behulp van die netwerkkoppelingsbeheerder en spoed beheerder,
- ondersoek rakende die afwind aandrywingstelsel se sensitiwiteit vir wringkragspulsasies by verskillende frekwensies en,
- die algehele funksionaliteit van die netwerkkoppelingsbeheerder wanneer die afwind aandrywingstelsel onderworpe is aan bogenoemde toestande.

Verder het die laboratoriumtoetsresultate ooreengestem met die onderskeie gesimuleerde toetsuitslae wat gedien het as bevestiging van die akkuraatheid van die ontwikkelde simulasiemodel.

Die 2.2 kW afwind turbine is opgerig by die Universiteit van Stellenbosch se Mariendahl klein windturbine toets fasiliteit. As gevolg van onvoorsiene gebeure en omstandighede kon egter geen veld-data versamel word met betrekking tot die afwind turbine. Die simulasiemodel en laboratoriumtoetse dui egter daarop dat die afwind turbine stabiel is wanneer dit netwerkgekoppel is en is nie beïnvloed deur die wringkragspulsasies wat veroorsaak word deur die toringskadu-effek nie en kan wel op die toetsveld funksioneer vir toekomstige studie.

Acknowledgements

I would like to express my sincere gratitude to the following people:

- Prof. Maarten Kamper, for his guidance and valuable input throughout this study.
- My parents, for their love and support throughout the entire process.
- Kenan Kloete, for his help with designing and setting up of the testbench and setting up of the downwind turbine at the Stellenbosch University Mariendahl wind turbine testing facility.
- Andre Swart and Murray Jumat for all their assistance.
- Everyone in the Electrical Machines Laboratory for their assistance and guidance throughout the entirety of the project.

Contents

Declaration	i
Abstract	ii
Uittreksel	iv
Acknowledgements	vi
Contents	vii
Nomenclature	ix
1 Introduction	1
1.1 Wind Energy in South Africa	1
1.1.1 Wind Energy as part of the National Energy Mix	1
1.1.2 Large-Scale Applications	1
1.1.3 Small-Scale Prospects	2
1.1.4 The Potential of Feed-In Based Decentralized Systems	2
1.2 Grid-Connected Wind Turbine Systems	2
1.2.1 Fixed-Speed Wind Turbine Systems	2
1.2.2 Variable-Speed Wind Turbine Concepts	3
1.2.3 Non-Conventional Wind Generator Concepts	3
1.2.4 Slip-Synchronous Permanent Generator Concept	4
1.2.5 A Drivetrain Based off of The SS-PMG	5
1.3 Generator Speed Control	6
1.3.1 Power in the Wind	6
1.3.2 Pitch Control	6
1.3.3 Stall Control	7
1.3.4 Active Stall Control	7
1.3.5 Yaw Control	7
1.3.6 Electro-Mechanical Braking	7
1.4 Generator Synchronization Conditions	8
1.5 Turbine Torque Pulsations	9
1.6 Statement of the Problem	9
1.7 Objective of Study	9
1.8 Significance of the Study	10
1.9 Thesis Structure	10
2 Modelling	11
2.1 PMSG	11
2.2 S-PMC	12
2.3 Turbine Blade Model	13
2.4 Gearbox	15
2.5 Grid Connection Controller	15
2.6 Downwind Turbine Simulation Parameters	16
2.7 Model Implementation	16

3	PI Speed Controller Design	17
3.1	Downwind Drivetrain System Identification	17
3.1.1	Dynamic Step-Test of the Downwind Turbine Drivetrain Process	17
3.1.2	First-Order Plus Dead Time Model	17
3.1.3	Discussion	18
3.2	PI Tuning	19
3.2.1	Internal Model Control Tuning	20
3.2.2	Integrator Windup Protection	21
3.2.3	Closed-Loop Speed Controller Implementation	21
3.2.4	Gain Scheduling	22
3.3	Chapter Summary	24
4	Grid Connection and On-Grid Dynamic Performance	26
4.1	Grid Connection	26
4.2	Grid Synchronization Parameters	27
4.2.1	Voltage Phase Angle Difference	28
4.2.2	Frequency and Phase Voltage Difference	28
4.2.3	Transient Grid-Connection Currents	29
4.3	On-Grid Dynamic Performance	30
4.3.1	Transient Turbine Torque Conditions	31
4.3.2	Turbine Pulsations and Bandwidth	32
4.3.3	Grid Disturbances	32
5	Laboratory Results	36
5.1	Laboratory Test Setup	36
5.2	Dynamic Step-Test	37
5.3	Speed Control	39
5.4	Grid Connection and On-Grid Dynamic Performance	42
5.4.1	Grid Connection	42
5.4.2	On-Grid Dynamic Performance	42
5.5	Field Testing Setup	45
5.6	Chapter Summary	46
6	Conclusion and Recommendations	48
6.1	Speed Control	48
6.2	Laboratory Grid Connection	48
6.3	On-Grid Dynamic Performance	48
6.4	Field Tests	49
6.5	Recommendations	49
6.5.1	System Modelling	49
6.5.2	Grid Connection	49
6.5.3	Field Testing	49
A	Appendix A	50
A.1	MATLAB/Simulink closed-loop controller blocks	50
A.2	Zero Crossing Algorithm Source Code - MATLAB	50
A.3	Digital PI-Controller Source Code - MATLAB	51
	Bibliography	52
	List of Figures	54
	List of Tables	56

Nomenclature

Variables

A	Swept area of wind turbine	[m ²]
C_p	Coefficient of wind power	[]
d_c	Duty cycle	[]
d_{\max}	Maximum duty cycle	[]
d_{\min}	Minimum duty cycle	[]
f_{gen}	PMSG frequency (electrical)	[Hz]
f_{grid}	Electrical network frequency	[Hz]
f_s	Drivetrain speed (electrical)	[Hz]
f_t	Turbine rotational frequency (mechanical)	[Hz]
G_c	Gain of the S-PMC	[]
I_s	Stator current	[A]
i_{abc}	Three-phase grid currents	[A]
J_m	Inertia of the generator	[kg·m ²]
J_t	Inertia of the turbine	[kg·m ²]
K_c	Controller gain	[]
\mathbf{K}_p	Park's transformation	[]
\mathbf{K}_p^{-1}	Inverse of Park's transformation	[]
k_i	Integrating process gain	[]
k_p	Process gain	[]
L_{ds}	Stator direct axis inductance	[H]
L_e	Per phase end winding inductance	[H]
L_{qs}	Stator quadrature axis inductance	[H]
N	Rotational Speed	[rpm]
n_m	Mechanical shaft speed	[rpm]
n_t	Turbine speed	[rpm]
n_{slip}	Mechanical shaft slip speed	[rpm]
n_{sync}	Mechanical shaft synchronous speed	[rpm]
P	Number of poles	[]
P_m	Extracted mechanical wind power	[W]
P_w	Available wind power	[W]
p	Rotational frequency of the turbine blades	[Hz]
R	Radius of rotor swept area	[m]
R_s	Stator per phase winding resistance	[Ω]
S	Apparant power	[VA]
s	Slip	[]
T_{rated}	Rated torque	[Nm]
τ_d	Process dead time	[seconds]
τ_c	Closed-loop time constant	[seconds]
τ_p	Process time constant	[seconds]
τ_r	Generated torque (S-PMC)	[Nm]

τ_s	Generated torque (PMSG)	[Nm]
τ_t	Generated turbine torque on the high speed side of the gearbox	[Nm]
$\tau_{t'}$	Generated turbine torque on the low-speed side of the gearbox	[Nm]
V_s	Grid or PMSG per-phase terminal voltage	[V]
v	Wind speed	[m/s]
v_{abc}	Transient three-phase grid voltages	[V]
v_{ds}	Stator direct axis phase voltage	[V]
v_{qs}	Stator quadrature axis phase voltage	[V]
Δf	Frequency difference	[Hz]
$\Delta\phi$	Voltage-phase angle difference	[°]
ΔV	Phase-voltage difference	[V]
η	Efficiency	[%]
λ_{ds}	Stator direct axis flux linkage	[Wb·turn]
λ_{qs}	Stator quadrature axis flux linkage	[Wb·turn]
λ_{ms}	PM flux linkage contribution on stator	[Wb·turn]
ρ	Density of air	[kg/m ³]
ω	Turbine rotor speed (mechanical)	[rad/s]
ω_e	PMSG speed (electrical)	[rad/s]
ω_t	Turbine speed (mechanical)	[rad/s]
ω_s	Synchronous speed (electrical)	[rad/s]
ω_{sl}	Slip speed (mechanical)	[rad/s]
ω_m	PM rotor angular speed (electrical)	[rad/s]
ω_r	Wound rotor angular speed (electrical)	[rad/s]

Abbreviations

CAD	Computer aided design
DFIG	Doubly fed induction generator
FE	Finite element
FEM	Finite element method
FOPDT	First-order plus dead-time
GCC	Grid connection controller
IG	Induction generator
IGBT	Insulated-gate bipolar transistor
IM	Induction motor
IMC	Internal Model Control
IPP	Independent power producer
IRP	Integrated resource plan
LVRT	Low voltage ride through
NERSA	National energy regulator of South Africa
PCC	Point of common connection
PI	Proportional-Integral
PID	Proportional-Integral-Derivative
PM	Permanent magnet
PMIG	Permanent magnet induction generator
PMSG	Permanent magnet synchronous generator
PUC	Point of utility connection

PWM	Pulse-width modulation
REIPPPP	Renewable energy independent power producer procurement program
REFIT	Renewable energy feed-in-tariff
RMS	Root mean square
RPP	Renewable power plant
SANEDI	South African National Energy Development Institute
SCIG	Squirrel-cage induction generator
SG	Synchronous generator
S-PMC	Slip permanent magnet coupling
S-PMG	Slip permanent magnet generator
SSC	Solid state converter
SSEG	Small-scale embedded generator
SS-PMG	Slip synchronous permanent magnet generator
SS-WTS	Slip synchronous Wind turbine systems
TS	Torque sensor
TSR	Tip-speed-ratio
VSD	variable speed drive
WRSG	Wound-rotor synchronous generator
WTS	Wind turbine systems

Chapter 1

Introduction

The objective of this chapter is to highlight the role of wind energy as part of the greater national energy mix of South Africa. The chapter begins with the plans and objectives set in place by the various governmental bodies to increase and promote the development and implementation of large, utility-scale wind energy projects in the form of the Renewable Energy Independent Power Producer Procurement Program (REIPPPP). Furthermore, this chapter highlights some of the different types of grid-connected wind turbine concepts as well as providing a brief overview of the different speed control strategies used to control wind turbines. Finally, the chapter concludes by stating the problem addressed in this thesis as well as the objectives and layout of the thesis as a whole.

1.1 Wind Energy in South Africa

The movement towards curbing global warming has accelerated the need for countries to phase out their dependence on coal fired power utilities and instead adopt a more balanced power generation scheme by implementing ever more renewable energy sources into their existing national grids. South Africa is one such country which heavily relies on coal to meet its energy needs. However, the South African government has stated its intentions to supplement its coal fired power stations by supporting the development and implementation of renewable energy sources for both small and large-scale applications [1]. Wind power (along with solar power) currently dominates South Africa's renewable energy market. Furthermore, it is predicted that wind power will be the technology most likely to contribute significantly to the South African energy mix due to the technology's existing maturity and established global capacity [2].

1.1.1 Wind Energy as part of the National Energy Mix

In 2010, the Integrated Resource Plan (IRP, 2010) was published with the intention to provide the preferred electricity mix and delivery timeline with which to meet the country's electricity needs for the period 2010 to 2030. The IRP estimates that by 2030, the demand for electricity will require an additional 46 gigawatts (GW) of generating capacity of which 13.8 GW is to be provided by renewable energy sources (wind, solar, biomass, small-scale hydro and biogas). In order to meet these needs, the Renewable Energy Independent Power Producer Procurement Program (REIPPPP) was established by which Independent Power Producers (IPP) could bid for ownership of a stake in the 13.8 GW set aside for renewable energy generation.

The procurement program has 5 bidding rounds used to select the IPP that will generate SA's renewable energy. As of 2015, 92 IPP have been selected to provide in excess of 6000 MW of renewable energy by 2020. Across the 5 bidding rounds, 3357 MW of wind energy has been procured, representing a third of the planned 9200 MW capacity set by the IRP for wind energy and more than 50% of the procured portfolio. As of August 2016, wind IPP are delivering 960 MW to the national grid [2].

1.1.2 Large-Scale Applications

The majority of South Africa's wind energy profile consists of large, utility-scale wind farms. Wind turbines with a generating capacity above 1 MW are considered to be utility-scale. The Darling Wind Farm was the first large renewable energy project in the country and the first of its kind to generate electricity from wind power on a commercial basis [2]. The wind farm has an installed capacity of 8 MW comprising of six 1.3 MW wind turbines. South Africa has a further 20 operational wind farms in the Western, Eastern and Northern Cape with generating capacities ranging from 5.2 MW to 140 MW [3].

1.1.3 Small-Scale Prospects

The market for small-scale wind turbines (with a generation capacity of under 100 kW) in South Africa is currently at an impasse. Before 2011, direct grid-connected small-scale wind turbines were thought to be the ideal solution for residential use in the sense that home-owners could exchange the electricity generated from their wind turbines (or solar panels) with the national grid for what was known as a Renewable Energy Feed-In-Tariff (REFIT), as a form of compromise to the rising electricity costs in South Africa. In 2009, home owners could expect a return of R1.25 per kilowatt hour (kWh) generated from wind energy [2]. However, in March 2011, the National Energy Regulator of South Africa (NERSA) announced a revision to the REFIT program in which the tariffs were downgraded in order to align the pricing with technology advancements and market trends at the time [2]. After this revision, home-owners producing their own electricity could expect to receive a tariff of R0.94/kWh generated from wind energy. Nevertheless, over time by selling energy back to the grid at a higher price than that of consumption (with the cost of consumption being R0.33/kWh at the time [4]) after a certain period, the overall income generated by electricity production would cover the initial costs of the system which was known as the "by-back" period. This by-back period was one of the main attraction points for investments in small-scale wind turbine systems. However, the legality of the REFIT programme was brought into question by the National Treasury and the Department of Energy and it was found that the REFIT programme contravened public procurement and finance regulations [2]. The REFIT programme was terminated by the NERSA in the later parts of 2011 with the REIPPPP launched to take its place.

1.1.4 The Potential of Feed-In Based Decentralized Systems

The termination of the REFIT program slowed the investment in small-scale wind turbine systems in South Africa. However, small-scale wind turbine systems have proved to be a successful means for generating renewable energy across Europe. In 1990, Germany became the first country to set up bylaws for decentralized grid-connected systems. Currently, over 250 000 homes, businesses and farms have installed solar photovoltaic panels on their roofs which produces nearly 4000 MW of solar energy while 20 000 wind turbines produce over 25 000 MW of wind energy [5]. The success of the decentralized grid system can be attributed to the higher feed in tariff provided by the German government - R1.25/kWh (when converted to Rands) [6]. The higher feed-in tariff allowed for a renewable energy investment boom in Germany resulting in a renewable energy contribution of nearly 55 TWh/year (55 000 000 MWh/year) or 10% of overall supply as well as creating over 150000 jobs in the renewable energy sector [5]. The success of small-scale wind turbines used in decentralized grid-connected systems in Germany provides hope for similar systems to be implemented in South Africa. Furthermore, it is true that SA's energy development program has been weighted towards large grid-tied projects, the South African National Energy Development Institute (SANEDI) has highlighted the significance of distributed decentralized projects as potential solutions to some of the country's energy challenges. However, the development of models and systems that can deliver those solutions are still much needed [2] as not much research has gone into the improvement of small-scale wind turbine systems when compared to utility-scale systems.

1.2 Grid-Connected Wind Turbine Systems

This section provides a review of the most common wind turbine systems (WTS) used for grid connection application.

1.2.1 Fixed-Speed Wind Turbine Systems

Figure 1.1 shows the first commercially successful grid-connected wind turbine, the so called "Danish concept" fixed-speed wind turbine. It consists of a squirrel-cage induction generator (SCIG) which is directly connected to the grid and driven by a fixed-speed turbine. This concept also makes use of a capacitor bank to provide reactive power compensation as well as a soft starter to aid in smooth grid connection.

The process of connecting the turbine to the grid is as follows [7], the turbine is accelerated by the wind to a speed of 5-30% below the synchronous speed of the generator, where synchronous speed is defined as the rotational speed required by the generator to produce voltages and currents with a frequency matching that of the grid's. The soft starter now starts to operate by sending delayed ignition pulses to the anti-parallel thyristors in order to limit the currents flowing in the generator needed for magnetization. Without the soft starter the inrush currents, which can be several times the rated current of the generator, could cause the generator to have a dangerously high start-up torque which would cause severe voltage disturbances on the grid. After the induction machine has been magnetized, the

soft starter is bypassed by a contactor to smoothly connect the generator to the grid and to reduce the overall losses of the system.

However, the variable nature of wind produces undesirable power fluctuations in the grid and this is especially true when fixed-speed wind turbines are used [8]. For this reason, only a small percentage of wind turbine installations make use of this concept today with market trends favouring variable speed wind turbine concepts [9].

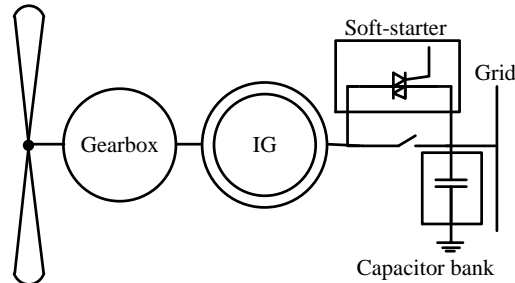


Figure 1.1: Danish concept fixed-speed wind turbine.

1.2.2 Variable-Speed Wind Turbine Concepts

Figure 1.2(a) shows a single-line diagram of the most common type of variable-speed wind turbine system (WTS) [9]. This configuration is made up of a variable-speed wind turbine connected to a doubly-fed induction generator (DFIG). The stator of the DFIG is directly connected to the grid while the rotor is connected to the grid via a partial-scale power converter which is typically rated at 20% - 30% of the generator power. The power converter is responsible for smooth grid connection and the variable speed range is $\pm 30\%$ around the synchronous speed. Figures 1.2(b) and (c) show two variations based on the WTS showed in (a) but instead of a partial-scale power converter, makes use of a full-scale power converter. The generator can be either a wound-rotor synchronous generator (WRSG), a permanent magnet synchronous generator (PMSG) or an induction machine as used in (a). This concept has full control over the speed range from 0 to 100% of synchronous speed [9]. However, this concept provides higher losses when compared to (a) as all the power generated flows through the power converter.

1.2.3 Non-Conventional Wind Generator Concepts

Large wind turbines typically rotate at 30 - 50 revolutions per minute (rpm). The generator, either induction or synchronous, is required to rotate at speeds of 1000 - 1500 rpm in order to obtain the frequency needed for grid synchronization. This speed increase is achieved through the use of a gearbox. However, the inclusion of a gearbox incurs additional cost, weight and inefficiencies to the drivetrain.

Direct connection of the generator to the wind turbine (without a gearbox) would require the generator to have a large number of poles as described by (1.1) in order to produce the frequency required for grid connection (50 Hz or 60 Hz) while rotating at the relatively low speeds of 30 - 50 rpm, where P and N refer to the number of poles and rotational speed (in rpm) respectively.

$$Frequency, f = \frac{P}{2} \times \frac{N}{60} \quad (1.1)$$

Permanent magnet synchronous generators (PMSG) are ideal for use in small-scale wind turbine applications. PMSG are synchronous machines where the rotor windings are replaced with permanent magnets. As a result, no external excitation is required so losses pertaining to rotor winding excitation are eliminated which allows for a higher power density at a small size. The permanent magnets allows for a smaller pole pitch which can yield a cost-effective design [10]. The small pole pitch also allows the PMSG to operate at lower speeds which either eliminates the need for a gearbox or allows for a single stage, low transfer ratio gears to provide for a more compact design.

However, synchronous generators (SG) exhibit oscillatory behaviour during load changes due to the limited amount of mechanical damping in the drivetrain and as a result, SG aren't suited for direct-grid connection. It is common practice in industry to make use of damper windings but the small pole pitch required for wind turbine generator designs precludes the use of damper windings and as a result, damper windings aren't considered suitable for wind energy applications involving PMSG.

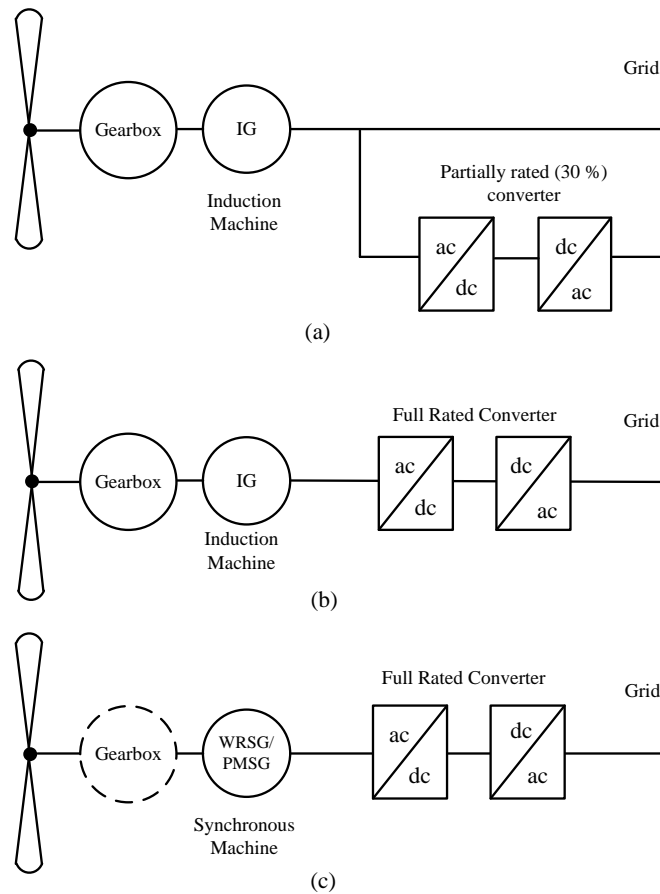


Figure 1.2: Most common wind turbine drive-train layouts currently in use with (a) the variable speed doubly-fed induction generator (DFIG) with gearbox and partially rated converter, (b) the variable-speed doubly-fed induction generator (DFIG) with gearbox and full rated converter, (c) direct-drive wound rotor synchronous generator (WRSG) or permanent magnet synchronous generator (PMSG) and full rated power electronic converter. The gearbox is optional in (c).

Further attempts to provide a form of damping to the drivetrain have been made in literature. Figure 1.3(a) shows a spring and mechanical damper system proposed in [11] in which the stator is mounted on an additional bearing arrangement and is connected to the nacelle structure by means of the spring damper configuration. In [12], a small series partially rated converter (20% of rated power) is placed in the star point of the generator as shown in Figure 1.3(b). The series converter provides the damping required during input power or grid disturbances.

Another type of generator, the permanent magnet induction generator (PMIG), evaluated in [13] for direct-grid connection is shown in Figure 1.3(c). The PMIG consists of a conventional 3-phase stator winding, however, the rotor consists of two sections: an outer squirrel-cage rotor and an inner permanent magnet (PM) rotor. The outer rotor is connected to the wind turbine shaft while the PM rotor is allowed to rotate freely against the shaft. The PMIG operates by allowing the squirrel-cage rotor to be driven by an external force, the PM rotor rotates with this rotor at a slightly slower speed where the difference in speed is referred to as slip. It is this 'slip' which provides a form of damping against torque pulsations. Once the squirrel cage rotor rotates at a speed greater than synchronous speed, the rotating PMs would induce a voltage in the stator with a frequency matching that of the grid's voltage and synchronization can thus occur [13].

1.2.4 Slip-Synchronous Permanent Generator Concept

Figure 1.4 shows a wind turbine concept known as the slip-synchronous permanent magnet generator (SS-PMG), developed in [14], the topology is based on the PMIG concept discussed in the previous section. The SS-PMG consists of two integrated generating units: a slip permanent magnet generator (S-PMG) where the short-circuited rotor is directly mounted to the turbine and a PMSG unit of which the stator terminals are connected directly to the grid. The two machines are mechanically linked via a common, free rotating permanent magnet rotor with separate sets of magnets for each of the generating units [15]. The S-PMG operates in a manner similar to that of an induction machine. The short-circuited

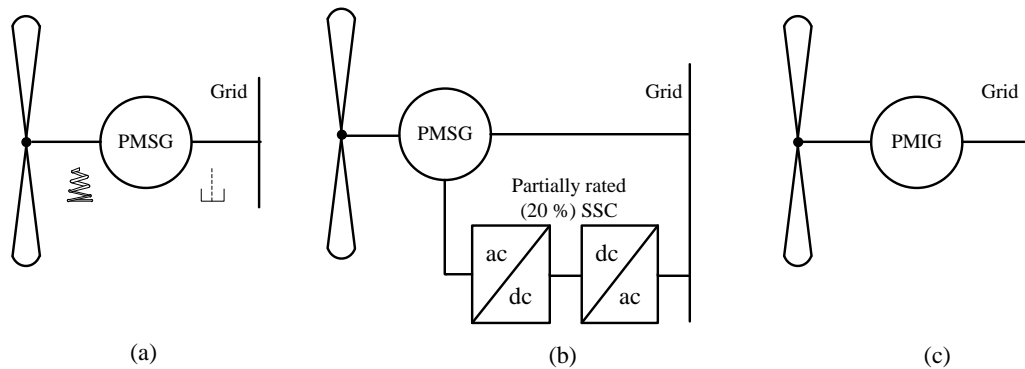


Figure 1.3: Attempts to provide damping to a drivetrain including a PMSG with, (a) a spring and mechanical damper being used, (b) a PMSG with a partially rated star point converter and, (c) A direct-grid connected permanent magnet induction generator.

cage rotor rotates at a speed relative to that of the common PM rotor, where the difference in speed is again referred to as slip speed. The common PM rotor transfers mechanical power from the S-PMG to the PMSG unit which in turn generates electrical power. With the turbine directly connected to the short-circuited rotor which is internally magnetically connected to the common PM rotor which itself is magnetically connected to the PMSG stator, there is no physical connection between the wind turbine and the grid connected PMSG. As a result, the S-PMG stage provides a form of damping in the drivetrain against sudden wind disturbances which allows the SS-PMG to be directly grid connected, without the need for a power converter [14].

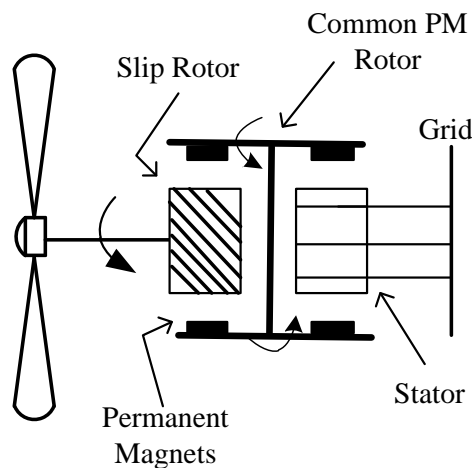


Figure 1.4: SS-PMG wind turbine drivetrain.

1.2.5 A Drivetrain Based off of The SS-PMG

Figure 1.5 shows a new wind turbine drivetrain (based on the SS-PMG concept) proposed and developed in [16]. In this drivetrain, the SS-PMG is separated into two distinct machines: with one being a S-PMG (which is referred to as a slip permanent magnetic coupling (S-PMC) or "slip coupler" in [16]) as previously described and the other being a conventional PMSG. The S-PMC is connected between the gearbox and the PMSG shown in Figure 1.5. The S-PMC, shown in Figure 1.6, consists of two rotating sections: the short-circuited rotor, (the inner section containing the windings), and an outer PM rotor. The drivetrain also includes a gearbox in order to provide greater flexibility with regards to speed selection.

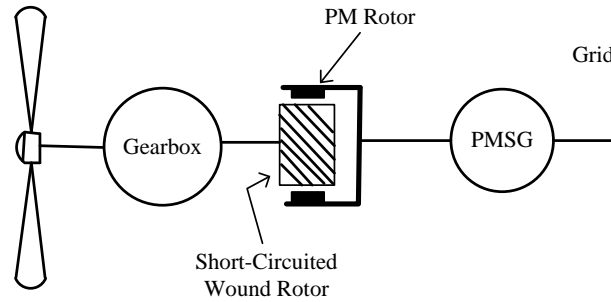


Figure 1.5: A wind turbine drivetrain concept based on the SS-PMG where the SS-PMG is separated into two distinct machines; with one being a S-PMC and the other a conventional PMSG.

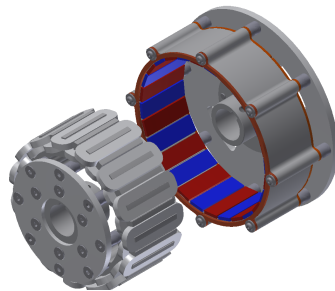


Figure 1.6: CAD representation of the S-PMC assembly [17].

1.3 Generator Speed Control

In grid connected wind turbine systems (WTS), in the events leading to grid connection or in the event of a grid outage, the wind turbine rotor will continue to accelerate due to torque produced as a result of the wind. As a result, the international standards and certification rules require that two independent braking systems be used for large wind turbine systems and at least one braking system be used for smaller WTS. It is common practice to provide an aerodynamic braking system on the low-speed shaft and a mechanical brake on the high-speed shaft [18]. This section provides a brief overview of the various methods used to control the speed of wind turbines.

1.3.1 Power in the Wind

Equation 1.2 describes the power available in the wind, P_w , which can be defined as the amount of kinetic energy passing through a given area over time [19].

$$P_w = \frac{1}{2} \rho A v^3, \quad (1.2)$$

where ρ represents the air density in measured in (kg/m^3), A is the swept area of the wind turbine and v is the speed of the wind (in m/s). However, the blades of a wind turbine cannot extract all of the energy in the wind and hence a term called the coefficient of wind power, C_p , is defined as the fraction of the wind power extracted by the wind turbine blades. Thus, the mechanical power, P_m , extracted from the wind by the turbine blades can be described as

$$P_m = \frac{1}{2} \rho C_p A v^3. \quad (1.3)$$

It is clear from 1.2 and 1.3 that the power produced by a wind turbine is heavily influenced by the speed of the wind, and consequently, the rotational speed of the turbine.

1.3.2 Pitch Control

For pitch controlled WTS, the turbine's electronic controller monitors the turbine's output power several times per second. When the turbine's power output becomes too high, the electronic controller signals

the blade pitch mechanism to turn the rotor blades slightly out of the wind which reduces the overall lift required to rotate the turbine rotor. Conversely, the blades are turned back into the wind whenever the wind drops to levels which allow safe power production.

1.3.3 Stall Control

Stall controlled wind turbines have their rotor blades bolted to the turbine hub at a fixed angle. However, the blades are designed to ensure that the moment the wind speed becomes too high, the geometry of the blades creates turbulence on the side of the blade not facing the wind. This turbulence, or stall, prevents the lifting force of the rotor blade from acting on the rotor which limits the power produced by the turbine. The advantage of using stall control is that it avoids the use of moving parts and a complex control system. However, successful implementation of stall control requires complex aerodynamic design challenges relating to the dynamics of the whole wind turbine.

1.3.4 Active Stall Control

A common concept for larger wind turbines is to use what is known as active stall-regulation. Active stall machines resemble pitch controlled machines in the sense that they too have pitchable blades. However, the difference between active stall and pitch controlled machines is that if the generator is about to be overloaded, the active stall machine will pitch the blades in the opposite direction of that from what pitch controlled machines does. This is done in order to force the blades into a deeper stall, thus wasting the excess energy in the wind. The advantage of active stall over normal passive stall controlled wind turbines is that the wind turbine can operate at near rated power at all high wind speeds.

1.3.5 Yaw Control

The yaw of a turbine refers to the angle between the incoming wind vector and the rotational axis of the turbine. To ensure maximum power extraction, the turbine should always be aligned with the wind, i.e., a yaw angle of zero. Wind turbines that make use of yaw control have what is known as a yaw drive which is responsible for directing the turbine into the wind based off signals received from various sensors located on the wind turbine nacelle. Furthermore, the yaw drive can also steer the turbine out of excessive incoming winds.

1.3.6 Electro-Mechanical Braking

One way to slow down and halt a wind turbine rotor involves converting the rotational kinetic energy into heat. This type of braking system is referred to as a mechanical disk brake. Disk brakes are mounted on the shaft (either the low-speed shaft, high-speed shaft or both) and slow the turbine down by providing braking torque in the form of friction. Disk brakes provide overspeed control, parking and emergency braking of wind turbines. However, one disadvantage of using a disk brake (in large wind turbines) is the inherent operating delay which can be as long as 10 seconds [20]. During this time, the rising rotor speed could accelerate to dangerous levels which could damage the wind turbine.

Another braking system proposed in [10] and shown in Figure 1.7(a) is known as electrodynamic braking in which counter-torque produced by the generator itself is used to brake the turbine. This system involves connecting a resistive bank to the terminals of the generator. The resistors are connected in parallel and with the appropriate switches, the value of resistance and hence the load on the generator can be varied to control the speed of the rotor.

A variation to the resistor bank braking method is proposed in [21] and shown in Figure 1.7(b) is used to provide speed control for a SS-PMG in which the resistor bank is replaced by a thyristor pack which is able to achieve variable braking torque with a single resistor. This is achieved by varying the thyristor firing angle. In this way, the generator counter-torque can continuously varied to respond to changing conditions without the need for multiple resistors [21].

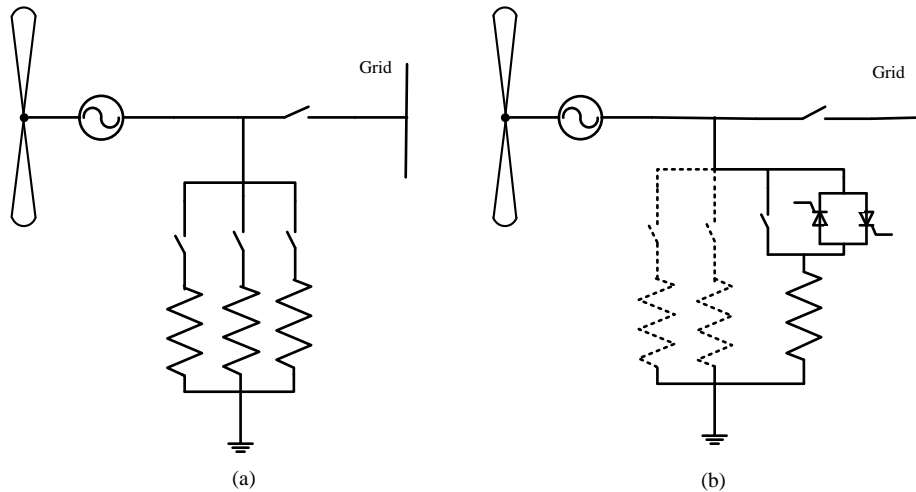


Figure 1.7: Line diagram of, (a) the resistive bank based speed control strategy and (b) the thyristor based single resistor strategy with optional resistor stages shown with dotted lines [21].

1.4 Generator Synchronization Conditions

Figure 1.8 shows a generator G_1 supplying power to a load with a second generator, G_2 about to be synchronized to the local network through contactor S_1 [22]. However, before G_2 can be connected to the network, each of its three phases must have exactly the same voltage magnitude and phase angle prior to S_1 closing. Additionally, G_1 's voltage frequency should be equal to that of G_2 . If S_1 is closed at any arbitrary moment where the voltages and frequency of G_2 aren't exactly the same in each conductor as those of G_1 , both generators are liable to be severely damaged by the large inrush currents and power transients that will occur before the generators stabilize at a common frequency [22]. Furthermore, these inrush currents and power transients could result in a loss of power to the load. Table 1.1 provides the general guidelines for synchronizing generators to existing power systems.

From Table 1.1, prior to synchronization, the difference in frequency, Δf , rms phase voltage ΔV , and, voltage-phase angle, $\Delta\phi$ between the oncoming generator and the connected generator must be less than a predetermined limit depending on the size of the generator.

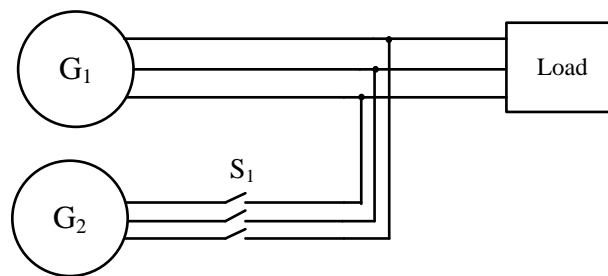


Figure 1.8: An oncoming generator (G_2) being connected to a power system [22].

Table 1.1: Parameter limits for synchronisation with the Eskom distribution network [23].

Embedded Generator Rating [kVA]	Maximum Frequency Difference [Hz]	Maximum Voltage Difference [%]	Maximum Phase Angle Difference [°]
$0 \leq S < 500$	0.3	10	20
$500 \leq S < 1500$	0.2	5	15
$S \geq 1500$	0.1	3	10

1.5 Turbine Torque Pulsations

The power produced by wind turbines under continuous operation often include periodic fluctuations at n times the rotational frequency of the blades (f_t) or nf_t where n is the number of blades [24, 25]. The most prominent of these frequency fluctuations are due to two phenomena known as wind shear and tower shadow. Wind shear refers to the variability of wind speed with respect to height [24], in other words, the wind speed at the tip of a turbine blade (when the tip of the blade is facing upwards) will be greater than the wind speed experienced at the blade's hub-point connection. Tower shadow refers to the disruption and redirection of airflow as a result of the turbine tower. Furthermore, each time a turbine blade passes in front of the tower, the disrupted airflow causes a fluctuation in the mechanical torque produced by the blade. This fluctuation in torque is then transferred to the generator which results in a small dip in output power [26]. The tower shadow effect is known to produce the most significant of turbine torque pulsations when compared to wind shear [24, 25, 26]. The nf_t frequencies are dependent on the rotational speed of the turbine and as a result, the generator will experience periodic dips in mechanical torque in the frequency range of 0.5 - 10 Hz [26]. This low frequency range tends to cause fluctuations in system rms voltage (known as voltage flicker) at the point of common connection (PCC) -where the wind turbine connects to the grid- which negatively effects the power quality supplied to the grid [26]. The tower shadow effect is known to be most prominent in downwind turbines due to the turbine tower being directly in the path of airflow prior to hitting blades. This in contrast to upwind turbines where the airflow strikes the blades *before* it hits the tower.

1.6 Statement of the Problem

Permanent magnet synchronous generators (PMSG) have shown to be an ideal solution for small-scale wind turbine applications. However, PMSG cannot be direct-grid connected as a result of a lack of damping present in conventional drivetrains. Attempts have been made in literature to provide damping to the drivetrain with a partial or full rated power converter being the favoured option in industry. However, full scale power converters (or even partial scale converters) impose penalties which include cost, reliability and efficiency.

The SS-PMG or the drivetrain based on the SS-PMG concept are wind turbine systems which can be connected to the grid without the need for a power converter. However, without a power converter providing smooth grid connection, a new means to synchronize slip-synchronous wind turbine systems (SS-WTS) to the grid is needed.

The wind turbine drivetrain from Figure 1.5 is to be used in a downwind configuration and is to be connected to an electrical network without the use of a power converter. That is to say, before grid connection, the new synchronization system would need to be able to allow the downwind turbine drivetrain to accelerate from rest to synchronous speed and then maintain the generators speed at synchronous speed prior to grid connection. Furthermore, the synchronization system would be required to disconnect the downwind turbine drivetrain from the grid in the event where the downwind turbine ceases to produce power and instead, starts to draw power from the grid.

Additionally, once grid connected, the downwind turbine's dynamic stability remains a concern. As stated in previous sections, PMSG exhibit oscillatory behaviour in the presence of load changes. Furthermore, with the wind turbine being in a downwind configuration, the effects of wind shear and tower shadow become more prevalent. It remains unknown whether or not a downwind turbine, making use of a slip coupler (S-PMC), can provide sufficient damping to the drivetrain in order to mitigate the oscillatory behaviour known to occur in direct grid connected PMSG-based wind turbine systems.

1.7 Objective of Study

The drivetrain shown in Figure 1.5 is to be used in a downwind configuration. However, before the downwind wind turbine can be considered for real world application, a speed controller which is to be used in conjunction with a grid connection controller (GCC) needs to be developed and tested which would allow the downwind turbine to synchronize with and connect to the grid. Consequently, the speed controller and GCC should be able to:

- Allow the wind turbine drivetrain to accelerate from rest until it reaches synchronous speed.
- Once the wind turbine has reached synchronous speed, the speed controller must be able to maintain the generator's speed at synchronous speed.
- Once synchronous speed as been established and maintained, the GCC will monitor and wait for the generator's voltage magnitude, frequency and phase to match that of the grid's.

- After all the necessary synchronization requirements have been met, the GCC will then connect the wind turbine to the grid.

The objectives are thus to determine a transfer function model of the downwind turbine drivetrain from which a speed controller can be designed and tested. The speed controller must be able to control and maintain the downwind turbine drivetrain speed (from rest) at synchronous speed regardless of the wind speed.

A further objective was, once the downwind turbine is connected to the grid, how well does it perform against turbulent winds, especially those pertaining to the $3f_t$ frequency which is known to cause substantial torque pulsations in downwind turbines.

The final objective was to evaluate the performance of the downwind turbine in real-world applications. The downwind turbine is to be tested at Stellenbosch's Mariendahl wind turbine testing facility.

1.8 Significance of the Study

The significance of the study is that it contributes to the development and understanding of direct-grid connected slip-synchronous wind turbine systems (SS-WTS). The slip-synchronous permanent magnet generator (SS-PMG), described in Section 1.2, has shown to be a suitable wind turbine system for direct-grid connection application. However the lack of a gearbox limits the SS-PMG to relatively low speeds which in turn forces the machine to be large and bulky. Furthermore, the design of the SS-PMG concept imposes a complexity in the design of the drivetrain as it requires two generating units which are magnetically coupled by a common PM rotor.

For these reasons, the separation of the two generating units as well as the inclusion of a gearbox allows for a greater speed selection which in turn allows for a physically smaller generator and a more compact wind turbine system. However, unlike the SS-PMG, the newly proposed and developed drivetrain of Figure 1.5 has yet to be tested in a laboratory or in the field. This fact furthers the significance of this study as the results may be utilized to develop and improve the overall design of SS-WTS as well as the systems used to synchronize these SS-WTS to utility grids without the need for power converters. The overall goal of the study is to further the knowledge of new, novel wind turbine systems.

1.9 Thesis Structure

The mathematical modelling of the downwind turbine is addressed in Chapter 2. Furthermore, the mathematical model is then used to develop a simulation model of the downwind drivetrain in MATLAB/Simulink. The design of the speed controller is handled in Chapter 3. Chapter 4 deals with the dynamic performance of the grid connected wind turbine model under turbulent wind/torque conditions. Chapter 5 attempts to verify the MATLAB/Simulink Model of the downwind drivetrain on a testbench in the laboratory. Chapter 6 deals with the real-world performance of the downwind turbine where field test results obtained from Stellenbosch's wind turbine testing facility will be presented.

Chapter 2

Modelling

This chapter develops a dynamic simulation model for the downwind turbine drivetrain shown in Figure 2.1. The drivetrain model will be implemented in MATLAB/Simulink in order to evaluate the downwind drivetrain's performance under varying simulated conditions. The dq -reference frame will be used to model the permanent magnet synchronous generator (PMSG) whereas the slip-magnetic coupling (S-PMC) will be modelled based off of it's linear slip versus torque relationship. The wind turbine is modelled using a function generator developed from the turbine's torque-speed curves and the gearbox is treated as a one-lump mass model for simplicity. Finally, a brief description of the grid connection controller (GCC) and it's functionality is provided at the end of the chapter.

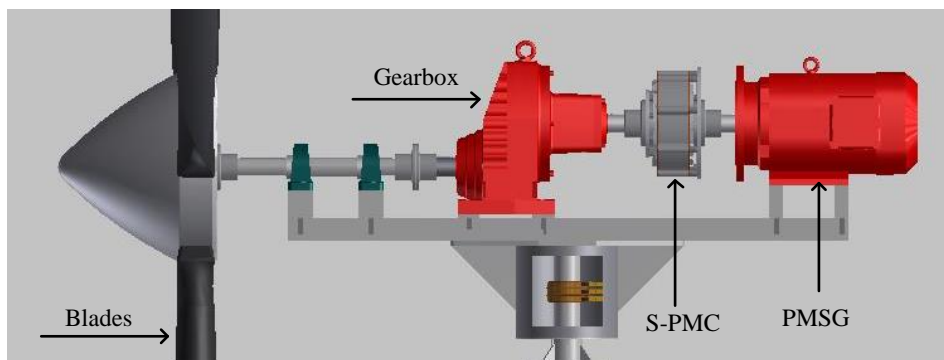


Figure 2.1: A CAD representation of the downwind turbine drivetrain.

2.1 PMSG

The permanent magnet synchronous generator (PMSG) was designed and constructed in [27]. Figure 2.2 (a) and (b) show the respective permanent magnet (PM) rotor and the wound stator of the PMSG. The PMSG consists of a 10/12 pole/slot combination with permanent magnets on the rotor providing the magnetic field. The stator is made up of double-layer, non-overlap copper windings with a fill factor of 40%. The PMSG is directly grid connected via a grid connection controller (GCC) and operates at a synchronous speed of 600 revolutions per minute (rpm). Furthermore, the rated power of the PMSG is 2200 W and its rated torque is 36 Nm.

The dq -equivalent circuits of the PMSG are shown in Figure 2.3 and the consequent dq -dynamic equations are given by

$$\begin{aligned} v_{qs} &= -R_s i_{qs} - L_{qs} \frac{di_{qs}}{dt} - \omega_e L_{ds} i_{ds} + \omega_e \lambda_{ms}, \\ v_{ds} &= -R_s i_{ds} - L_{ds} \frac{di_{ds}}{dt} + \omega_e L_{qs} i_{qs}, \end{aligned} \quad (2.1)$$

where ω_e represents the electrical speed in radians per second (rad/s). The stator winding resistance is given as R_s and the flux-linkage due to the permanent magnets is given by λ_{ms} . The PMSG dq -inductances are given by L_{ds} and L_{qs} and are determined by

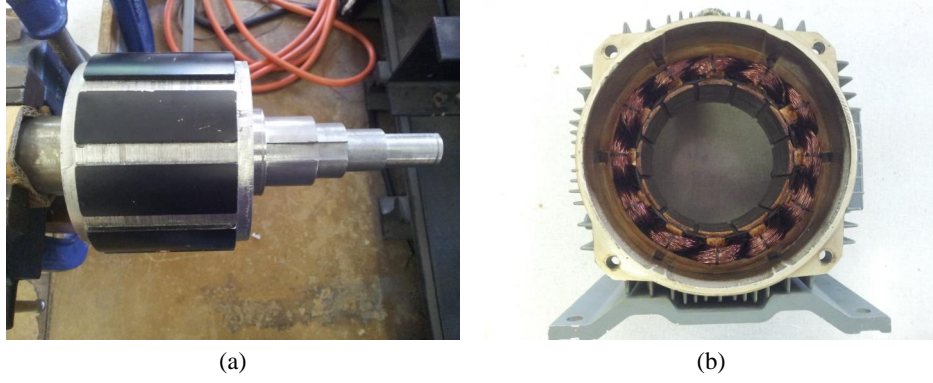


Figure 2.2: Figure showing the constructed PMSG rotor (a) and wound stator (b) [27].

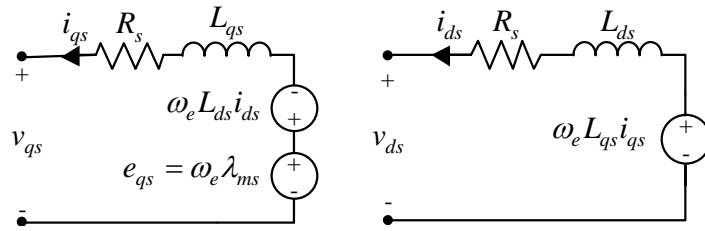


Figure 2.3: The dynamic dq -equivalent circuits of the PMSG.

$$L_{ds} = \frac{\lambda_d - \lambda_{ms}}{-I_d} + L_e; \quad L_{qs} = \frac{\lambda_q}{-I_q} + L_e, \quad (2.2)$$

where L_e represents the end-winding inductance. Finally, the torque generated by the PMSG is given by

$$\tau_s = \frac{3}{4} p [(L_{qs} - L_{ds}) i_{ds} i_{qs} + \lambda_{ms} i_{qs}]. \quad (2.3)$$

where p represents the number of generator poles.

2.2 S-PMC

The slip-magnetic coupling (S-PMC) used in the drivetrain was designed and constructed in [16]. The S-PMC consists of two rotating sections which are shown in Figure 2.4. The first section, Figure 2.4(a), consists of a short-circuited rotor (the inner section containing the windings) whereas the second section, Figure 2.4(b), consists of a PM rotor (the outer section, lined on the inside with PMs). The magnetic coupling allows for the transfer of torque between the gearbox and the PMSG and acts as a filter for torque transients with the aim of improving the quality of the torque transmitted to the PMSG. The S-PMC consists of a 28/30 pole/slot combination, with all 30 non-overlap coils short-circuited and has an efficiency of 97% [16]. Furthermore, like an induction machine, the S-PMC operates under slip conditions where the slip is proportional to the amount of torque being transferred. The formal definition for slip speed is defined as

$$n_{slip} = n_{sync} - n_m \quad (2.4)$$

where n_{slip} is the slip speed, n_{sync} is the synchronous speed and n_m is the mechanical shaft speed (all in rpm). The term *slip* is the relative speed expressed on a per-unit basis [22] and is defined as

$$s = \frac{n_{slip}}{n_{sync}} (\times 100\%) = \frac{n_{sync} - n_m}{n_{sync}} (\times 100\%). \quad (2.5)$$

If equations (2.4) and (2.5) are expressed in terms of angular velocity ω , then for the S-PMC,

$$\omega_{sl} = \omega_m - \omega_s = \left(\frac{\omega_m - \omega_s}{\omega_m} \right) \times \omega_m = s \times \omega_m \quad (2.6)$$

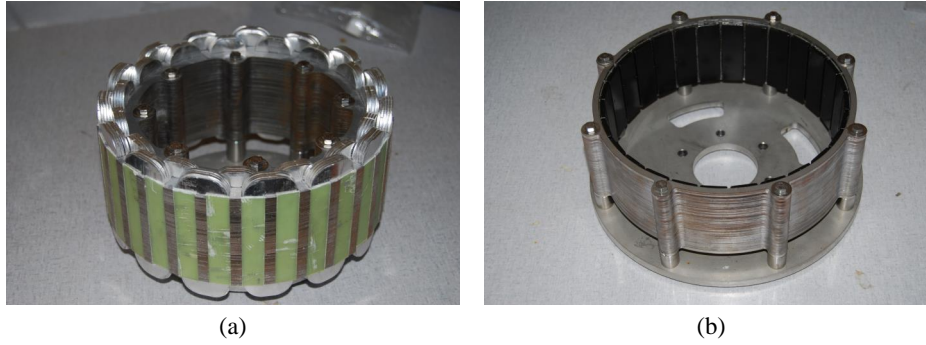


Figure 2.4: Figure showing the constructed S-PMC short-circuited rotor (a) and the PM rotor (b) [16].

where ω_{sl} is the slip speed, $\omega_m = \omega_e \times \frac{2}{p}$ is the rotor speed (on the high-speed side of the gearbox) and ω_s is the PMSG rotor speed or if grid connected, synchronous speed, all in rad/s.

Figure 2.5(a) [16] shows the linear relationship between slip and the output torque produced by the S-PMC. The output torque, τ_r , is described by

$$\tau_r = G_c \times \omega_m \times s, \quad (2.7)$$

where the S-PMC gain (G_c) is given by

$$G_c = \frac{\tau_r}{s \times \omega_m} \quad (2.8)$$

and shown in Figure 2.5(b).

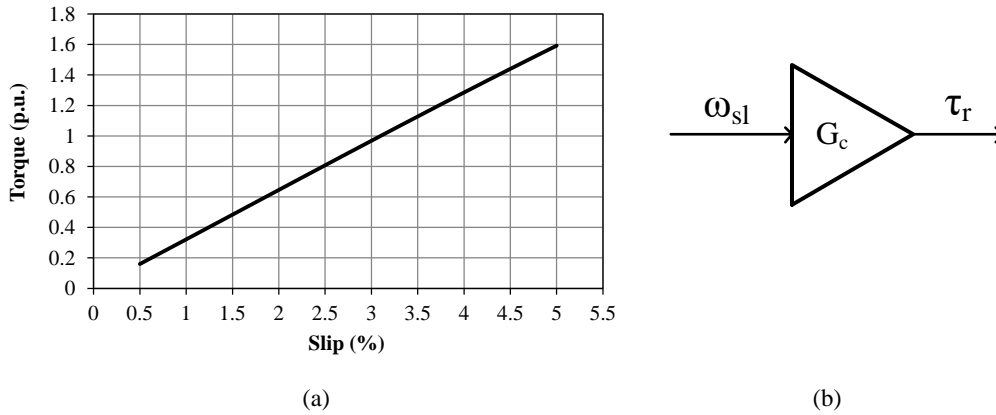


Figure 2.5: S-PMC modelling with (a) the linear relationship between slip and torque for slip values between (0 - 5%)[16] and (b) the S-PMC gain block model.

2.3 Turbine Blade Model

Figure 2.6 shows the three blades of the downwind turbine fitted to the nacelle. Wind turbine blade sets are characterised by their wind power coefficient (C_p) versus Tip-Speed-Ratio (TSR) curve where the TSR is defined as

$$TSR = \frac{\omega R}{v}, \quad (2.9)$$

where ω is the turbine angular velocity (in rad/s), R is the length of one of the blades and v is the wind speed (in m/s). The C_p versus TSR curve for the 1.9 m blades used for the downwind turbine is shown in Figure 2.7. Figure 2.8(a) shows the wind turbine's power-speed curves and Figure 2.8(b) shows a function



Figure 2.6: Downwind turbine blades.

generator representation model which provides the aerodynamic torque produced by the turbine as an output based off of the wind turbine's power-speed curves with wind speed, v and turbine rotational speed, ω_t as inputs to the function generator.

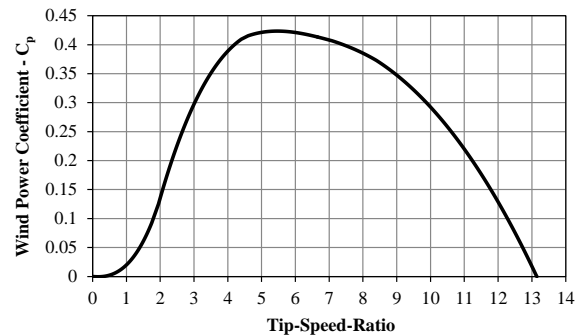
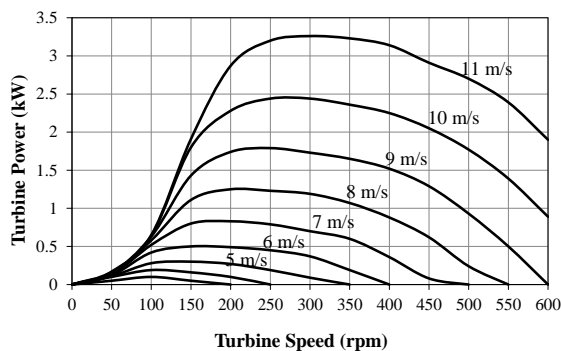
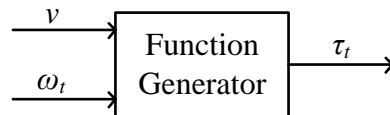


Figure 2.7: Wind power coefficient versus tip-speed-ratio curve for the 1.9 m blade set used for the downwind turbine [16].



(a)



(b)

Figure 2.8: Wind turbine power versus turbine speed curves (a) [16] and equivalent simulation block model (b).

2.4 Gearbox

The drivetrain gearbox is an *SEW Eurodrive* with a gear ratio of 1:3.78, a maximum torque rating of 305 Nm, and a power rating of 5 kW. It is a single stage, helical gear unit which is used as an up-speed gearbox to increase the drivetrain's rotational speed by a factor of 3.78. Tests conducted in [16] determined the gearbox efficiency and it was found to be 96-97% at a load of 132 Nm. However, it should be noted that this efficiency could only be reached once the gearbox is brought to the rated operating temperature by running the gearbox under rated load for 1.5 hours [16].

For simplicity, the gearbox is modelled as a gain-block where its magnitude is that of the gear ratio, 1 : 3.78, as its purpose in the simulation model is to reduce the turbine torque τ_t by a factor of 3.78. As a result the dynamics of the turbine and slip-rotor are expressed as

$$\tau_t' - \tau_r = J_t \frac{d\omega_t}{dt}, \quad (2.10)$$

while the dynamics of the PM rotor section and the PMSG are given by

$$\tau_m = \tau_r - \tau_s = J_m \frac{d\omega_s}{dt}, \quad (2.11)$$

where τ_t' is the torque generated by the turbine reduced by a factor of 3.78, τ_r is the torque generated by the S-PMC and τ_m is the resultant torque acting on the PMSG rotor. The respective inertias of the turbine (plus the S-PMC's short-circuited rotor) and the PMSG (plus the S-PMC's PM rotor) are represented by J_t and J_m .

2.5 Grid Connection Controller

Figure 2.9 shows a simplified model of the grid connection controller (GCC). The GCC is responsible for controlling the speed of the downwind turbine prior to grid connection as well as synchronizing and connecting the downwind turbine to the grid. The GCC achieves this by comparing the frequency of both the generator and the grid through the method of counting the zero crossings of their respective terminal voltages over a specified time period. The error in frequency is then fed into a digital PI-controller which adjusts the duty cycle of a dumpload chopper circuit which regulates the effective load at the terminals of the generator, which in turn controls the speed of the wind turbine. Once the frequency of the generator matches that of the grid, the GCC waits for the respective voltage phase angles of the generator and grid to align before closing S_1 (normally open) and opening S_2 (normally closed) and connecting the generator to the grid.

Additionally, the GCC will disconnect the grid-connected wind turbine (by opening S_1 and connecting the dumpload to the stator terminals) in the event where: the generator no longer produces power, the power produced by the wind turbine exceeds operational conditions, or in any event where the grid code is violated.

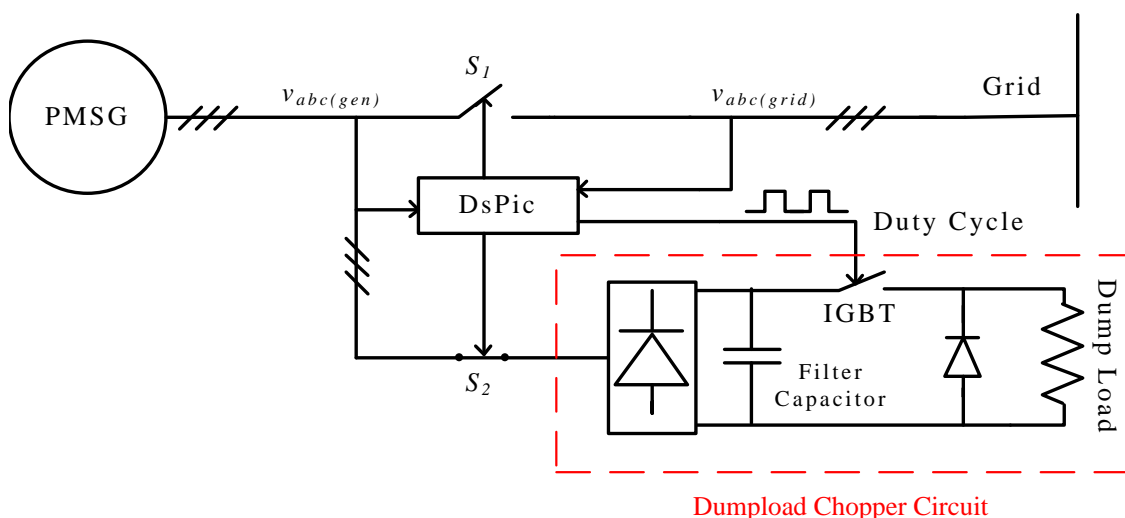


Figure 2.9: GCC circuit diagram.

2.6 Downwind Turbine Simulation Parameters

Table 2.1 provides the relevant parameters used in the chapters and sections that follow.

Table 2.1: Downwind turbine simulation parameters.

Parameter	Value	Parameter	Value
$V_{s(rated)}$	230 V / 400 V	Generator poles, p	10
$I_{s(rated)}$	3.2 A	Gear ratio, η	1:3.78
f_s	50 Hz	$s^{(rated)}$	3 %
R_s	5.2 Ω	G_c	18.5
L_{ds}	66.6 mH	Switching frequency (GCC)	5 kHz
L_{qs}	67.8 mH	Dumpload Resistor	20 Ω
L_e	16.1 mH	Filter Capacitor	2200 μF
λ_{ms}	1.17 Wb.t	$v^{(rated)}$	11 m/s
J_m	0.2 kg.m ²	J_t	0.8 kg.m ²
$T_t^{(rated)}$	145 Nm	Turbine Speed, $n_t^{(rated)}$	163 rpm

The turbine inertia referred to in Table 2.1 represents the estimated turbine inertia transferred to the generator side of the simulation according to $J_t = J_T/\eta^2$ where J_T is the actual turbine inertia and η is the gear ratio of the gearbox.

2.7 Model Implementation

From the mathematical equations in the previous sections a complete simulation model of the downwind turbine is obtained and shown in Figure 2.10. The input to the simulation model is wind speed, v_{wind} whereas the outputs are the PMSG's terminal 3-phase voltages v_a , v_b and, v_c . The simulation model is implemented in MATLAB/Simulink in order to evaluate the drivetrain's performance under various simulation conditions.

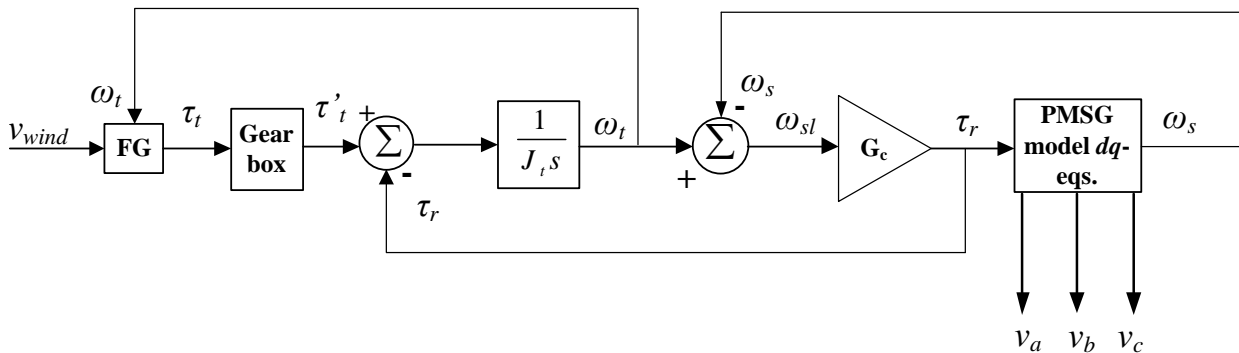


Figure 2.10: A block diagram representation of the open-circuited downwind turbine simulation model.

Chapter 3

PI Speed Controller Design

In this chapter, the necessary proportional (P) and integral (I) components of a PI-controller are developed. The PI-controller is implemented in MATLAB/Simulink in conjunction with the downwind turbine model developed in Chapter 2. A closed-loop block diagram model of the downwind turbine drivetrain, the PI-controller, and the GCC is then used to evaluate the the PI-controller's ability to maintain the downwind turbine's speed at synchronous speed for any given wind speed.

3.1 Downwind Drivetrain System Identification

One of the first steps in designing a control system is to identify and understand the dynamic performance of the *process* which is to be controlled [28]. This can be done theoretically where the process is modelled using mathematical equations or by using experimental data to generate a model for the process. In this section, the downwind turbine drivetrain model is treated as an "unknown" process for which a simplified first-order plus dead time (FOPDT) is developed.

3.1.1 Dynamic Step-Test of the Downwind Turbine Drivetrain Process

In the presence of consistent wind, wind turbines will accelerate indefinitely if not connected to a load or braking mechanism. This kind of behaviour is referred to as *non-self-regulating* or *integrating*. In contrast, *self-regulating* processes are those which naturally settle at some steady-state value for a given input. The downwind drivetrain, from Figure 2.10, is a *non-self-regulating* process with regards to its input (wind speed) and its output (frequency). However, by connecting a pulse-width modulated (PWM) controlled dumpload chopper circuit to the terminals of the generator, for any given wind speed (referred to as input torque from here on) and for a predetermined duty cycle, the downwind drivetrain's output will settle at some steady-state speed and consequently behave as a *self-regulating* system.

Figure 3.1 shows a block diagram representation of a dynamic step-test performed on the downwind turbine drivetrain and Figure 3.2 shows the result of the dynamic step-test. The dynamic step-test involved providing the simulated drivetrain and chopper circuit model with an initial disturbance, in this case a constant input torque signal of 100 Nm, while the duty cycle to the chopper circuit is initially held at a constant level of 30%. Due to the input torque, the drivetrain will initially accelerate before settling at a steady-state speed as a result of the counter-torque produced by the generator due to the effective load at its stator terminals. After the drivetrain's speed has settled at a steady-state level, the duty cycle is then stepped down to 15% (with no change to the input torque disturbance signal) to allow the drivetrain's speed to accelerate and once again settle at a new steady-state level. From this dynamic step-test, a FOPDT model for the downwind turbine drivetrain and dumpload chopper circuit can be developed which describes the relationship between the duty cycle, (d_c), and speed (f_s) for a constant input torque.

3.1.2 First-Order Plus Dead Time Model

A first-order plus dead time dead time transfer function model is, in general, described by

$$G(s) = \frac{k_p e^{-\tau_d s}}{\tau_p s + 1}, \quad (3.1)$$

where $G(s)$ represents the transfer function of the identified process. The process gain (k_p) is defined as the change in process output (Δf_s) over the change in controller output (Δd_c). The process time constant (τ_p) is defined as the time taken before the process output reaches 63% of its final value and

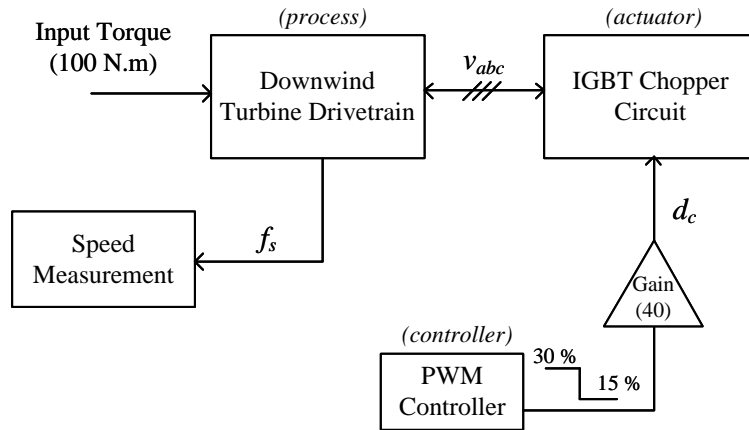


Figure 3.1: Block diagram model of the dynamic step-test performed on the downwind turbine drivetrain.

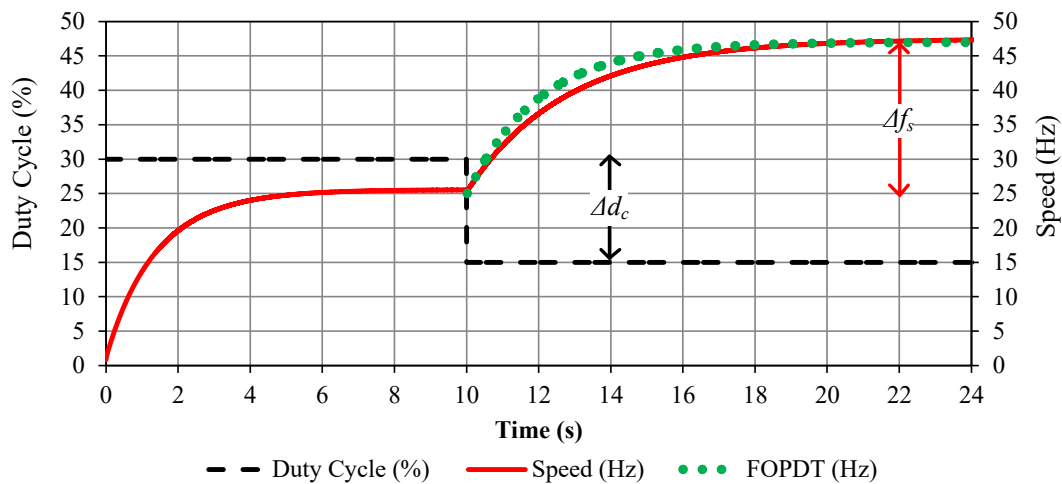


Figure 3.2: Simulated dynamic step-test results for a change in duty cycle (d_c) from 30% to 15% for a constant input torque of 100 Nm, and a dumpload resistor value of 20 Ω .

the process dead time (τ_d) is defined as the delay in time before the process responds to the change in controller output.

From Figure 3.2 over the time range $t \geq 10$ seconds,

- $k_p = \left| \frac{\Delta f_s}{\Delta d_c} \right| = \left| \frac{(47-25)}{(15-30) \cdot 40} \right| = 0.03667$
- $\tau_p \simeq 2$ seconds and,
- $\tau_d \simeq 0.02$ seconds.

The FOPDT transfer function model for the downwind turbine drivetrain and IGBT chopper circuit is thus

$$G(s) = \frac{0.03667e^{-0.02s}}{2s + 1}, \quad (3.2)$$

where the accuracy of the FOPDT transfer function model is shown in Figure 3.2.

3.1.3 Discussion

The downwind turbine drivetrain simulation model behaves as a self-regulating process for a constant torque input and set duty cycle. That is to say, in the presence of a torque input, the drivetrain will accelerate before settling at a steady-state speed as a result of the set duty cycle. However, the downwind drivetrain can also be seen as a near-integrating process. A near-integrating process is defined as a self-regulating process whose process time constant is much larger than its process dead-time. For this

reason, the downwind turbine drivetrain can be viewed as a near-integrating process. Furthermore, the downwind drivetrain exhibits further integrating characteristics in the sense that the dynamic step-test will yield different process values (k_p and τ_p) for different input torque and duty cycle combinations. This is problematic when considering that most PI-control algorithms are designed off of the values of k_p and τ_p . Consequently, a suitably robust PI-control algorithm is needed in order to implement speed control regardless of changing process dynamics. Furthermore, the PI-controller will replace the manually controlled PWM-controller shown in Figure 3.1 and will automatically control the duty cycle input to the chopper circuit based on the difference in frequency between the downwind drivetrain and a predetermined reference frequency. Figure 3.3 shows the resulting block diagram required to provide automatic, closed-loop speed control.

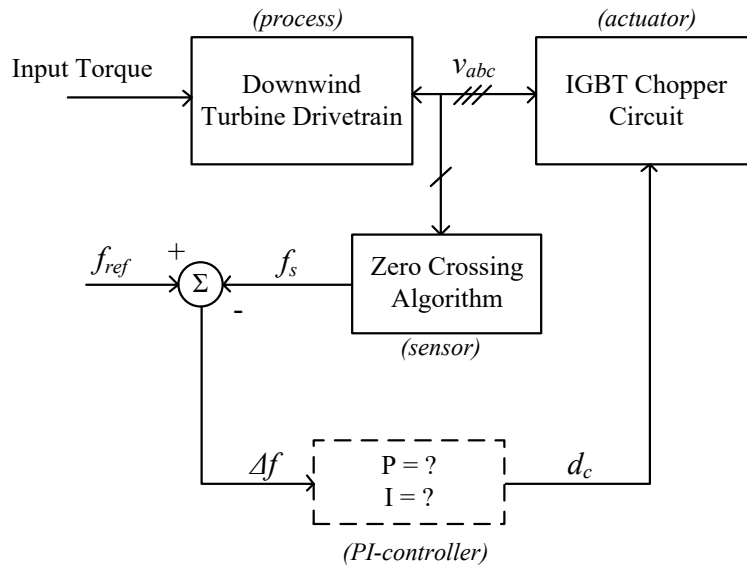


Figure 3.3: Block diagram model of the required PI-controlled speed controller.

3.2 PI Tuning

There are more than 400 PI and PID tuning methods from which to develop a controller [29] with the most common of those being:

1. Ziegler-Nichols Tuning,
2. Cohen-Coon Tuning,
3. Lambda Tuning and,
4. Internal Model Control (IMC).

The Ziegler-Nichols tuning rules work well for processes whose time constant (τ_p) is at least two times as long as the process dead time (τ_d) whereas the Cohen-Coon tuning method works well for processes where the process time constant is greater than at least half of the process dead time [30]. As a result, the Cohen-Coon tuning method is suited to a wider variety of processes than the Ziegler-Nichols method [30]. Both the Ziegler-Nichols and Cohen-Coon tuning rules are based off of the Quarter Decay Ratio [28] otherwise known as Quarter Amplitude Damping [30] where the control objective is to eliminate any error between the set-point and process output as quickly as possible. However, the speed of the controller often results in the process output overshooting the set-point and oscillate around the set-point before reaching the set-point steady-state value [29].

Lambda and Internal model control (IMC) tuning offer an alternative to quarter amplitude tuning. Both Lambda and IMC tuning aim for a first-order plus dead time response to a change in set-point [29]. Furthermore, both Lambda and IMC tuning rules have the following advantages [30]:

- Lambda and IMC tuning rules are much less sensitive to any errors made when determining the process dead time through dynamic step-tests.

- The tuning is very robust, in other words, the control loop will remain stable even if the process dynamics/characteristics change from the ones used for tuning.
- The Lambda and IMC control loops absorbs a disturbance better, and passes less of it on to the rest of the process.

One of the drawbacks of Lambda and IMC tuning is that the controller's integral time (T_i) is set equal to some multiple of the process time constant [30]. Consequently, if the process has a long time constant, the resulting lengthy integral time will result in a slow recovery time from disturbances. [30].

However, due to the flexibility towards changes in the dynamics of the process model as well as the robustness of the control loop that IMC and Lambda tuning methods provide makes them the ideal choice for developing the PI speed controller used by the GCC to control the speed of the downwind drivetrain.

3.2.1 Internal Model Control Tuning

The internal model control (IMC) tuning rules are based off of the values:

- k_p - process gain,
- τ_p - process time constant,
- τ_d - process dead time,

which are determined from the results of the process' dynamic step-test. The above listed parameters are used to determine the necessary proportional (P) and integral (I) parameters of a PI-controller. The controller gain, K_c , for a self-regulating process is calculated as [30]

$$K_c = \frac{1}{k_p} \times \frac{\tau_p}{(\tau_d + \tau_c)}. \quad (3.3)$$

However, the process gain of a self-regulating process whose process time constant is much larger than its dead time can be converted to an integrating process gain k_i by using [31],

$$k_i = \frac{k_p}{\tau_p}. \quad (3.4)$$

The parameter, τ_c , is referred to as the closed-loop time constant where a small value of τ_c results in a faster control loop. Furthermore, it is suggested in [30] that the value of τ_c be 1-to-3 times that of τ_p . Using (3.3) with the values obtained from the downwind drivetrain dynamic step-test, the proportional P term is set equal to the controller gain and is subsequently determined by [30]:

$$\begin{aligned} P &= K_c \\ &= \frac{1}{0.03667} \times \frac{2}{(0.02 + 2)} \\ &= 27. \end{aligned}$$

If the downwind drivetrain is treated as a near-integrating process, the proportional term is calculated as

$$\begin{aligned} P &= K_c \\ &= \frac{1}{k_i} \times \frac{\tau_p}{(\tau_d + \tau_c)} \\ &= \frac{1}{0.018335} \times \frac{2}{(0.02 + 2)} \\ &= 54, \end{aligned}$$

where k_i is calculated as

$$\begin{aligned} k_i &= \frac{k_p}{\tau_p} \\ &= \frac{0.03667}{2} \\ &= 0.018335. \end{aligned}$$

In both instances, τ_c is initially set equal to τ_p to ensure a fast control loop. For both self-regulating and near-integrating processes, the integral I term is determined by

$$\begin{aligned} I &= \frac{1}{\tau_p} \\ &= \frac{1}{2} \\ &= 0.5. \end{aligned}$$

The values for P and I for both self-regulating and near-integrating process designs are compared and used to develop a digital PI-controller which is used by the GCC in conjunction with the dumpload chopper circuit to control the speed of the downwind turbine simulation model.

3.2.2 Integrator Windup Protection

All actuators have limitations. If a controller with integrating action is used where the control algorithm isn't properly designed, the integral term may become very large once the controller output reaches the actuator limits. This happens when the control error becomes too large and causes the the actuator output to saturate at its upper or lower limits. During this time, the integral will continue integrating the error signal and consequently continue increasing the value of the integral term. This becomes problematic after the control error is eventually reduced but by that time the total accumulated error in the control algorithm might be so large that by the time the integral term assumes normal values, the control-loop may already be unstable [32]. Furthermore, during this time where the integral winds down, the output of the controller may oscillate around the set point which can result in an oscillating process output. There are many ways to avoid integrator windup with the the two most common strategies being *back-calculation* and *integral clamping* [32]. The integral clamping method is used in this thesis due to its simplicity as the integral simply stops updating the integrating term at some pre-determined boundary value. The integrating term boundary (I_{limit}) value for the PI-controller developed in the previous section was initially set to 15% of the maximum duty cycle, see the source code provided in Appendix A.3.

3.2.3 Closed-Loop Speed Controller Implementation

Figure 3.4 shows a closed-loop block diagram representation of the speed controller developed in the previous sections where, f_{grid} represents the frequency of the utility grid and poses as the reference signal for the speed controller. The frequency of the generator, f_s , is determined by counting the number of zero-crossings per generator phase voltage v_{abc} . Furthermore, Δf represents the frequency difference between the grid and generator while the input torque disturbance signal remains unchanged. The output of the PI-controller, d_c , is the duty cycle which is used to control the chopper circuit and consequently, the speed of the drivetrain. The resulting MATLAB/Simulink block-model contents of the respective blocks in Figure 3.4 are shown in Appendix A.

The performance of the PI speed controller is shown in Figure 3.5. Overall, the PI-controller is able to control and maintain the downwind drivetrain's speed within the upper and lower speed boundary values for torque inputs up to 100 Nm (0.7 p.u.). However, Figure 3.5(d) shows one of the PI-controller limitations where it is unable to regulate the downwind drivetrain's speed within the necessary boundaries. This is as a result of the controller gains being designed from a dynamic step-test where the resulting FOPDT model was linearised around a specific operating condition namely, an input torque value kept constant at 100 Nm. Consequently, the PI-controller is unable to regulate the drivetrain's speed for torque inputs greater than 100 Nm.

Additionally, for relatively low input torque conditions (Figure 3.5(a)-(b)), the downwind drivetrain displays increasing oscillatory behaviour at low values of input torque. This oscillatory behaviour was found to be due to the integral clamping limit of 15%. For relatively high values of input torque, the integral clamping limit (and consequently the controller output) is sufficient to control the drivetrain speed with minimal oscillations (Figure 3.5 (c)-(d)). However, for low input torque values, the controller output becomes too large and forces the downwind drivetrain's speed to oscillate around the set-point.

Figure 3.6 shows the PI-controller's performance after the proportional term was increased to 54 (treating the drivetrain as a near-integrating process) and the integral clamping limiting term was reduced to 7%. It is clear from Figure 3.6 (a) and (b) that the oscillatory behaviour during steady-state decreases with a decrease in the integral clamping limit. Additionally, the increased proportional gain improved the overall steady-state performance of the PI-controller at higher torque inputs.

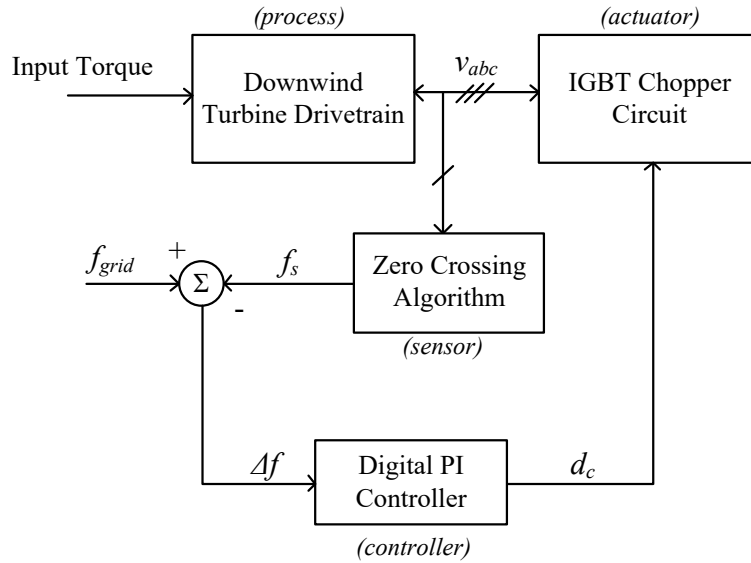
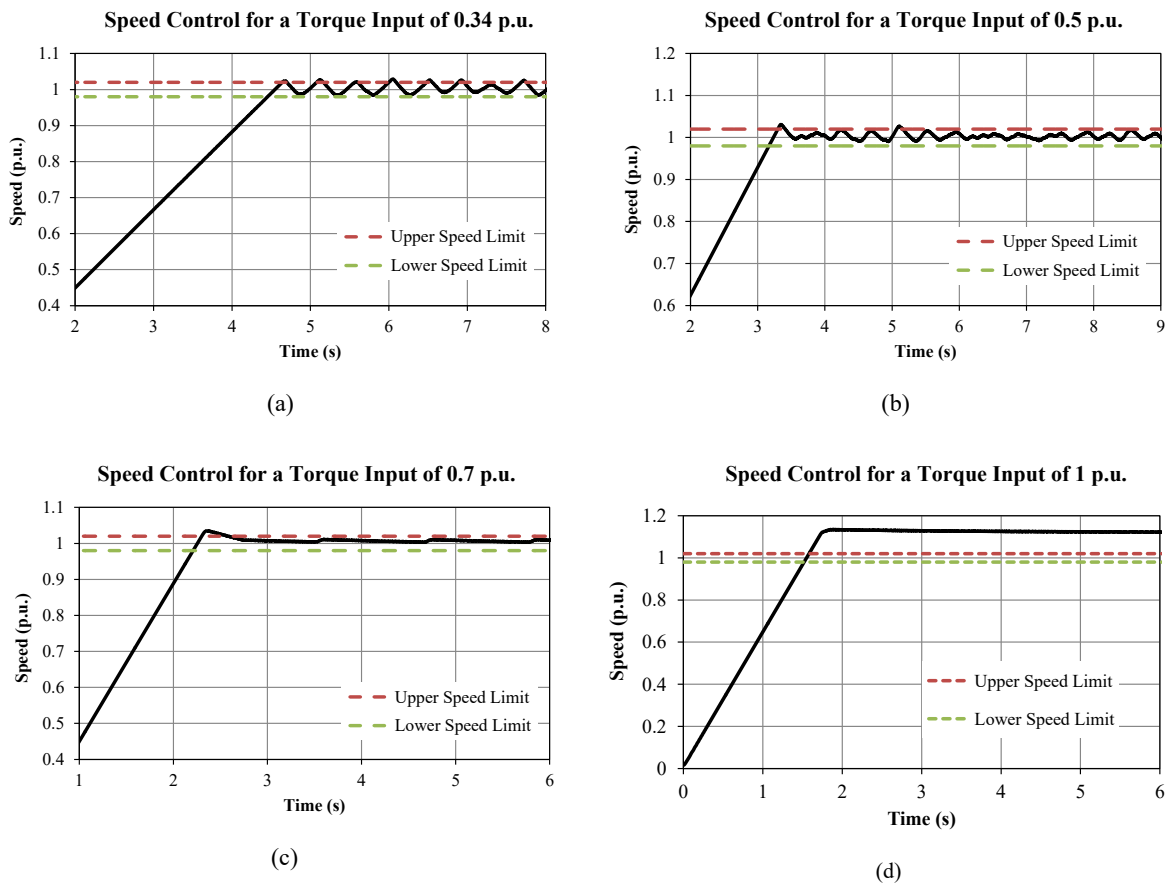


Figure 3.4: Closed-loop speed controller block diagram.

Figure 3.5: Simulated results for the implemented PI-controller for different torque inputs where: $P = 27$, $I = 1$ and $I_{(limit)} = 15\%$

3.2.4 Gain Scheduling

Gain scheduling is a well-known tuning method for controlling nonlinear process. Gain scheduling involves computing linear approximations of the process for different operating points and then tabulating the controller gains as a function of those operating conditions [33]. However, manually tuning and tabulating the resulting controller gains imposes additional complexity towards the overall speed controller design.

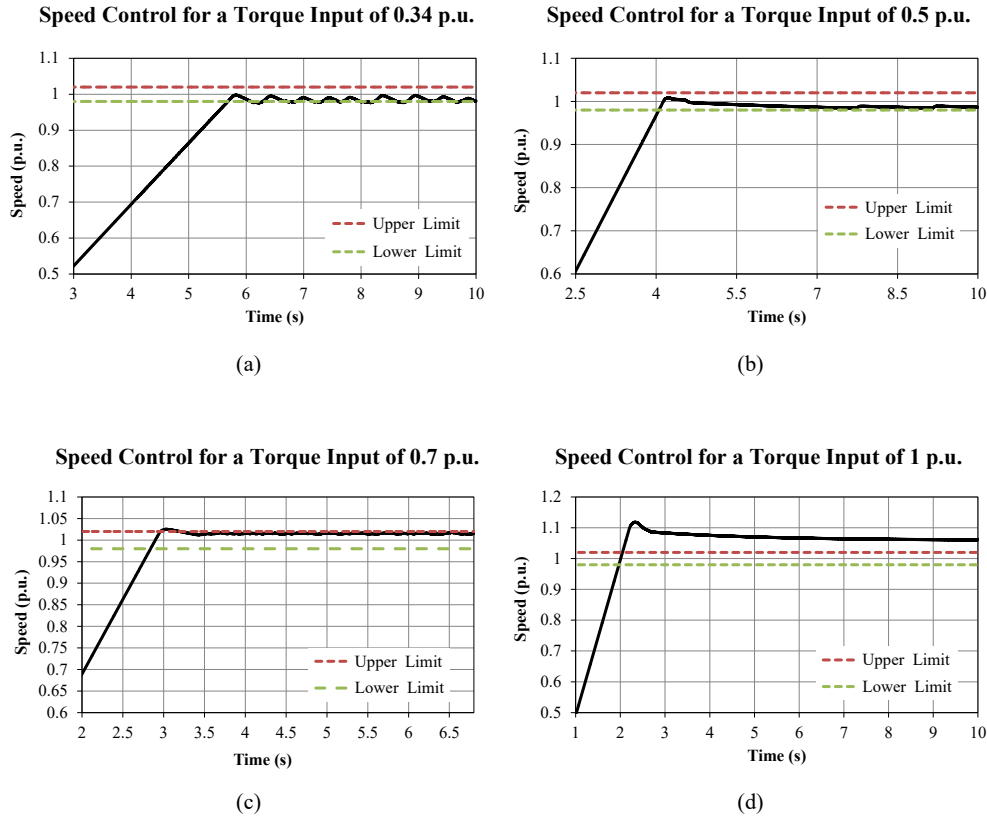


Figure 3.6: Simulated results for the implemented PI-controller for various torque inputs with adjusted controller gains: $P = 54$, $I = 1$ and $I_{(limit)} = 7\%$.

Therefore, this section proposes a simplified gain scheduling PI-controller tuning methodology specifically for the downwind drivetrain. The methodology involves the following steps:

1. Select 3 design operating points where the operating points corresponds to different input torque conditions.
2. Using the dynamic step-test model from Figure 3.1, find the duty cycle values which results in a steady-state error of zero for each respective operating point.
3. Set the integral term limit (I_{limit}) equal to the lowest of the duty cycle values.
4. The proportional gain (P) is determined from the following equation:

$$P = \frac{(d_{c(max)} - d_{c(min)}) \times 40}{(2 \times error)} \quad (3.5)$$

where $d_{c(max)}$ and $d_{c(min)}$ represents the highest and lowest duty cycle values determined in Step 2 and the $error$ term is the maximum allowed steady-state error corresponding to the greatest input torque condition.

For the downwind drivetrain and chopper circuit model the corresponding steps result in:

1. Selected input torque (T) operating conditions:
 - $T = 50 \text{ Nm}$ (0.34 p.u.)
 - $T = 100 \text{ Nm}$ (0.7 p.u.)
 - $T = 145 \text{ Nm}$ (1 p.u.)
2. Duty cycles (d_c) corresponding to the respective input torque conditions:
 - $d_c = 7\%$

- $d_c = 15\%$
 - $d_c = 25\%$
3. The integral limiting term set to prevent against integer windup:
 $\hookrightarrow I_{limit} = 7\%$.
 4. The proportional gain, calculated using (3.5):
 $\hookrightarrow P = 180$, where:
 - $d_{c(min)} = 7\%$,
 - $d_{c(max)} = 25\%$ and,
 - the maximum steady-state error at $T = 145 \text{ Nm}$ is set to 2 Hz.

Figure 3.7 shows the results of the proposed *gain scheduled* PI-controller tuning methodology. The resulting PI-controller is able to control the speed of the downwind drivetrain within the set speed boundaries for the three identified operating points. Figure 3.7(a) still has a degree of oscillation during steady-state however the severity of the oscillations are less pronounced when compared to those of Figures 3.5(a) and Figures 3.6(a). Furthermore, the *gain scheduled* tuning methodology's ability to maintain the downwind drivetrain's speed within the set speed boundaries for relatively high input torque conditions can be attested to the substantially higher proportional gain term, $P = 180$, compared to $P = 27$ and $P = 50$ from Figures 3.5 and 3.6 respectively. In addition, when comparing Figures 3.5, 3.6 and 3.7 the integral limiting term (I_{limit}) is shown to be responsible for the degree of oscillations for relatively low input torque conditions. It is for this reason that the integral limiting term is set equal to the duty cycle value of the lowest input torque condition in step 3 of the proposed tuning methodology as it assures that for low input torque values, the integral term (I) doesn't allow the PI-controller output to force the drivetrain speed into oscillation. Furthermore, the proportional term (P) corresponds to the highest input torque conditions. This ensures that for the highest operating point condition, the value chosen for the allowed steady-state error will provide the necessary proportional gain value for all subsequent operating conditions. It is for this reason that the proposed *gain scheduled* methodology is favourable as it produces a single set of P and I values which are suitable to provide acceptable steady-state performance for each of the three selected operating conditions. This reduces the overall complexity of traditional gain scheduling tuning while maintaining the overall benefits it provides for nonlinear processes.

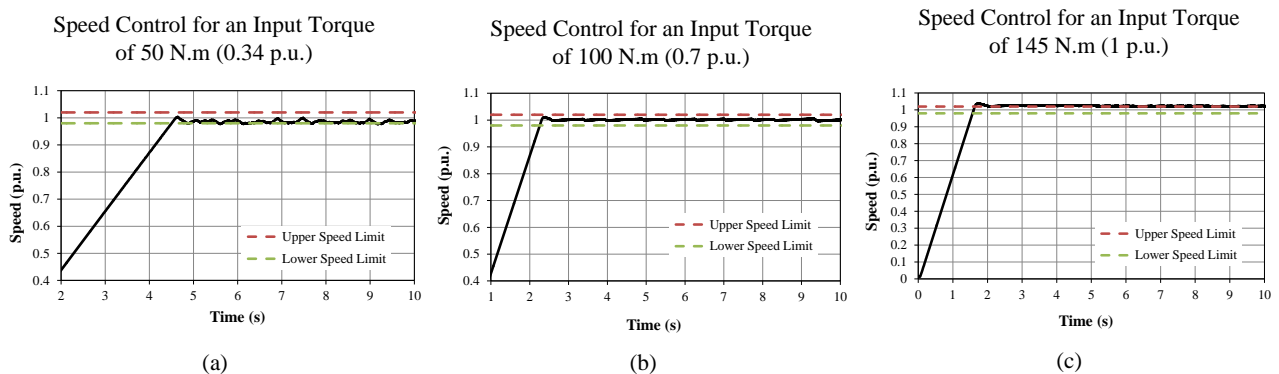


Figure 3.7: Simulated results for the implemented PI-controller for different torque inputs using the proposed *Gain Scheduling* methodology, where: $P = 180$, $I = 1$ and $I_{(limit)} = 7\%$

3.3 Chapter Summary

This chapter provided a methodology for designing the proportional (P) and integral (I) components required for a PI-controller which is to be used to control and maintain the speed of the downwind turbine drivetrain from rest to synchronous speed regardless of wind conditions (input torque). The chapter started by treating the combined downwind turbine drivetrain and dumpload chopper circuit models from Chapter 2 as an unknown *process* for which a first-order plus dead time (FOPDT) model was developed. The FOPDT model was obtained in MATLAB/Simulink by conducting a dynamic step-test on the downwind drivetrain and dumpload chopper circuit models. From this dynamic step-test, the process gain k_p , process time constant τ_p , and process dead time τ_d , were identified. From these parameters, the

consequent P and I parameters were determined by using the Internal Model Control (IMC) tuning rules. The resulting IMC tuned PI-controller was able to control and maintain the downwind drivetrain's speed at synchronous speed for varying input torque conditions. However, the drivetrain's speed displayed significant oscillatory behaviour under relatively low input torque conditions. This was found to be as a result of the integral clamping limiting term's (I_{limit}) contribution towards the controller output. After the integral limiting term's influence on the controller output was reduced, the resulting oscillations at low values of input torque subsided. It was found that when using (3.3), the process gain should be converted to an integral gain k_i . The integral gain is necessary due to the downwind drivetrain's process time constant being significantly larger than its process dead time and consequently a larger proportional gain was required.

Section 3.2.4 provided a solution to some of the deficiencies of IMC tuning in the form of a proposed *gain scheduled* tuning methodology. Unlike traditional gain scheduled tuning, which provides different proportional (P) and integral (I) gains for different process operating conditions, the proposed tuning methodology produced a single set of (P) and (I) gains which proved acceptable for each of the three identified operating conditions. The resulting PI-controller was able to control the speed of the downwind drivetrain within the the set speed boundary conditions for each of the identified operating conditions while minimizing steady-state oscillations for low input torque conditions. However, the *gain scheduling* method heavily relies on the accuracy of the simulated model and requires a degree of trial and error in order to determine the P and I terms required for speed control across all input torque conditions.

Chapter 4

Grid Connection and On-Grid Dynamic Performance

This chapter focuses on connecting the simulated, PI-controlled downwind turbine model to a 400 V, 50 Hz three-phase grid. Furthermore, this chapter investigates the consequences of not adhering to the recommended synchronization conditions as outlined in Table 1.1. Additionally, once grid connected, the dynamic performance of the downwind turbine model is investigated when subjected to various turbulent wind conditions.

4.1 Grid Connection

Figure 4.1 shows a simplified line diagram of the downwind turbine drivetrain and dumpload chopper circuit. The process of connecting the downwind turbine to the grid involves allowing the turbine to accelerate under the influence of the wind. During this time, the grid connection contactor (S_1) is open while the dumpload chopper circuit contactor (S_2) remains closed. The IGBT switch, however, only activates once the downwind turbine's speed is near synchronous speed. In other words, the dumpload is not connected to the generator terminals and the generator is consequently operating under no-load (open-circuit) conditions. Under no-load conditions, the generator will continue accelerating until it approaches synchronous speed. The grid connection controller (GCC) will only initiate speed control once the speed of the generator is near synchronous speed. As mentioned in previous chapters, speed control involves comparing the speed (in Hz) of the generator to the frequency of the grid. The difference in frequency is the error signal the PI-controller uses to control the IGBT in the dumpload chopper circuit which in turn controls and maintains the turbine speed within the set speed limits. Once the turbine's speed is at steady-state, the (GCC) compares the voltages of both the generator and the grid to the grid-synchronisation code outlined in Section 1.4 before disconnecting the dumpload chopper circuit (opening S_2) from the generator terminals and connecting the generator to the grid (closing S_1).

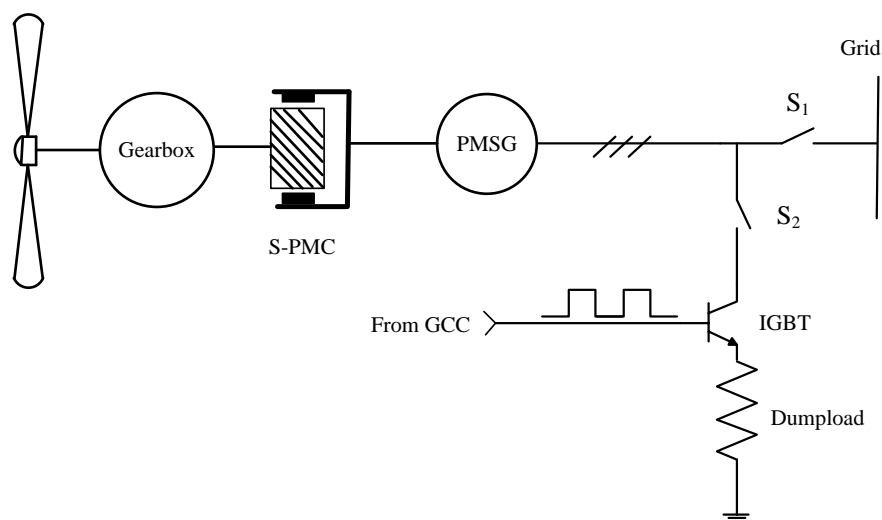


Figure 4.1: Simplified line diagram showing the downwind turbine drivetrain and dumpload chopper circuit.

The recommended grid synchronization conditions that all oncoming generators must adhere to prior to connecting to a power network was detailed in Section 1.4 and those conditions pertaining to smaller-scale wind turbines are repeated below:

1. $\Delta\phi < 20^\circ$
2. $\Delta V < 10\%$
3. $\Delta f < 0.3$ Hz

where $\Delta\phi$, ΔV , and Δf , represents the respective difference in: voltage phase angle, per-phase voltage magnitude, and frequency between the grid and generator prior to grid connection. Furthermore, Figure 4.2 shows a flow diagram representation of the grid connection procedure where, $|\Delta f_s|$, $|\Delta\phi_s|$, and $|\Delta V_s|$ represents the absolute tolerance allowed for each of the respective frequency, voltage phase angle and per-phase voltage magnitude difference between the grid and generator prior to grid connection.

Put into words, the grid connection algorithm monitors and waits for the wind-turbine generator to speed up until it reaches synchronous speed. Once the generator's speed enters the lower speed limit, the speed controller activates in order to slow down the generator's acceleration and eventually force the speed into a steady-state condition within the set upper and lower speed limits. Once in steady-state, the grid connection methodology shown in Figure 4.2 becomes active. The grid connection controller (GCC) will only connect the generator to the grid once all three synchronising conditions are adhered to.

Figure 4.3 shows a visual representation of all three synchronisation conditions in which prior to grid connection, at time $3.12 \leq t \leq 3.128$ seconds, the respective generator and grid phase voltages are in phase, $\Delta\phi \simeq 0^\circ$, the difference in magnitude between the generator and grid's phase voltages is within specification, $\Delta V < 10\%$ and the the difference in frequency between the generator and grid is less than than the tolerance limit, i.e., $\Delta f < 0.3$ Hz.

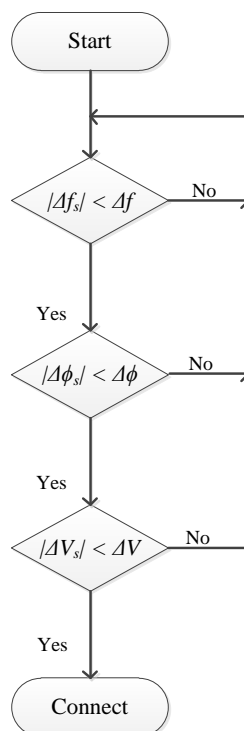


Figure 4.2: Flow diagram representation of the methodology used to determine whether or not the oncoming generator can be connected to the grid.

4.2 Grid Synchronization Parameters

The grid synchronization parameters and their respective tolerance limits must be adhered to in order to ensure a safe and stable connection to the grid. The magnitude of the peak transient currents that flow in the moments just after grid connection are directly proportional to the values of $\Delta\phi$, ΔV , and Δf

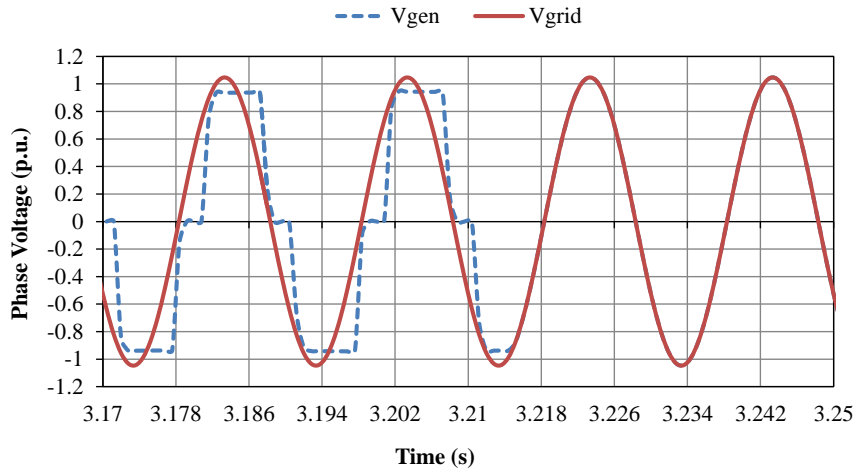


Figure 4.3: Simulated downwind turbine generator (V_{gen}) and grid (V_{grid}) phase voltage prior to and after grid connection where grid connection occurs at time $t = 3.215$ seconds

prior to grid connection. This section will illustrate the consequences of not adhering to the tolerance limits set in the grid-synchronisation code.

4.2.1 Voltage Phase Angle Difference

If the respective generator and grid voltage waveforms are approximated as sinusoidal waves, the difference in voltage phase angle can be defined as the relative displacement between the two waveforms or; the time interval by which one waveform leads by or lags the other waveform.

Figure 4.3 shows the distorting effect the diode rectifier has on the generator voltage waveform. As a result, determining the precise phase angle of the generator voltage waveform from its frequency (determined using the method of zero-crossings) is a challenging process. However, the effect of varying the voltage phase angle tolerance limit ($\Delta\phi_s$) prior to grid connection on the magnitude and stability of the resulting grid current will be illustrated using simulation results.

Figure 4.4 shows the effect that varying the voltage phase angle tolerance limit ($\Delta\phi_s$) has on the resulting grid current after grid connection for a constant input torque of 100 Nm. Figure 4.4(a) shows the ideal scenario where $\Delta\phi_s = \Delta\phi \simeq 0^\circ$. The resulting current shows a peak magnitude of just under 2.5 p.u. Furthermore, Figures 4.4(b) and (c) depict scenarios where the difference in voltage phase angles ($\Delta\phi$) between the grid and generator are 43.2° and 68.4° respectively. For the case where $\Delta\phi_s = \Delta\phi \simeq 43.2^\circ$, the resulting peak current magnitude is just under 3 p.u. whereas for the case where $\Delta\phi_s = \Delta\phi \simeq 63.4^\circ$, the resulting peak current magnitude is substantially greater than that of Figures 4.4(a) and (b) where the peak current magnitude is nearly 6 p.u. It is clear from Figure 4.4 that the difference in phase angle between the generator and the grid should be kept well within the recommended tolerance limit of $\Delta\phi_s = 20^\circ$ in order to prevent excessive peak magnitude grid-connected currents.

4.2.2 Frequency and Phase Voltage Difference

The effect of varying Δf while keeping $\Delta\phi \simeq 0$ is shown in Figure 4.5. Figures 4.4(a) and 4.5(a) show the results from the same simulation where the recommended synchronisation conditions of Table 1.1 were adhered to. Furthermore, Figures 4.5(b) and (c) follow a similar trend to that of figures 4.4(b) and (c) where the peak magnitude of the grid current increases as the difference in frequency tolerance limit increases. Additionally, Figure 4.5(c) shows a condition where the frequency-difference-tolerance limit was severely reduced and where the speed controller had not yet been activated which resulted in an extra current transient (between time $2.05 \leq t \leq 2.15$) with a peak value of 3.56 p.u. before settling at a steady-state value.

The open-circuit terminal voltage of a permanent magnet synchronous generator is purely a function of frequency. Consequently, it is not possible to vary the phase voltage magnitude of the generator as it has been designed to produce a certain rms voltage at a specific frequency. However, Figure 4.5 shows the importance of the tolerance limits placed on the generator frequency prior to grid connection. Furthermore, the resulting grid currents' magnitude is directly proportional to the tolerance limit. As

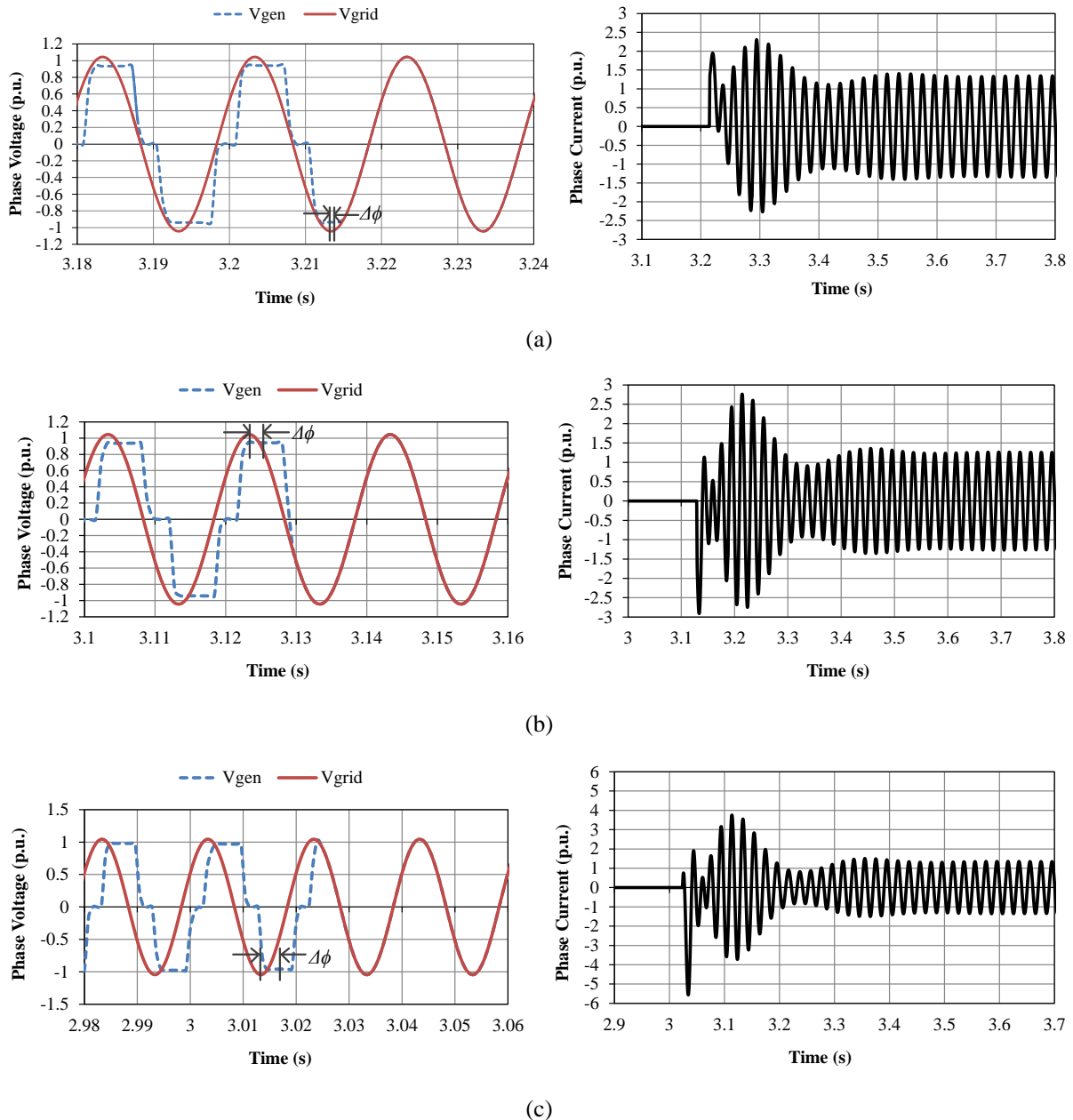


Figure 4.4: Simulated grid current response for varying voltage-phase-angle differences conditions prior to grid connection where in (a) $\Delta\phi \simeq 0^\circ$, (b) $\Delta\phi \simeq 43.2^\circ$ and (c) $\Delta\phi \simeq 68.4^\circ$

a result, in order to ensure safe and stable grid connection, the difference in frequency between the generator and the grid should be kept at a minimum.

4.2.3 Transient Grid-Connection Currents

From a safety point of view, the post-grid-connection current magnitude should be kept as low as possible. In order to provide perspective regarding the current magnitudes resulting from grid connection, the grid currents will be assumed to be as a result of three-phase fault at the terminals of the generator. This assumption is plausible as at the moment of grid connection, the effective load on the generator (the dumpload resistor) is assumed to be greater than the load imposed by the grid, which is ideally regarded to have negligible impedance. The official South African grid code does not cater to low-voltage (LV) generating units however guidelines for small-scale embedded generating (SSEG) units are provided in [34]. From [34], under the section pertaining "Protection equipment" (Section A.7); the fault level contribution of the SSEG will not exceed the ratings of circuit-breakers installed in the system. However, if the SSEG fault level contribution is unavailable then in the case of synchronous generators, the fault

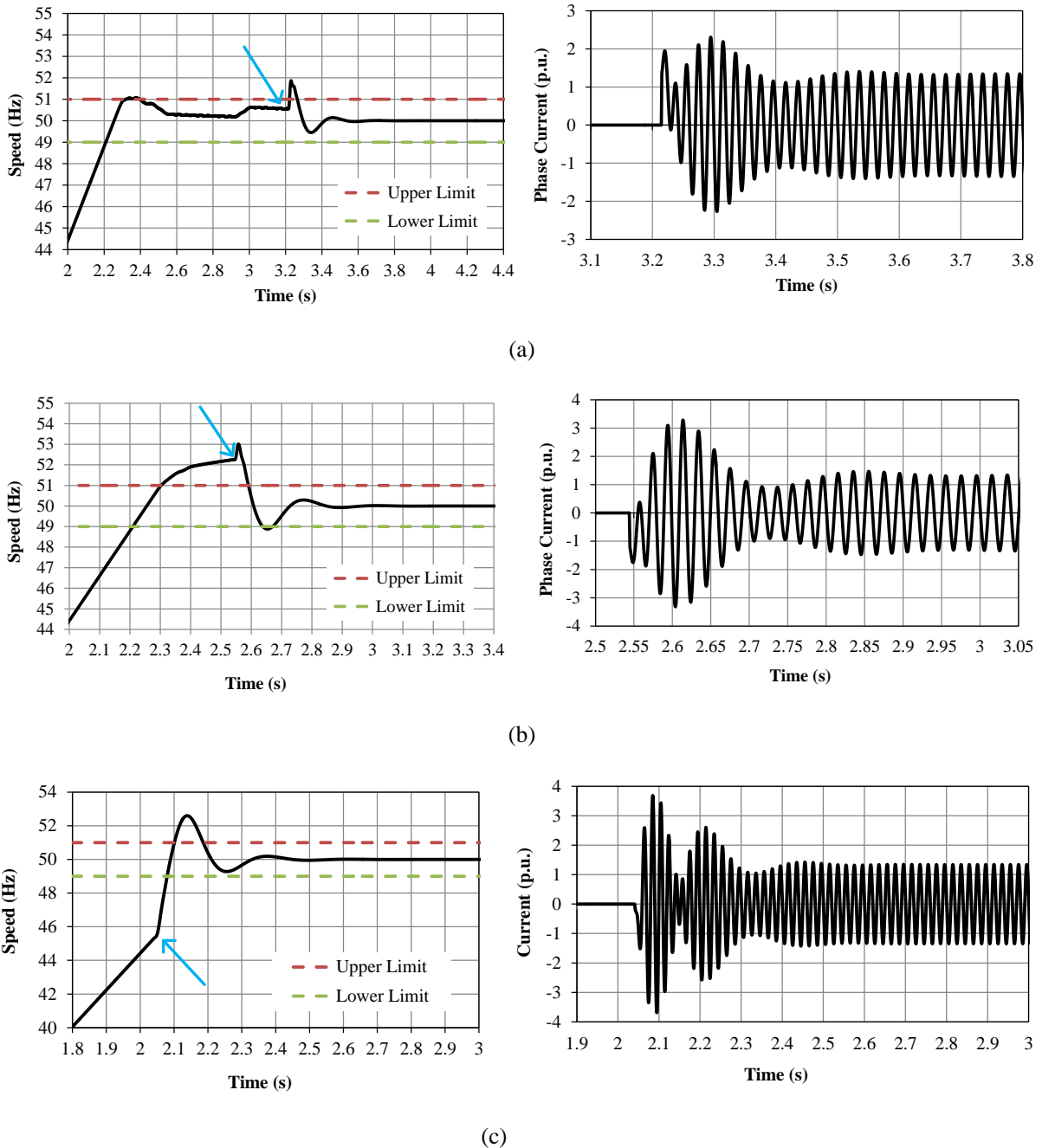


Figure 4.5: Simulated grid current response for varying difference-in-frequency conditions where (a) $\Delta f \simeq 0.5$ Hz, (b) $\Delta f \simeq 2.5$ Hz and (c) $\Delta f \simeq 5$ Hz. Grid connection is indicated by the arrow.

current contribution must not exceed eight times the rated current (8 p.u.) of the generator.

It is clear from Figures 4.4 and 4.5 that the grid-connection current produced by downwind-turbine generator falls well within the 8 p.u. suggested limit and is thus eligible to connect to the grid provided that a suitably rated circuit-breaker is installed at point of utility connection (PUC). However, the GCC is programmed to disconnect the wind turbine from the grid should the transient grid-connection currents exceed 4 p.u.

4.3 On-Grid Dynamic Performance

An important aspect of any wind turbine system is its ability to remain stable under varying wind conditions while providing an acceptable level of power quality to the grid. In this chapter, the downwind turbine simulation model developed in Chapter 2 is altered such that the downwind turbine is now already

grid connected and its performance pertaining to turbulent wind conditions is investigated. Consequently, the PI speed controller and the grid connection controller (GCC) model isn't used in the proceeding simulations.

Figure 4.6 shows an altered block diagram representation of the downwind turbine. From Figure 4.6, the input to the the simulation model is the wind speed (v_w), which along with the turbine rotational speed (ω_t), are fed into a function generator (FG) which provides the aerodynamic torque (τ_t) provided by the turbine using the turbine's torque-speed curves from Figure 2.8. Additionally, the three-phase grid voltages (v_{abc}) are transformed to v_{dq} by means of the Park Transformation K_p . The input to the permanent magnet synchronous generator (PMSG) is the electrical speed, $\omega_e = \omega_m \cdot \frac{p}{2}$, (in rad/s) where p represents the number of generator poles and ω_m represents the mechanical shaft speed (in rad/s). Furthermore, the outputs of the PMSG model are its dq -equivalent currents i_{dq} and the electromagnetic counter torque (τ_s) produced by the PMSG. The output to the simulation model are the grid currents, i_{abc} , which are calculated by means of the Inverse Park Transform K_p^{-1} .

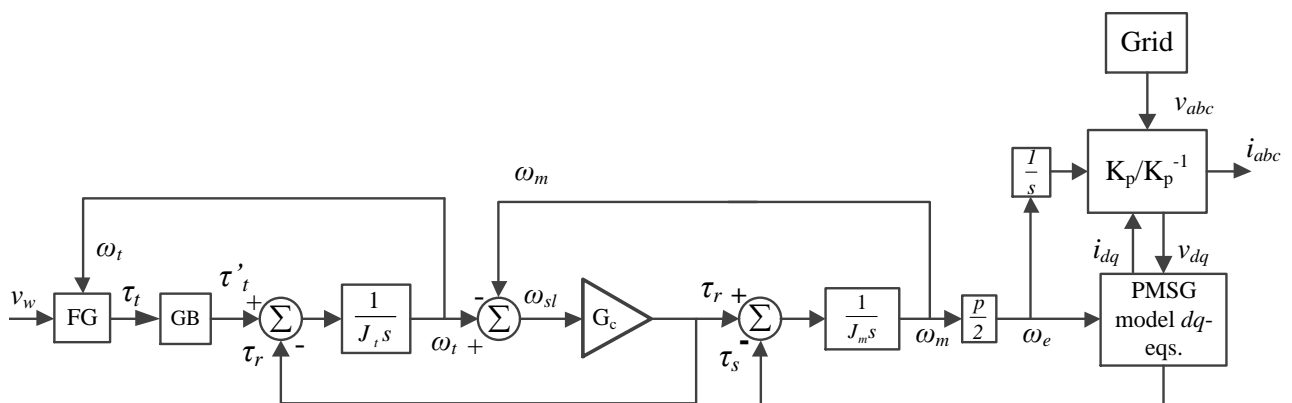


Figure 4.6: Block diagram representation of the grid connected downwind turbine.

4.3.1 Transient Turbine Torque Conditions

Transient turbine conditions refer to the torque response of the downwind turbine due to varying wind conditions. In Figure 4.7(a) the transient response of the stator counter torque, τ_s , is shown for a step in turbine torque from 0 to 1 p.u. (which represents a step in wind speed from 0 to 12 meters per second) and Figure 4.7(b) shows the resulting current response. Furthermore, Figure 4.8(a) and (b) shows the respective rotor speed and power angle responses for the 1 p.u. step in turbine torque. Such a server change in wind conditions will seldom occur in nature but Figures 4.7 and 4.8 show the inherent stability of the grid-connected downwind turbine system.

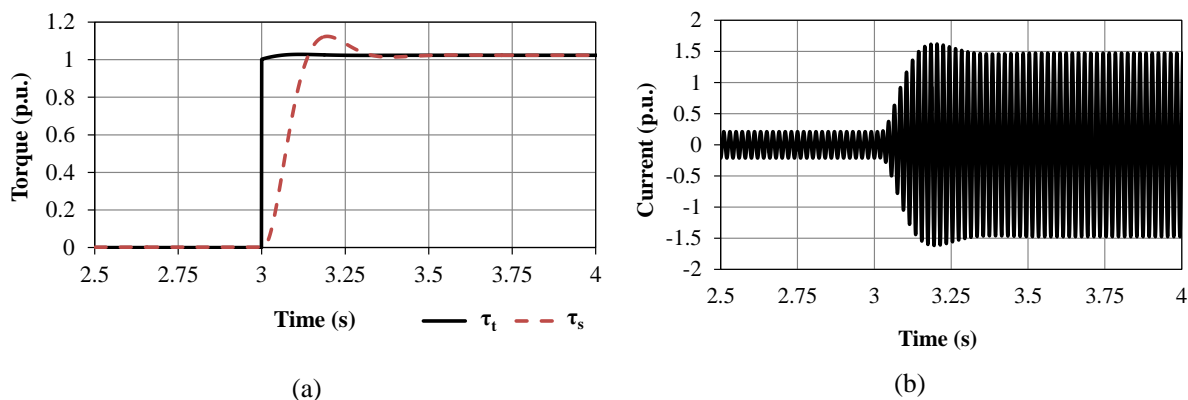


Figure 4.7: Simulated turbine torque response (a) and current response (b) for a 0 to 1 p.u. step in turbine torque.

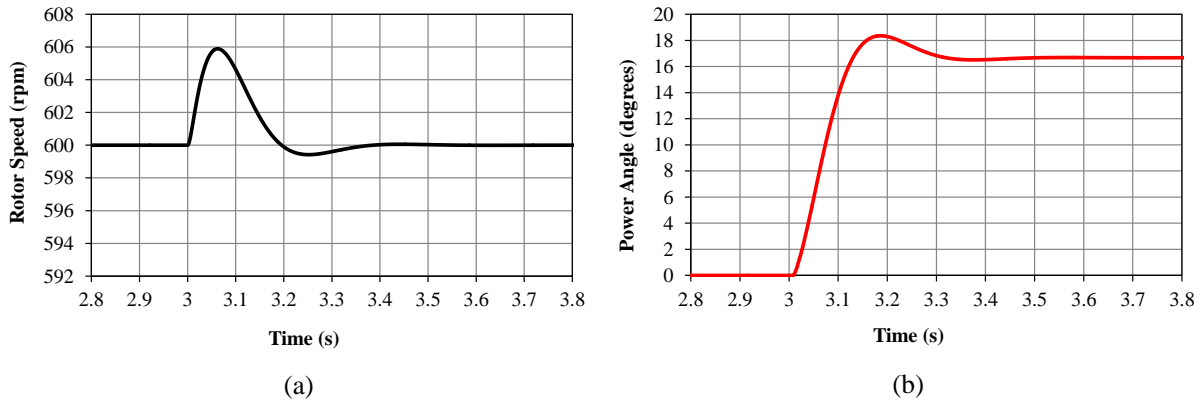


Figure 4.8: Simulated rotor speed response (generator side) (a) and power angle response (b) for a 0 to 1 p.u. step in turbine torque.

4.3.2 Turbine Pulsations and Bandwidth

As mentioned in Section 1.5, the power produced by wind turbines under continuous operation are subjected to periodic pulsations around a certain frequency with the largest of these fluctuations occurring as a result of the tower shadow effect. The tower shadow effect is as a result of the disruption in airflow due to the tower. Furthermore, each time one of the turbine blades passed in front of the tower, the disrupted airflow causes a fluctuation in the mechanical torque produced by the blade. The tower shadow effect is dependant on the rotational speed of the turbine with the rotational frequency of the wind turbine (in Hz) defined by

$$f_t = \frac{n_t}{60}, \quad (4.1)$$

where n_t is the rotational speed of the turbine in revolutions per minute (rpm). Furthermore, any disturbances to the wind speed experienced by the turbine blades will generate torque pulsation frequencies of nf_t where n is the harmonic order of the frequency component. As a result, for a three-bladed wind turbine, the torque pulsations caused by tower shadow will occur at $n = 3$. Additionally, the torque pulsations due to wind sheer occur at $n = 1$. For the downwind turbine, with a rotational frequency of $f_t = \frac{150}{60} = 2.5$ Hz, the respective torque pulsations due to wind sheer and tower shadow occur at frequencies of 2.5 Hz and 7.5 Hz.

In Figure 4.9 the bandwidth of the grid-connected downwind turbine is shown where the input is the turbine torque (low-speed side) τ'_t and the output is the generator counter torque τ_s . From Figure 4.9, the bandwidth of the downwind turbine is roughly 4 Hz. Figure 4.10 shows what effect a turbine torque input with a frequency of 8 Hz and a peak-to-peak amplitude of 2.5 Nm ($\simeq 10$ Nm on the low-speed side of the gearbox) has on the grid current. From Figure 4.10, it can be seen that the 8 Hz torque pulsation is substantially attenuated by the downwind turbine and as a result has little to no effect on the grid current. The peak-to-peak amplitude of 2.5 Nm was chosen due to the fact that the peak-to-peak tower shadow-induced power fluctuations can be up to 10% of the average input torque value for downwind turbines [35]. Additionally, Figure 4.11 shows what effect a turbine torque input with a frequency of 2.5 Hz and a peak-to-peak amplitude of 0.45 Nm has on the grid current response. The value of 0.45 Nm for the peak-to-peak amplitude of the torque input was chosen due to the minimal contribution (around 1%) wind sheer has on the overall fluctuations caused by $3f_t$ frequency [36]. Figure 4.11(a) shows the minimal influence that the wind sheer effect has on the grid current. However, Figure 4.11(b) shows the downwind turbine's inability to attenuate the 2.5 Hz torque input due to the fact that the wind sheer frequency component of 2.5 Hz is lower than the downwind turbine's bandwidth and as a result, the full magnitude of the 2.5 Hz fluctuation is transmitted to the generator.

Nevertheless, both Figures 4.10 and 4.11 show that the respective effects of tower shadow and wind sheer have no significant bearing on the grid current and consequently, any concerns regarding voltage flickering are mitigated.

4.3.3 Grid Disturbances

Grid disturbances refer to variations in grid frequency and voltage. Two common grid disturbances are sudden variations in voltage at the point of connection (POC) between the wind turbine and the grid

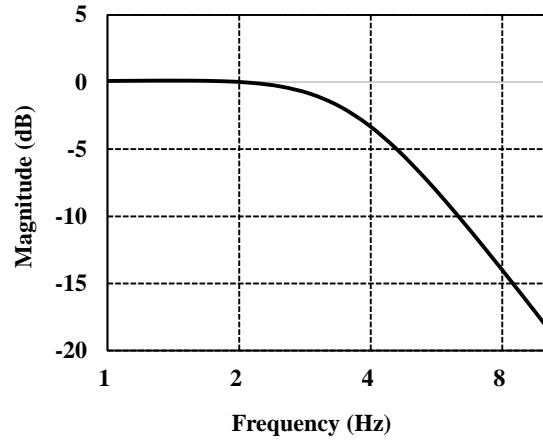


Figure 4.9: Simulated frequency response of τ_s/τ_t' for the 2.2 kW downwind turbine.

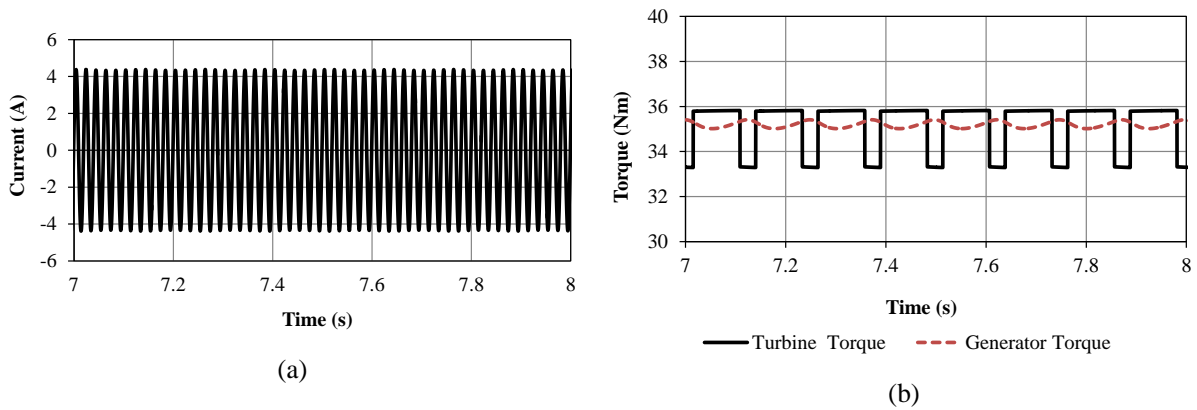


Figure 4.10: Simulated grid current response (a) for an input turbine torque with an 8 Hz frequency component and a peak-to-peak amplitude of 2.5 Nm which models the effect of tower shadow on turbine and generator torque (b).

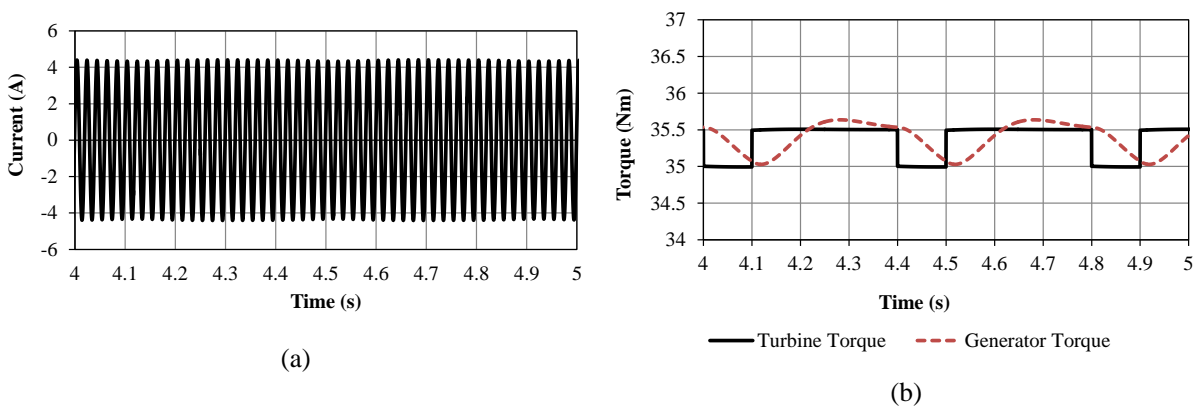


Figure 4.11: Simulated grid current response (a) for an input turbine torque with a 2.5 Hz frequency component and a peak-to-peak amplitude of 0.5 Nm which models the effect of wind shear on turbine and generator torque (b).

as well as sudden grid frequency variations. Figure 4.12 shows the rules and guidelines, as stated in [37], pertaining to the low voltage ride through capabilities of renewable power plants (RPP) with a generating capacity of 0 - 13.8 KVA (Category A1). Figure 4.12 shows that wind turbines which fall in Category A1 should remain grid connected in the event where the grid voltage falls by 15% or rises by 10%. Furthermore, Table 4.1 shows the respective maximum disconnection times for RPP of Category A1 for different voltage ranges at the POC.

Figure 4.13(a) shows a simulated LVRT condition as stated in [37] as well as, (b), the effect on the grid current. Figure 4.13(b) shows the grid current as a result of a momentary 15% drop in grid voltage followed by a rise in grid voltage from 0.85 p.u. to 1.1 p.u. It can be seen that the simulated downwind turbine grid current remains stable with short-lived transients at the moments when the grid voltage changes. Furthermore, the simulated downwind turbine is able to remain within the continuous operating range as shown in Figure 4.12.

Table 4.1: Maximum disconnection times for Renewable Power Plants (RPPS) of Categories A1 [37].

Voltage range at POC	Maximum trip time [Seconds]
$V < 50\%$	0.2 s
$50\% \leq V < 85\%$	2 s
$85\% \leq V < 110\%$	Continuous operation
$110\% < V < 120\%$	2 s
$120\% \leq V$	0.16 s

All wind turbines should remain grid connected should the grid frequency vary between 49 Hz - 51 Hz. In other words, wind turbine generators should remain grid connected in the event where the grid frequency varies by ± 1 Hz. Moreover, wind turbines are required to remain grid connected during rate of change of frequency values up to and including 1.5 Hz per second, provided the grid frequency is still within operating range range of 49 Hz - 51 Hz [37]. However, wind turbines are required to disconnect from the grid in the event where the grid frequency is higher than 52 Hz for longer than 4 seconds or when the grid frequency is less than 47 Hz for longer than 200 milliseconds [37].

Figure 4.14 shows the respective speed responses of the turbine and the PM-rotor as a result of a change in grid frequency from 50 Hz to 49 Hz at a rate of 1.5 Hz per second as specified in [37]. The grid frequency (in Hz) was converted to an equivalent radians per second value using $\omega_s = 2\pi f_s \times \frac{p}{2}$ for comparison purposes. Figure 4.14 shows no oscillatory behaviour for a 1.5 Hz per second change in grid frequency.

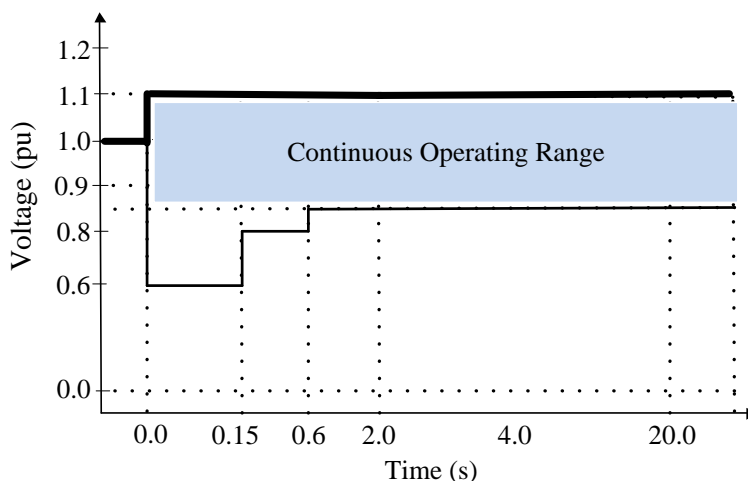
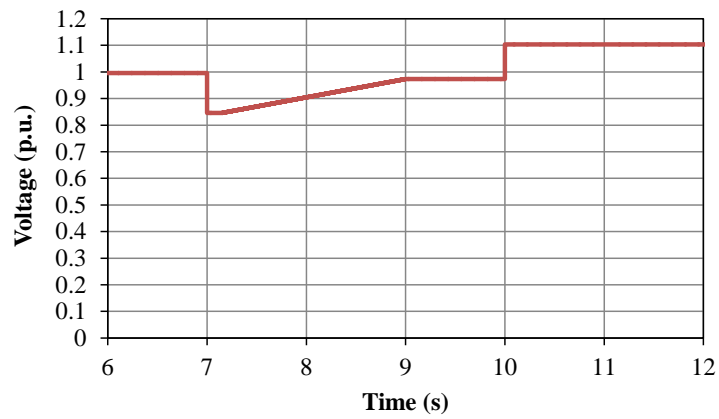
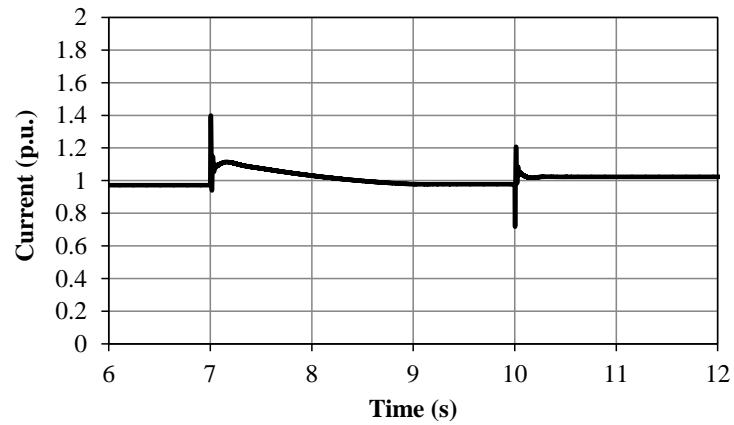


Figure 4.12: Low voltage ride through (LVRT) specifications for wind turbines with a power rating of 0 - 13.8 kVA as per [37].



(a)



(b)

Figure 4.13: Simulated (a) Low voltage ride through (LVRT) condition as per [37] and (b) its effects on the grid current.

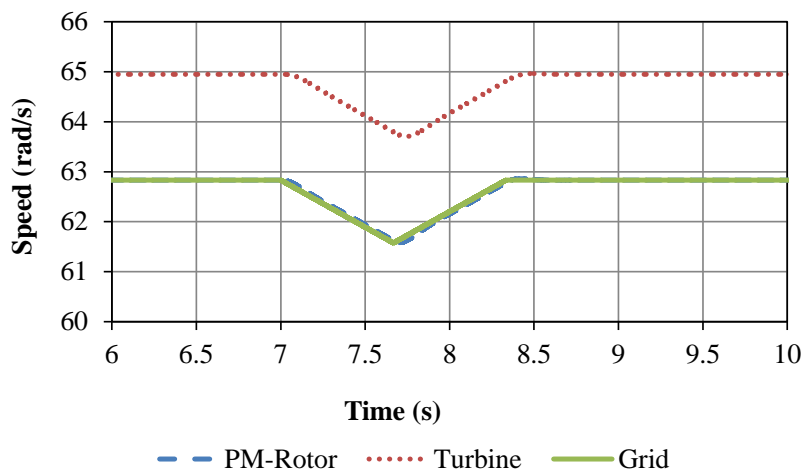


Figure 4.14: Simulated turbine and PM-rotor mechanical speeds (ω_t and ω_m) as a result of a 1.5 Hz per second change in grid frequency where the grid speed is given as $\omega_s = 2\pi f_s \times \frac{p}{2}$.

Chapter 5

Laboratory Results

In this chapter, the 2.2 kW downwind turbine drivetrain is placed on a mechanical test bench and its dynamic performance is evaluated. Furthermore, the grid connection controller's (GCC) ability to provide speed control under various torque conditions is also evaluated. Additionally, the GCC's ability to connect the downwind turbine drivetrain to the grid under varying torque condition is also tested. Finally, once grid connected, the downwind turbine drivetrain's on-grid stability is evaluated.

5.1 Laboratory Test Setup

Figure 5.1 shows a top level schematic of the laboratory wherein the practical evaluation and testing of the downwind turbine drivetrain was performed. From Figure 5.1, the wind turbine blades are replaced by a 5.5 kW geared induction motor (IM) driven by an Allen-Bradley *powerflex* 700 variable speed drive (VSD). The VSD can be set to regulate the torque produced by the IM which in-turn acts as the torque input to the downwind turbine drivetrain. It should be noted that the torque provided by the VSD-IM combination is markedly different from the torque provided by turbine blades. That is to say, the torque provided by wind turbine blades is highly dependent on rotational speed whereas the the VSD-IM combination is able to produce a relatively instantaneous torque output from zero to rated torque. In other words, the VSD-IM combination is able to produce faster rates of acceleration than what would be expected in field tests.

A *Lorenz* DR-300 in-line torque sensor is placed between the VSD-IM combination and the downwind drivetrain gearbox (GB) and is used to measure and record the torque input provided to the downwind drivetrain. Additionally, the torque sensor is also able to measure and record the drivetrain's rotational speed. Moreover, the dotted arrows shown in Figure 5.1 represents points of measurement which include measurements of both the generator's and grid's respective phase voltages as well as the current produced by the permanent magnet synchronous generator (PMSG).

Finally, the laboratory is supplied by a 1 MVA distribution transformer. The VSD and PMSG (when grid connected) forms a feedback loop as both are connected to the same distribution transformer. This feedback loop has the potential to produce unwanted effects with regards to the measurements however it is assumed that the electrical network is sufficiently stiff such that any undesired effects can be regarded as negligible.

Figure 5.2 (a) shows a side-on view of the 2.2 kW downwind turbine drivetrain on a mechanical test bench and (b) shows a front-on view of the 2.2 kW downwind turbine drivetrain which includes the dumpload and GCC. The "inertia disk" shown in Figure 5.2 is used to provide additional inertia to the drivetrain. The inertia disk was designed to replicate the inertia of the wind turbine blades (between 5 kg·m² and 8 kg·m²) which are estimated to be substantially greater than that of the drive IM ($\simeq 0.03$ kg·m²).

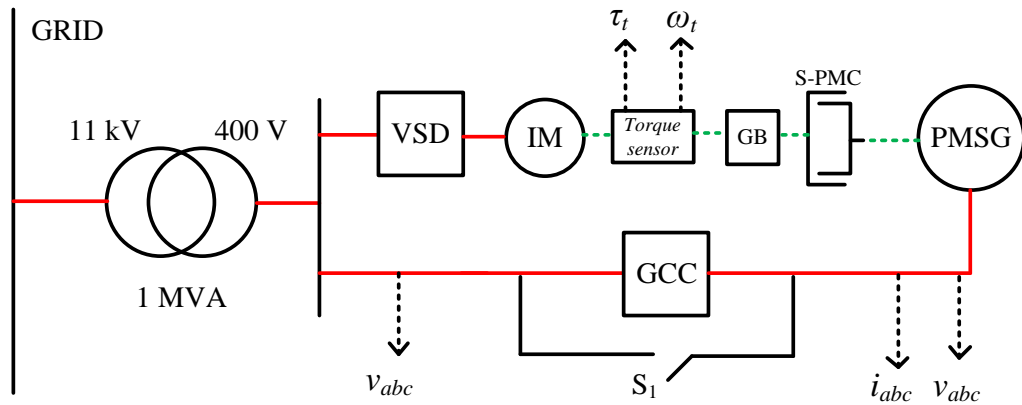


Figure 5.1: Top level schematic of the downwind turbine drivetrain testing setup. The solid red lines indicate electrical connections and the dotted green connections represent mechanical connections.

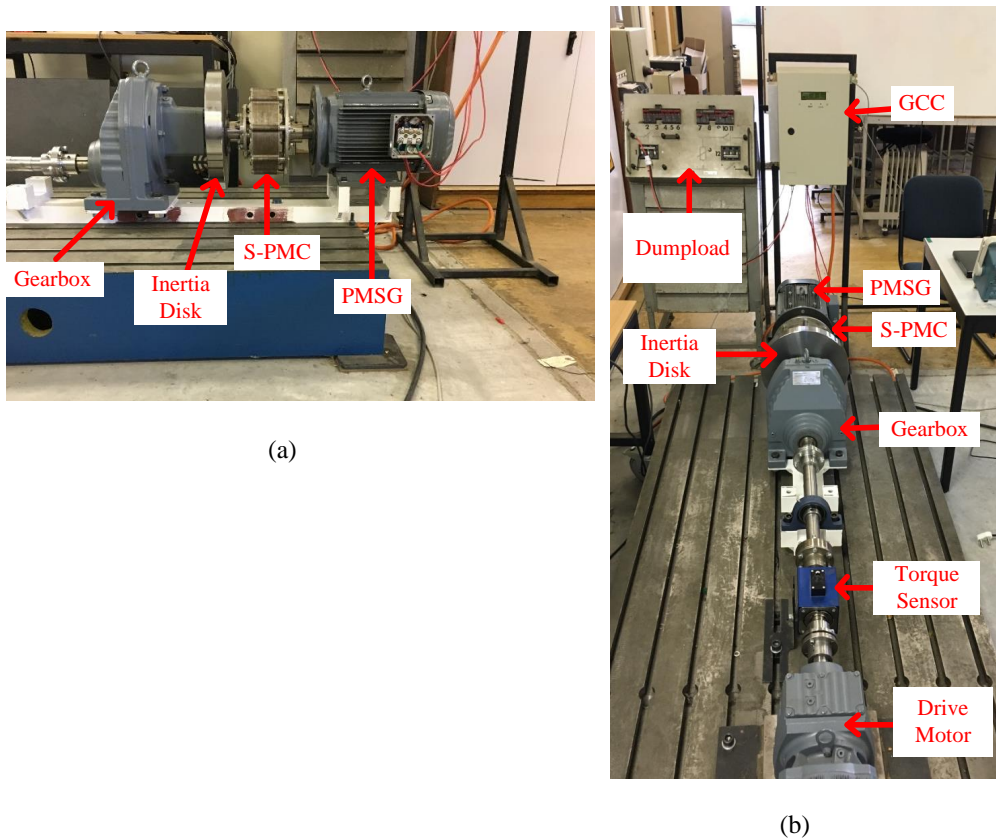


Figure 5.2: Figure showing (a) a side view of the 2.2 kW downwind turbine drivetrain on test bench and (b) a front view of the 2.2 kW downwind turbine drivetrain which includes the dumpload and GCC.

5.2 Dynamic Step-Test

Figure 5.3 shows the results of an initial laboratory test where the outcome was to identify the relationship between duty cycle and drivetrain speed for a fixed torque input. Two tests were performed where a fixed torque input of 30 Nm (0.21 p.u.) and 50 Nm (0.34 p.u.) respectively was supplied to the drivetrain by the VSD and IM. During these initial tests, the dumpload resistor was arbitrarily set to 4 Ω and the duty

cycle to the dumpload chopper circuit was varied and the resulting drivetrain speed was measured and recorded. The relationship between duty cycle and speed is shown to be highly nonlinear. However, as shown in Figure 5.3, the accuracy of the simulated test for both (a) and (b) closely correlate to the same tests performed on the mechanical test bench. It can be seen that the simulated speed response closely matches that of the actual speed response of the downwind drivetrain for duty cycle values greater than 6% for an input torque of 30 Nm and for duty cycle values greater than 10% for an input torque of 50 Nm. From this test, it is clear that the simulation model's accuracy decreases for low values of duty cycle for any given value of torque input. This is problematic in the sense that low values of duty cycle are required to provide sufficient speed control at rated speed. However, it was found that increasing the value of the dumpload resistor resulted in an overall increase in duty cycle values required to provide speed control at rated speed. It is for this reason that the dumpload resistor value was increased to 20 Ω . However, due to time constraints, a comprehensive study of the relationship between dumpload resistor value and duty versus speed for a given torque input could not be conducted.

The simulated dynamic step-test of section 3.1.1 was replicated on the mechanical test bench setup in order to identify the actual dynamics of the downwind drivetrain as well as to further verify the accuracy of the simulation model. Figure 5.4 shows a schematic of the dynamic step-test replicated in the laboratory. The VSD is initially programmed to provide a fixed, 100 Nm torque input to the drivetrain while the duty cycle of the GCC is manually set at 30%. Due to the fixed 100 Nm torque input, the downwind drivetrain initially accelerates before settling at a steady-state speed due to the counter-torque by the produced by the generator as a result of the dumpload chopper circuit. Once the drivetrain has reached a steady-state speed, the duty cycle is stepped down to 15% which in turn causes the drivetrain to accelerate before settling at a new steady-state speed. Figure 5.5 shows the results of the practically implemented dynamic step-test with the simulated response from section 3.1.1 included for comparison purposes. Figure 5.5 illustrates the accuracy of the downwind turbine simulation model. The simulated and practical dynamic step responses are near identical bar a slight deviation during the time interval prior to the step down in duty cycle. Consequently, the actual downwind drivetrain's transfer function $G(s)$ is shown to be the same as the simulated transfer function identified in section 3.1.2

$$G(s) = \frac{0.03667e^{-0.02s}}{2s + 1}, \quad (5.1)$$

where the process gain is $k_p = 0.03667$, the process time constant is $\tau_p = 2$ (seconds) and the drivetrain dead time is $\tau_d = 0.02$ (seconds).

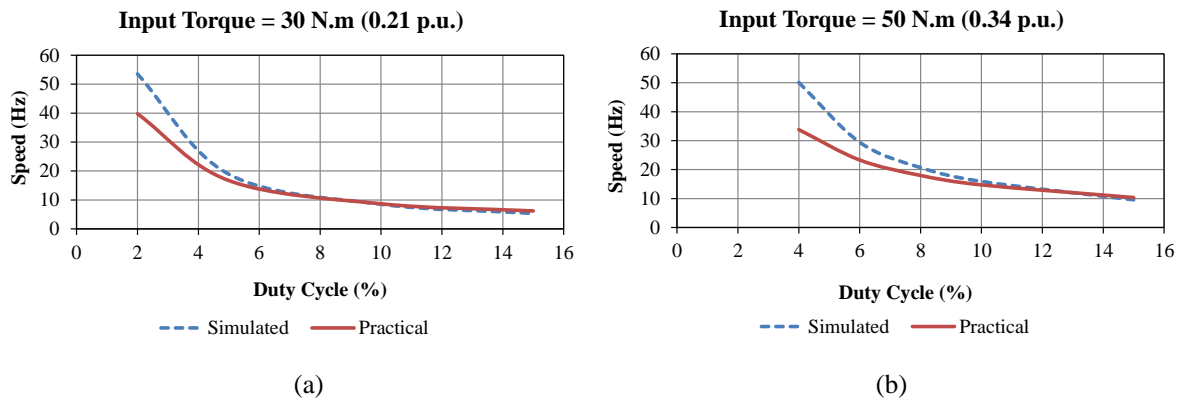


Figure 5.3: Results of a test to identify the relation between duty cycle and drivetrain speed for a fixed input torque of (a) 20 Nm (p.u.) and (b) 50 Nm (0.34 p.u.).

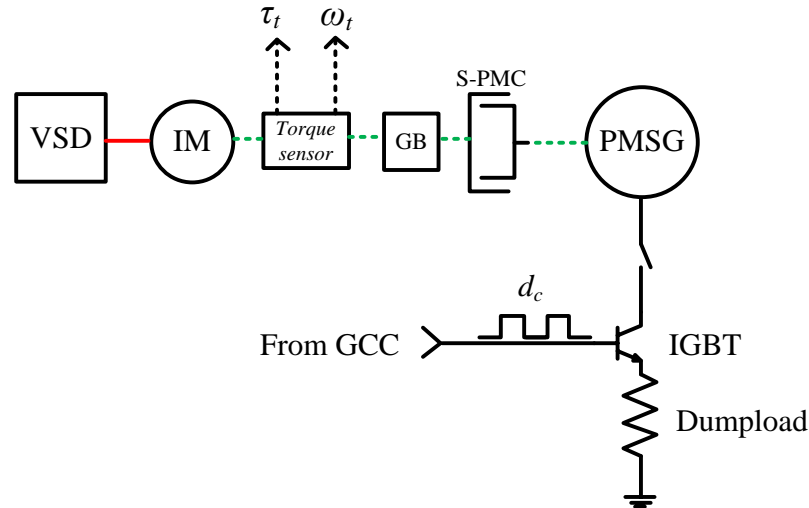


Figure 5.4: Schematic of the practical implementation of the dynamic step-test from section 3.1.1 where the value of the dumpload resistor is 20Ω .

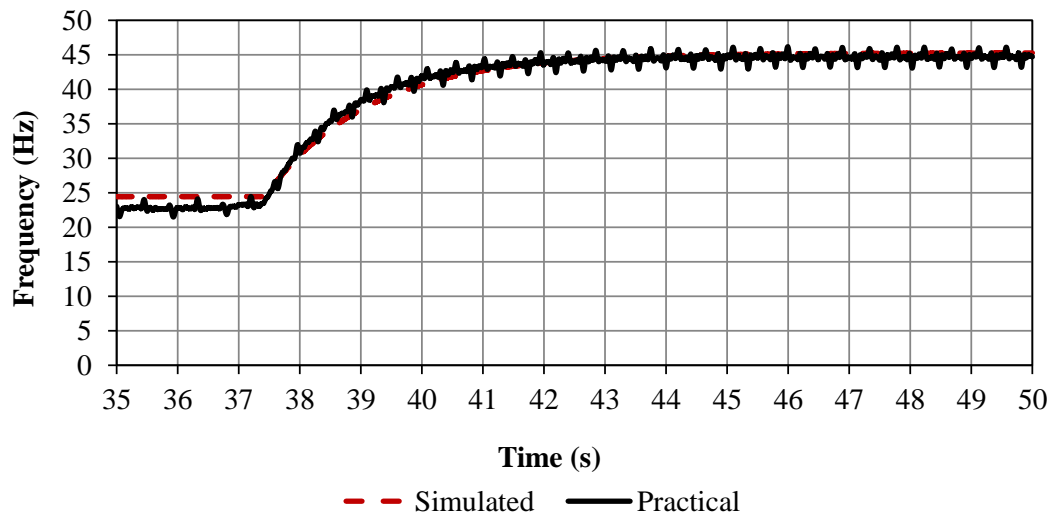


Figure 5.5: Dynamic step-test results of the downwind turbine drivetrain for a fixed 100 Nm torque input and a step in duty cycle from 30% to 15%.

5.3 Speed Control

Figure 5.6 shows a top level schematic of the laboratory layout used for the speed control tests. The VSD is set to torque regulation mode but unlike the dynamic step-tests, the duty cycle to the dumpload chopper circuit is automatically controlled by the GCC in order to regulated the downwind drivetrain's speed. Figure 5.7 shows a classical closed-loop block diagram representation of Figure 5.6 in which the grid frequency f_{grid} is used as the reference input to the PI speed controller and the electrical frequency of the PMSG f_{gen} is the controlled output. The difference in electrical frequency between the grid and PMSG is denoted as Δf whereas the duty cycle (the output of the controller) is denoted as d_c .

Figure 5.8 shows the results of four separate speed control tests where the input torque supplied by the VSD was set to 50 Nm, 70 Nm, 100 Nm and 145 Nm respectively. The downwind drivetrain's speed ω_t was measured and recorded using the in-line torque sensor. The PI-controller's ability to control the downwind drivetrain's speed within the necessary boundary conditions is evident in Figures 5.8 (a)-to-(c). However, the designed PI-controller is unable control the drivetrain's speed within the boundary conditions for torque inputs greater than 100 Nm (0.7 p.u.) as shown in Figure 5.8(d). This is partly due do the fact that the speed controller was designed to handle a maximum torque input of 100 Nm. Consequently, the proportional and integral gains proved insufficient for torque inputs greater than 100 Nm.

The simulated speed control results from Figure 3.6 and the measured results of Figure 5.8 compare favourably (barring Figure 5.8(d)). Figure 5.8 (a) shows significantly less steady-state oscillation when compared to Figure 3.6 (a) however the measured results of Figure 5.8 shows a persistent ripple during steady-state throughout the range of torque inputs which can be attested to minor vibrations due to the effects of the chopper circuit as well as unwanted frequencies emanating from the mechanical test bench. However, the results of Figure 5.8 further validates the accuracy of the downwind turbine drivetrain simulation model as well as the effectiveness of the PI speed controller design procedure.

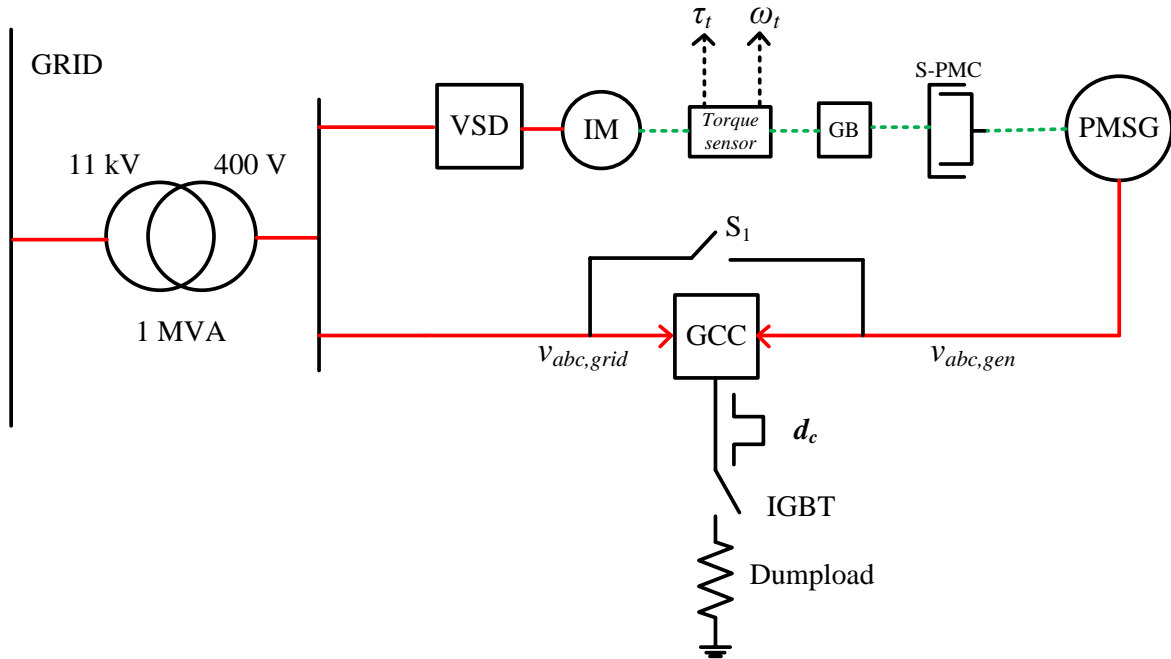


Figure 5.6: Top level schematic of the laboratory setup used to conduct speed control tests on the downwind turbine drivetrain.

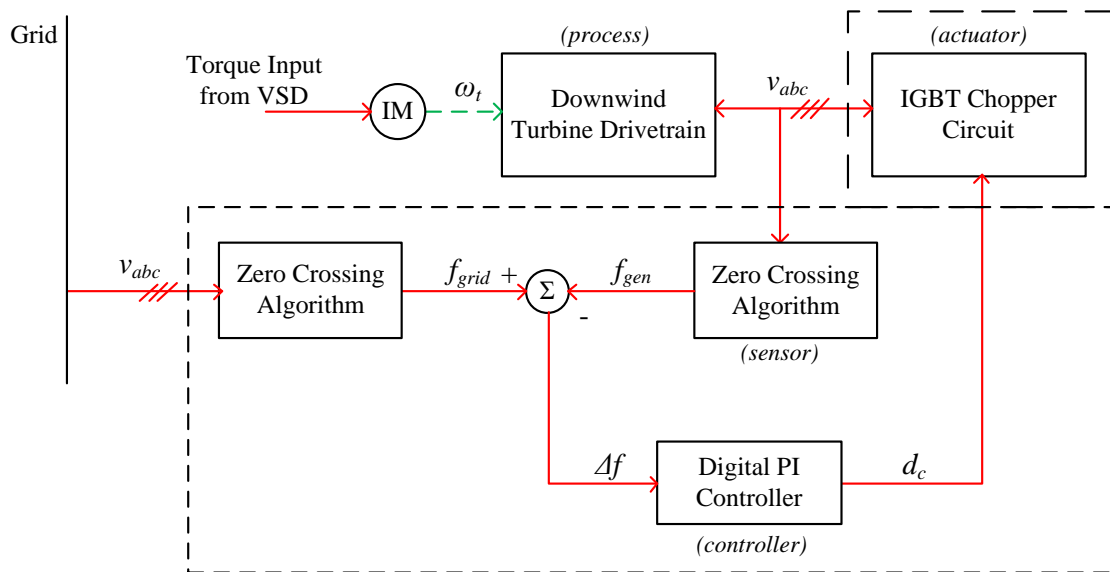


Figure 5.7: Closed-loop block diagram representation of Figure 5.6 where everything contained within the dotted lines are controlled within the GCC.

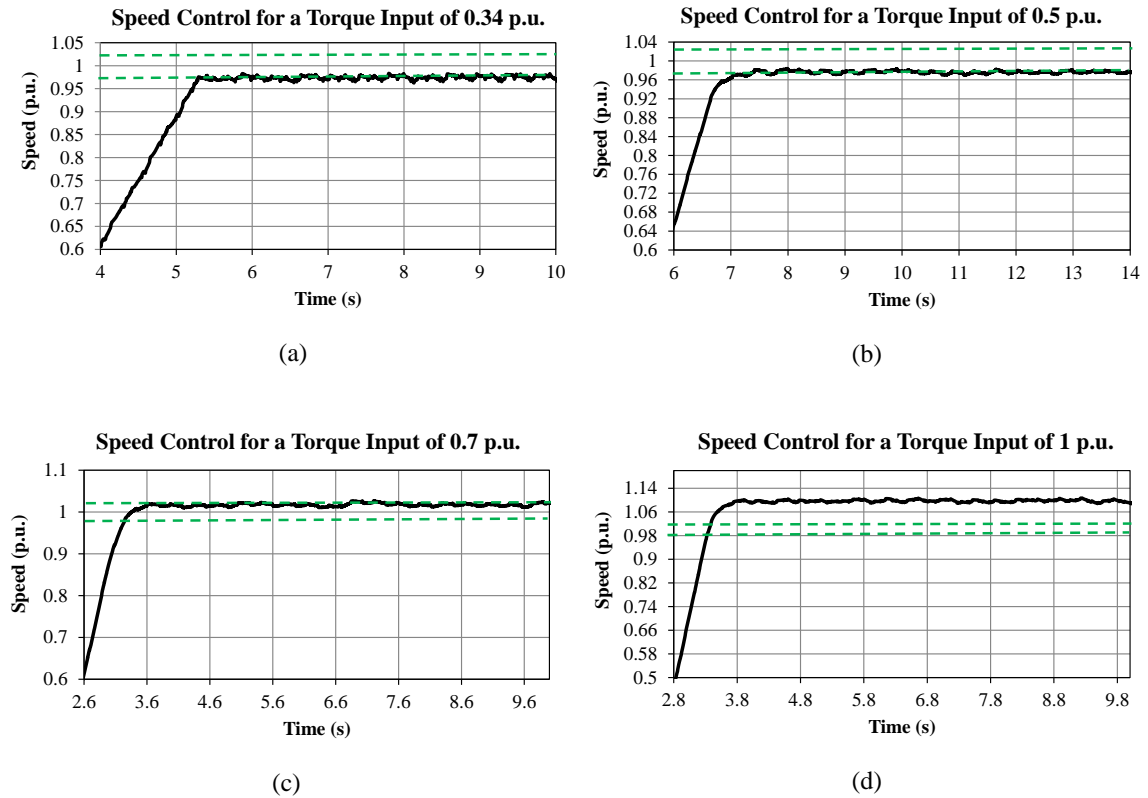


Figure 5.8: Measured speed control results for various torque inputs: (a) 50 Nm (0.34 p.u.), (b) 70 Nm (0.5 p.u.), (c) 100 Nm (0.7 p.u.), and (d) 145 Nm (1 p.u.). The dotted lines represent the suggested boundary restrictions as outlined in [37].

Figure 5.9 shows the PI-controller's disturbance rejection capabilities. For this test, the VSD was instructed to provide an initial fixed 100 Nm torque input to the downwind drivetrain. After 15 seconds, the torque supplied by the VSD was manually (and randomly) varied. From Figure 5.9, the PI-controller is able to control and maintain the drivetrain speed within a speed range of ± 0.1 p.u. for the range of torque variations. The PI-controller is shown to react quickly to any variations in torque and consequently is able to regulate the drivetrain speed within acceptable boundaries even during large variations in input torque. The PI-controller's disturbance rejection capabilities validates the robustness of the Internal Model Control (IMC) tuning method as was outlined in section 3.2.

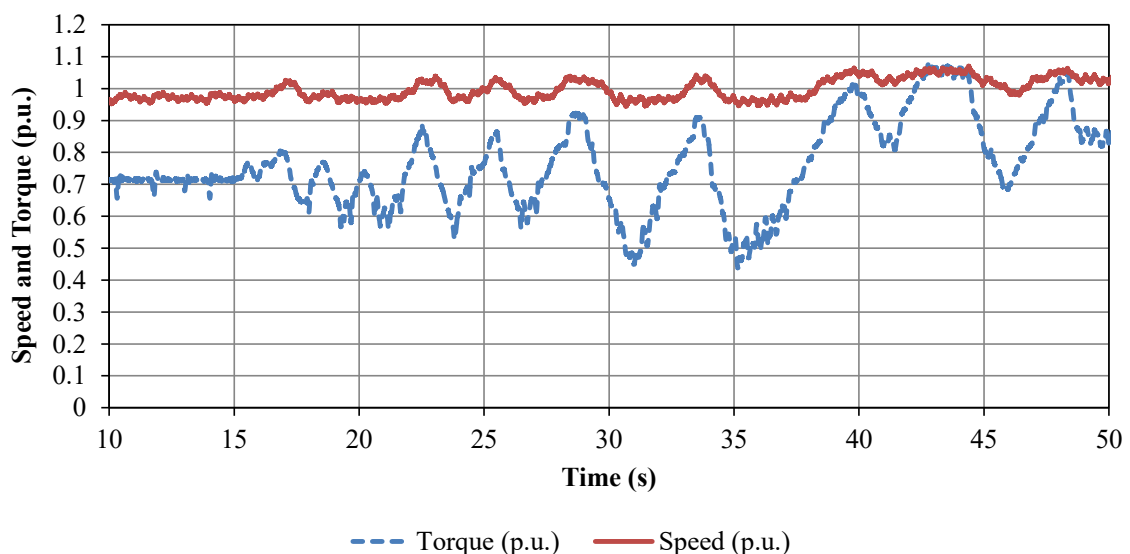


Figure 5.9: Measured results showing the PI-controller's disturbance rejection capabilities.

5.4 Grid Connection and On-Grid Dynamic Performance

In this section, the grid connection controller's (GCC) ability to synchronize the downwind drivetrain to the grid is evaluated. Additionally, once grid connected, the downwind drivetrain's ability to filter torque pulsations in the frequency range of 2.5 Hz - 8 Hz (the 3p frequencies) is evaluated. Finally, the GCC's ability to disconnect the downwind drivetrain from the grid during excessive input torque conditions tested.

5.4.1 Grid Connection

Figure 5.10 shows a grid connection test where the downwind drivetrain was accelerated from rest by a torque input of ± 110 Nm. Figures 5.10 (a), (b), and (c) show the drivetrain speed, grid and PMSG phase voltages and generator current prior to and after grid connection. It should be noted that Figure 5.10 (a) was generated from the data obtained from the torque sensor whereas Figures 5.10 (b) and (c) were generated from data obtained from an oscilloscope. As a result, the times displayed on the horizontal axis of Figures 5.10 (b) and (c) don't correlate to that of Figure 5.10 (a). However, the respective grid connection instances are indicated by the arrow.

Figure 5.10 shows that the GCC is able to connect the downwind drivetrain to the grid within the grid connection synchronization requirements as outlined in [37]. However, when grid connected, the generator current is shown to have multiple transients before settling at a steady-state. These transients are most likely due to the acceleration of the generator at the moment of grid connection as alluded to in section 4.4, Figure 4.5 (c). It was found that the GCC connected the the drivetrain to the grid as soon as possible (when all grid synchronization parameters were within specification) and as a result, all subsequent grid connection test resulted in grid/generator currents with multiple transients before settling at a steady-state. Furthermore, the peak magnitude of the current response is directly proportional to the value of the torque input which further suggests that the acceleration of the generator prior to grid connection is a crucial parameter when it comes to grid connection. The extra transients can theoretically be avoided if grid connection is delayed until the speed controller has brought the drivetrain speed to steady-state (where the acceleration of the drivetrain is zero).

Figure 5.11 shows how the GCC would typically behave during field tests. From Figure 5.11, the drivetrain is accelerated from rest by a torque input of 0.45 p.u. and the GCC subsequently connects the the drivetrain to the grid (indicated by the solid arrows) once the necessary synchronization conditions have been met. The input torque is then increased above rated conditions and the GCC subsequently disconnects the downwind drivetrain from the grid (indicated by the dotted arrows) and connects the dumpload to the terminals of the generator. Once the dumpload is connected, the drivetrain speed slows down and settles at a much lower steady-state level. After a while, once the input torque has returned to normal operating conditions and once the drivetrain speed is slow enough, the GCC disconnects the dumpload from the generator terminals and allows the drivetrain to accelerate to rated speed before implementing speed control and reconnecting the drivetrain to the grid.

5.4.2 On-Grid Dynamic Performance

Figure 5.12 shows a schematic of the laboratory setup used to conduct the on-grid dynamic performance tests. For this test, the GCC was replaced with a set of synchronizing lights and a mechanical three-phase switch. Furthermore, the VSD was set to speed regulation mode and the downwind drivetrain was brought up to rated speed using the VSD and IM drive motor. The synchronization lights were used to determine the phase alignment between the generator and the grid while an oscilloscope was used to monitor the grid and generator phase voltages prior to grid connection. Once the generators voltage-frequency, voltage-phase angle, and voltage magnitude aligned to that of the grid's voltage-frequency, voltage-phase angle, and voltage magnitude, the mechanical switch S_1 was manually closed to connect the generator to the grid. Once grid connected, the speed command to the VSD was increased which resulted in torque being generated by the PMSG due to the PMSG being grid connected. The subsequent generator/grid current was measured and recorded using an oscilloscope and the drivetrain speed was measured using the torque sensor.

Dynamic Step Test

Figure 5.13 shows the results of the laboratory implementation of the simulated torque step-test of Figure 4.7. Figure 5.13 (a) and (b) show the respective step in torque and stator current response. For this test, the downwind drivetrain was manually connected to the grid using the synchronizing lights and the mechanical switch. After grid connection, the speed command of the VSD was increased which resulted in a step in input torque provided to the drivetrain. The resulting stator current was measured

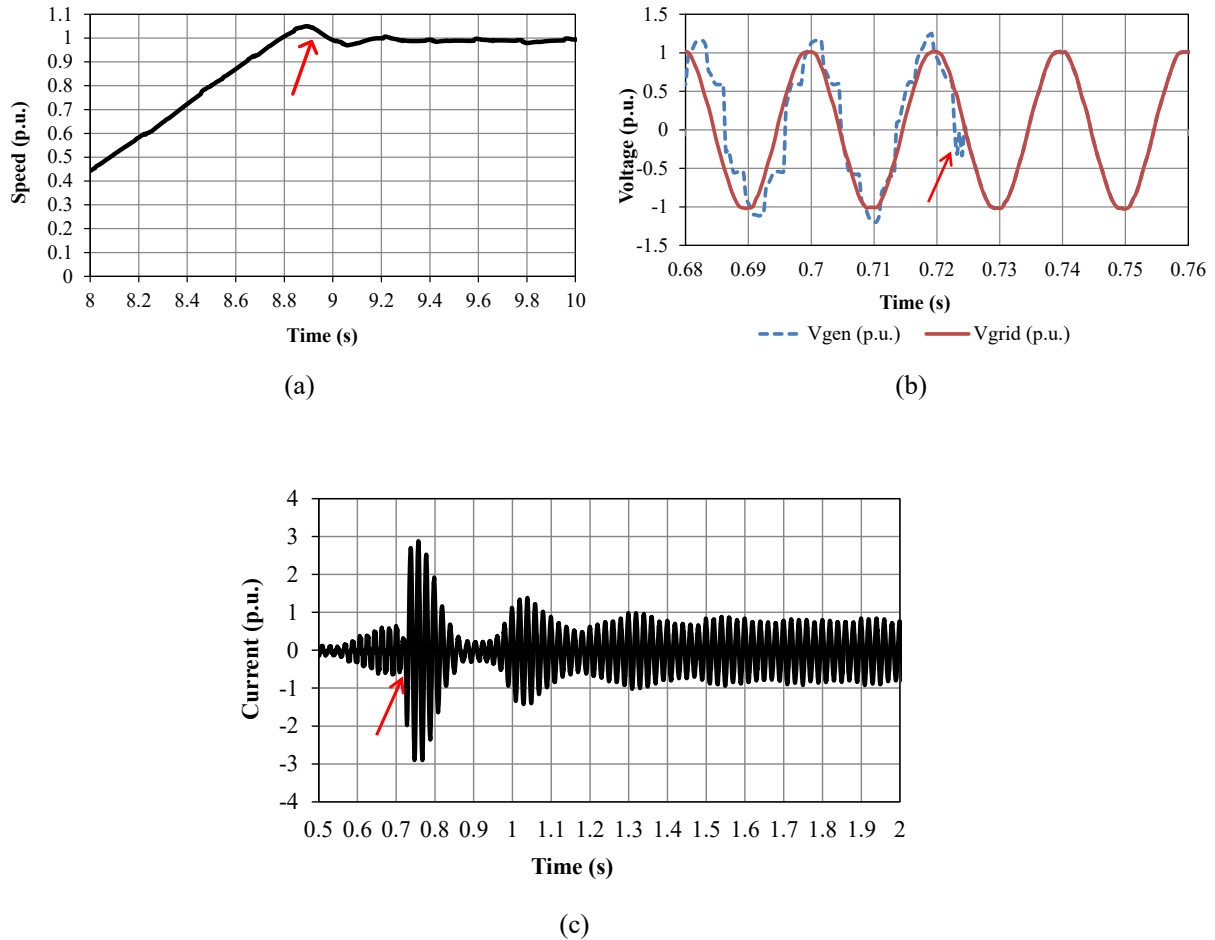


Figure 5.10: Figure showing: (a) drivetrain speed, (b) grid and PMSG phase voltages, and (c) generator current prior to and after grid connection for a torque input of 110 Nm (0.78 p.u.). Grid connection is indicated by the arrow.

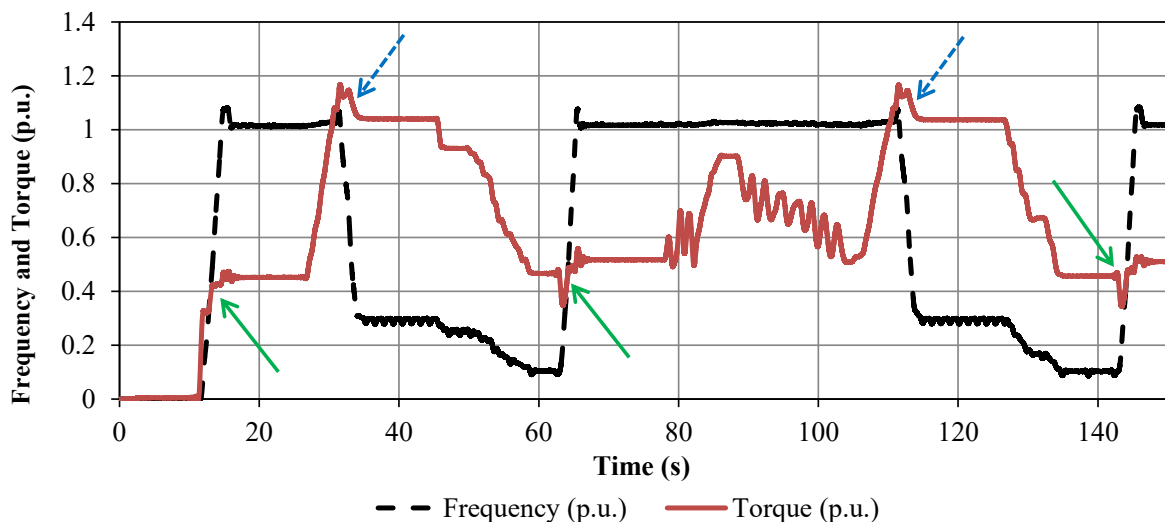


Figure 5.11: Figure showing how the GCC connects the downwind drivetrain to the grid (solid arrows) and how and when the GCC disconnects the drivetrain from the grid (dotted arrows).

and recorded on an oscilloscope. The torque-step response of Figure 5.13, closely resembles that of the simulated torque-step response of Figure 4.7. Furthermore, the grid-connected downwind drivetrain is

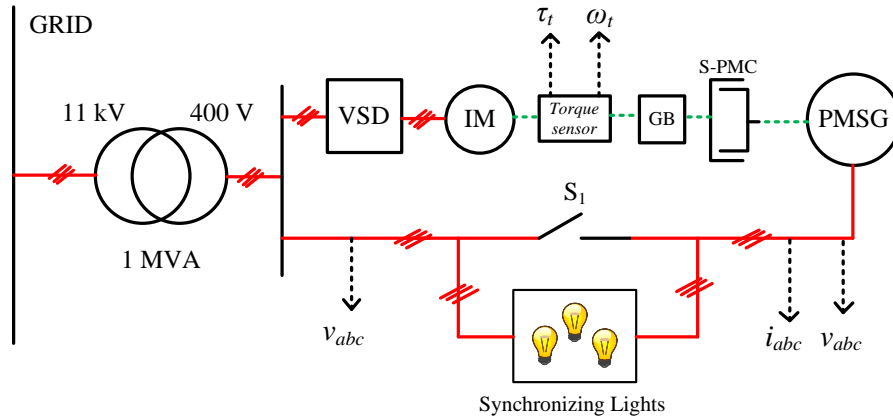


Figure 5.12: Schematic of the laboratory setup used to conduct the on-grid dynamic performance tests. The dotted arrows represent measurement points.

shown to be stable for a 0.8 p.u. step in torque input. Moreover, the results of the torque-step test further verifies the accuracy of the simulated model.

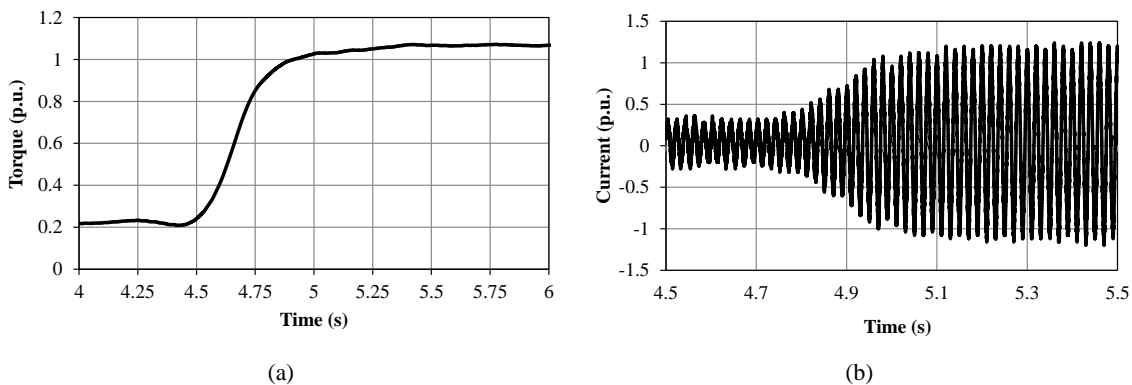


Figure 5.13: Figure showing: (a) step in torque input and (b) stator current response.

Torque Pulsations

Figure 5.14 shows the results of two tests which were conducted to evaluate the downwind turbine's sensitivity to turbine torque pulsations as identified in section 1.5. Figure 5.14 (a) shows the grid current response for a 1 p.u. torque input with a 2.5 Hz pulsation frequency component. The 2.5 Hz frequency pulsation is used to simulate the effect wind shear would have on the turbine blades. However, Figure 5.14 (a) differs from the simulated 2.5 Hz frequency test of Section 4.3, Figure 4.11, with regards to the magnitude of the wind shear effect. In Figure 5.14 (a) the magnitude of the wind shear frequency was increased to that of the tower shadow effect. This was done to illustrate what effect low frequency events can have on the downwind drivetrain. From Figure 5.14 (a), the downwind drivetrain is unable to attenuate the $\Delta 0.1$ p.u. peak-to-peak 2.5 Hz frequency pulsation. However, in theory, the wind shear component contributes a small fraction towards the overall magnitude of the 3p pulsation frequency and, as shown in Figure 4.11 (a), the downwind drivetrain would otherwise filter out any effects caused by the 2.5 Hz frequency component.

Figure 5.14 (b) shows the grid current response for a 1 p.u. torque input with a 8 Hz pulsation frequency component. The 8 Hz frequency pulsation arises as a result of the tower shadow effect which is a function of the turbine's rotational speed as explained in Section 4.3.2. The tower shadow effect is known to be more severe in downwind turbines where the resulting peak-to-peak turbine torque pulsations are known to be up to 10% of the average value. However, Figure 5.14 (b) shows that the 8 Hz pulsation frequency with a peak-to-peak magnitude of 0.1 p.u. has no noticeable effect on the grid current (when compared to Figure 5.14 (a)) which suggests that the S-PMC will be able to attenuate the effects of tower shadow and as a result, prevent any voltage flicker on the grid. The results of Figure 5.14 also suggest that the downwind drivetrain has a bandwidth of 4 Hz as was shown in Figure 4.9.

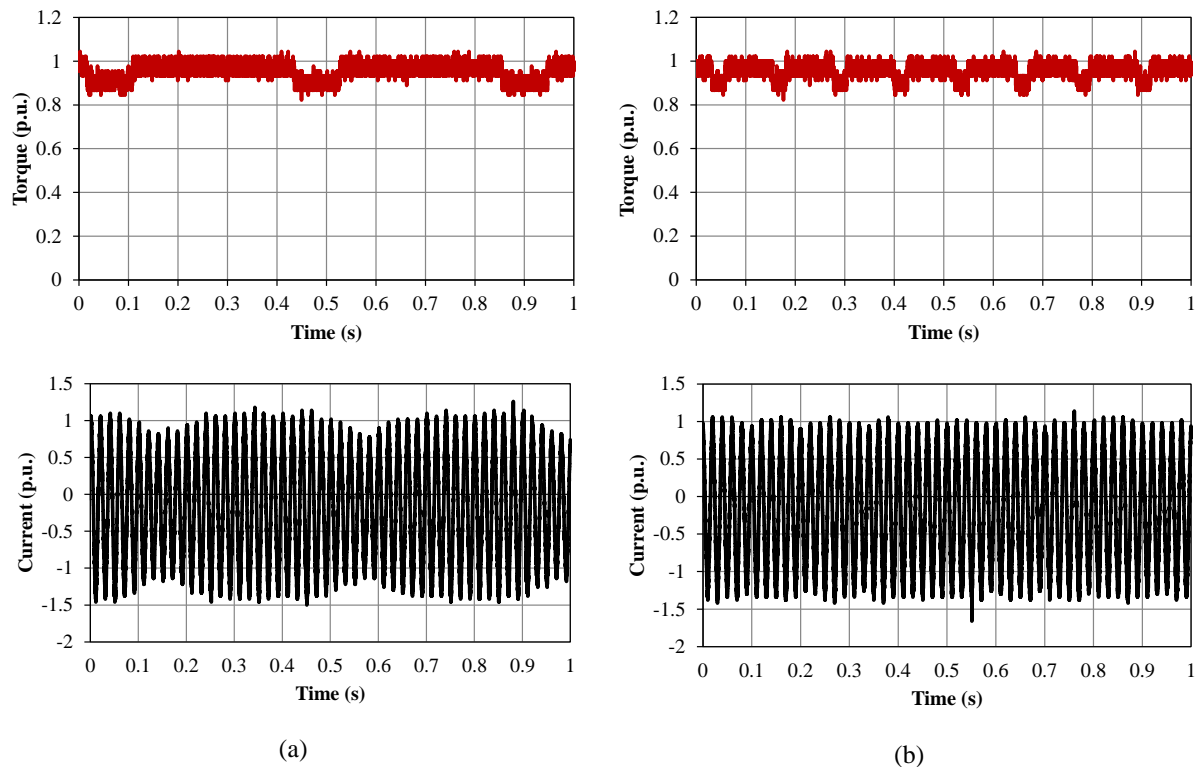


Figure 5.14: Downwind drivetrain’s on-grid dynamic performance for (a) a rated torque input with a 2.5 Hz frequency component (resulting from the wind shear effect) and (b) a rated torque input with a 8 Hz frequency component (resulting from the tower shadow effect).

5.5 Field Testing Setup

The downwind turbine was erected at the Stellenbosch University Mariendahl small wind turbine testing facility as shown in Figure 5.15. The downwind turbine nacelle sits atop a 18 m tower and an addition 2 m extension which brings the hub height to ± 20.5 m. The power output from the wind turbine is measured using a *Lovato* DMG-700 Digital Multimeter and recorded (logged) using an EXP 1010 USB expansion module. The data is stored on a desktop computer situated on-site.

Figure 5.16 shows the average wind speed at the Mariendahl testing site over the weekend of 04 November 2017 to 06 November 2017. The wind speed at the testing facility is monitored using a Wind Monitor-JR Model 04101 wind speed and wind direction sensor. The wind speed is recorded using CR-300 datalogger from *Campbell Scientific*. From Figure 5.16, the average wind speed indicates that the wind turbine testing facility has strong wind conditions during the afternoon periods. The wind speed tends to level off in the evenings before retuning to average speeds between 4 m/s and 7 m/s.

Unfortunately, no meaningful wind turbine power data could be collected due to various time constraints which includes a robbery of the pre-existing on-site measuring equipment and power cables. However, much of the equipment has now been replaced and further wind turbine testing can now be conducted at the testing facility. Additional problems arose during the initial speed control tests conducted on-site. The downwind turbine nacelle and 2 m tower extension exhibits oscillatory behaviour in the presence of strong winds while under speed control (prior to grid connection). However, further field-testing showed that at low wind speeds, the wind turbine’s speed can be controlled at rated speed without any turbine oscillations. It was concluded that the severity of the oscillations is shown to be proportional to the speed of the wind at any given moment. A further issue is in the event where the downwind turbine blades are facing into the wind (the wrong direction). The 1.9 m blades aren’t always able to redirect the nacelle in the correct direction and as a result, no thrust is produced on the blades and the downwind turbine remains idle. Without a yaw drive, the downwind turbine is unable to turn itself in a direction where the blades are facing ”downwind” and consequently, no drivetrain acceleration is achieved.



Figure 5.15: 2.2 kW downwind turbine at the Stellenbosch University Mariendahl small wind turbine testing facility.

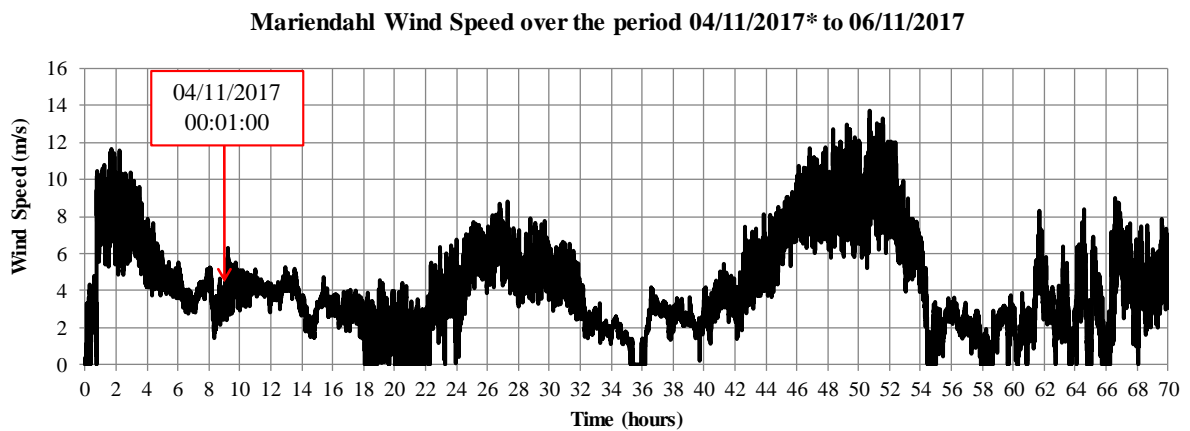


Figure 5.16: Average wind speed measurements recorded at the Mariendahl wind turbine testing facility over the weekend of 04 November 2017 to 06 November 2017.

5.6 Chapter Summary

In this chapter, the downwind turbine drivetrain's dynamic performance was tested and evaluated in a laboratory setup. The downwind drivetrain (consisting of a gearbox, S-PMC and PMSG) was placed on a mechanical testbench and the turbine blades were replaced by an Allen-Bradley *powerflex* 700 variable speed drive (VSD) and an induction motor (IM). The VSD-IM combination was used as a means to provide a source of torque to the drivetrain in order to simulated the torque that conventional turbine blades would provide in the presence of wind.

A dynamic-step test was performed in order to identify the step-response of the downwind drivetrain. During this test, the grid connection controller (GCC) was placed in "manual" mode where the duty cycle to the dumpload chopper circuit was manually stepped in order to record the speed response of the drivetrain when subjected to a 0.7 p.u. (100 Nm) input torque condition. The resulting speed-step response matched results of the simulated dynamic-step test. Consequently, the physical drivetrain's

step response yielded identical *process* constants as those determined in Chapter 3. The subsequent process gain (k_p), process time constant (τ_p) and process dead time (τ_d) were used to develop a digital PI-controller using the tuning rules as outlined by the Internal Model Control (IMC) method.

The digital PI-controller was used in conjunction with the GCC and dumpload chopper circuit to control and maintain the downwind drivetrain speed at synchronous speed regardless of the input torque conditions. The PI-controller was able to control and maintain the drivetrain speed within the necessary boundaries as set out in [37] for torque inputs up until 100 Nm. However, the speed controller failed to maintain the drivetrain speed within the set boundaries for torque inputs greater than what was used in the dynamic step-test.

The GCC's ability to connect the downwind drivetrain to the grid was also tested. The GCC was able to connect the drivetrain to the grid once all the synchronization conditions were met however the resulting grid-current transients proved to be a point of concern especially for torque inputs of 0.7 p.u. (100 Nm). The reason for the excessive grid current transients were shown (in Chapter 4) to be as a result of the acceleration of the generator prior to grid connection. It was shown that the GCC connected the drivetrain to the grid once the synchronization conditions were met but before the PI-controller had an opportunity to completely arrest the drivetrain's acceleration.

Finally, the downwind drivetrain's on-grid dynamic stability was evaluated. Two tests were conducted to determine what effect a 2.5 Hz and 8 Hz torque pulsation would have on the grid current. The 2.5 Hz and 8 Hz torque pulsation frequencies are as a result of wind sheer and tower shadow respectively. As was shown in Chapter 4, the downwind drivetrain was able to attenuate a 0.1 p.u. peak-to-peak torque pulsation component at a frequency of 8 Hz. Consequently, the tower shadow frequency had no effect on the grid current. Additionally, a 2.5 Hz, 0.1 p.u. peak-to-peak torque pulsation test was conducted in order to gauge and verify the bandwidth of the downwind drivetrain. The downwind drivetrain was unable to attenuate the 0.1 p.u. torque pulsation at 2.5 Hz and the effects of the 2.5 Hz torque pulsation was evident on the grid current. Further testing suggested that the downwind drivetrain has a bandwidth of 4 Hz, as was shown in Chapter 4.

Chapter 6

Conclusion and Recommendations

The two main aims of this thesis were: (1) to design and develop a speed controller which has the ability to regulate the speed of a 2.2 kW downwind turbine at the synchronous speed required for grid connection; and (2) evaluate the dynamic performance of the downwind drivetrain.

6.1 Speed Control

In order to conduct speed control, an accurate simulation model of the downwind turbine drivetrain was formulated in MATLAB/Simulink. The downwind turbine simulation model was used to develop a PI-controller by simulating a dynamic step test in order to identify the drivetrain's step response as well as its transfer function. From the step response, the relevant proportional (P) and integral (I) components of the PI-controller were derived using the internal model control (IMC) tuning rules. During laboratory testing, the same dynamic step-test was performed and the resulting drivetrain step response was shown to match the simulated results with a high degree of accuracy and as a result, the physical system proved to have the same transfer function as was found in simulation. Moreover, the resulting PI-controller was shown to provide acceptable performance in both the simulated and laboratory tests. It can therefore be concluded that the simulation methods and models used in this thesis provide a large degree of accuracy when it comes to predicating the response of the actual system. This is especially useful in the case of larger drivetrains where practical laboratory testing isn't always possible.

6.2 Laboratory Grid Connection

The grid connection controller (GCC) was able to connect the downwind drivetrain to the grid within the specified grid synchronization tolerance limits. However, the GCC lacked the functionality to wait until the PI-controller had completely arrested the drivetrain's acceleration. Consequently, the resulting grid transient currents reached magnitudes of 3 p.u. or 3 times the rated current for a 0.7 p.u. (100 Nm) torque input. The magnitude of the largest current transient is within acceptable levels however the simulations conducted in Chapter 4 suggested that the excessive grid current transients can be avoided if the GCC 'waits' until the drivetrains acceleration is near zero. This additional functionality is easily implementable but was overlooked due to time constraints. However, provision was made to disconnect the downwind turbine should the transient grid current exceed 4 p.u..

6.3 On-Grid Dynamic Performance

The 2.2 kW downwind turbine is shown to be stable under a variety of input torque conditions. The main torque condition prevalent to downwind turbines are those as a result of the tower shadow effect. For the 2.2 kW downwind turbine, the tower shadow effect produces a torque pulsation at a frequency of 8 Hz. The tower shadow effect was simulated in MATLAB/Simulink and in the Laboratory. In both cases, the downwind turbine was able to attenuate the 8 Hz torque pulsation frequency to an extent where it had no effect on the resulting grid current. Moreover, once grid connected, the downwind drivetrain was shown to be stable during a sudden near-rated step in input torque. The results from the simulations and laboratory tests indicate that the downwind turbine would be stable during field testing and the likelihood of power fluctuations as a result of the tower shadow effect are mitigated due to the 4 Hz bandwidth of the drivetrain. The accuracy of the simulation model was further verified during the on-grid torque pulsation test as it correctly predicted the bandwidth of the drivetrain and how the drivetrain would respond to torque pulsations at various frequencies.

Additionally, the downwind drivetrain was shown to comply (in simulation) with the low voltage ride through (LVRT) requirements for small-scale wind turbines as well as the requirements pertaining to fluctuation in grid frequency. However, these tests could not be conducted in the laboratory.

6.4 Field Tests

Time restrictions due to a series of unfortunate events saw to it that no meaningful wind turbine power data could be recorded. A burglary saw to it that the on-site measuring equipment had to be completely replaced. However, the Stellenbosch University small wind turbine testing facility is now, at the time of writing, ready to measure, record and log data for any further wind turbine projects. Further delays were brought about due to severe oscillatory behaviour shown by the downwind turbine in the presence of strong winds. The 2 m wind turbine tower extension is thought to be the cause of the oscillations due to its significantly smaller diameter when compared to the 18 m tower. The 2 m tower extension's natural frequency is suspected to be near to that of the turbine blades' rotational frequency which can cause resonance. Furthermore, the downwind turbine blades aren't always able to turn the nacelle in the direction needed for blade rotation. Without a yaw drive, the wind turbine will remain idle even in the presence of strong winds.

6.5 Recommendations

From the conclusions, a number of recommendation can be made for further research and investigations:

6.5.1 System Modelling

The Internal Model Control (IMC) tuning rules proved to be an effective methodology for designing a speed controller for the downwind turbine. However, the IMC tuning rules aren't suited for integrating or near-integrating processes. Furthermore, it was shown that *gain scheduling* provides a better framework for designing control systems for integrating or near-integrating processes. The gain scheduling design process is more complex than that of the IMC design process, however, the improved all-round steady-state performance shown by the adapted gain scheduling methodology implemented in Section 3.2.4 suggests that it should be considered for future wind turbine speed control projects.

6.5.2 Grid Connection

The grid connection controller (GCC) is responsible for connecting the downwind turbine to the grid. However, the GCC was shown to connect the downwind drivetrain to the grid before the speed controller was able to arrest the drivetrain's acceleration. This resulted in large grid-current transients. Simulations conducted in Chapter 4 suggests that the magnitude and number of grid-current transients can be minimized and reduced respectively by connecting the drivetrain to the grid only after the speed controller has brought the drivetrain's speed to a steady-state where its acceleration is effectively zero. It is suggested that a form of delay (in software or otherwise) be introduced that monitors and evaluates when the drivetrain's acceleration is zero before grid connection takes place. Additionally, a more sophisticated method for determining the frequency (speed) of the drivetrain should be considered. The method of zero crossings is inaccurate at low drivetrain speeds and the distorting effects of the diode rectifier on the generator voltage further hinders the GCC's ability to determine the voltage-phase angle and voltage frequency.

6.5.3 Field Testing

Downwind turbine drivetrain designers need to ensure that the wind turbine's rotational frequency f_t isn't within the tower's first natural frequency. This was the case with the 2.2 kW downwind turbine and is suspected to be the reason for the oscillatory behaviour of the nacelle at high wind speeds. It is thus recommended that the frequency of the wind turbine tower be taken into account during the initial design process.

If the same 1.9 m blades are used for subsequent downwind turbine designs; it is suggested that a yaw controller be designed in order to ensure the turbine blades remain 'downwind' to the direction of the wind. It was shown that the 1.9 m blades weren't always able to reposition the nacelle in the correct direction when the turbine blades are facing 'upwind'. Additionally, a wind turbine blade simulation package can be used to ensure that geometry of the blades allows the nacelle to be positioned and repositioned in the event of sudden changes in wind direction.

Appendix A

Appendix A

A.1 MATLAB/Simulink closed-loop controller blocks

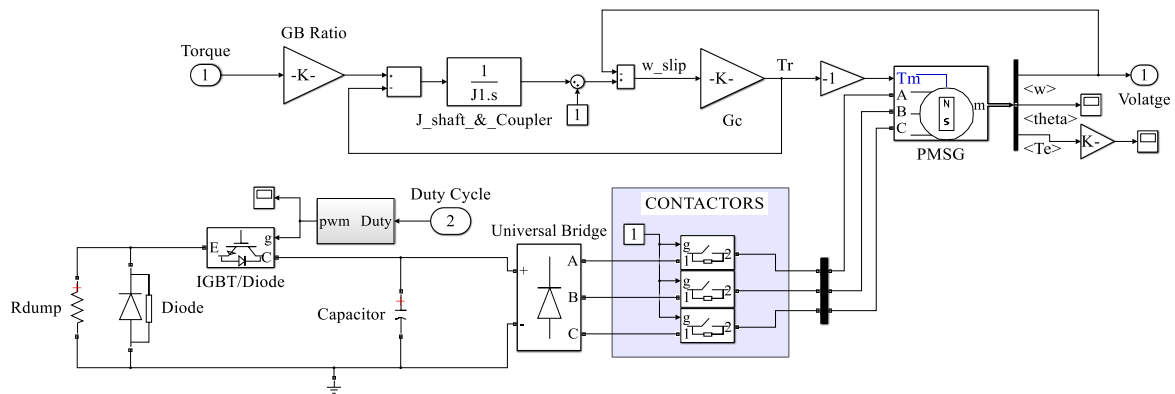


Figure A.1: Contents of the "Downwind Turbine and Chopper Circuit" block model of Figure 3.4

A.2 Zero Crossing Algorithm Source Code - MATLAB

```
function Fgen = duty_cycle(Vab, freq_count)

global Freq_gen ;

if(Vab > 210 && freq_count > 50)

    if ((freq_count > Freq_gen) && (Freq_gen < 200))
        Freq_gen = Freq_gen + 1;
    end

    if (freq_count < Freq_gen)
        Freq_gen = Freq_gen - 1;
    end

    end

    %%%%%%%%%%%%%%%
    if ((Freq_gen - freq_count) > 10)
        Freq_gen = Freq_gen - 10;
    end

    end

    if ((freq_count - Freq_gen) > 10)
        Freq_gen = Freq_gen + 10;
    end
end
```

```

    end

end

Fgen = Freq_gen ;

```

A.3 Digital PI-Controller Source Code - MATLAB

```

function pwm = duty_cycle(fgrid, fgen)

global PDC ; % Controller output - duty cycle
global errSum ; % Integral update term

error = (fgrid - fgen); %% Error Signal

errSum = error + errSum ; %% Updating the Integral Term (I)

%%%%%%%%%% Anti Windup Protection%%%%%%%%%%
if(errSum < 0)
    errSum = 0 ;

elseif(errSum >= 600) % 600 = 15 percent for Figure 3.6
    errSum = 600 ; % 200 = 5 percent for Figure 3.7
                    % 280 = 7 percent for Figure 3.8
end

%%%%%%%%%% PI CONTROL %%%%%%%%%%%
PDC = 27*error + (1)*errSum ; % P = 27 for Figure 3.6, I rounded up to 1.
                                % P = 50 for Figure 3.7, I = 1.
if(PDC < 0)                      % P = 180 for Figure 3.8, I = 1.
    PDC = 0 ;
elseif(PDC > 2000)
    PDC = 2000 ;
end

%%%%%%%%%% PWM OUTPUT %%%%%%%%%%%
pwm = PDC ; %% OUTPUT

end

```

Bibliography

- [1] S. SHABANGU. White paper on renewable energy. White paper, DEPARTMENT OF MINERALS AND ENERGY REPUBLIC OF SOUTH AFRICA, 2003.
- [2] L. Aphane and K. Breytenbach. State of renewable energy in south africa. Report, DoE, 2015.
- [3] energyblogs. Onshore wind database, 2017. URL www.energy.org.za/knowledge-tools/projectdatabase.
- [4] National Energy Regulator Of South Africa. Eskom price increase application, 2009. URL <http://www.nersa.org.za/Admin/Document/Editor/file/Electricity/PricingandTariffs/Eskom>.
- [5] Kestrel Wind. Home energy system in south africa, 2012. URL <http://www.kestrelwind.co.za/content.asp?pageid=418>.
- [6] Dr. Matthais Lang and Annette Lang. German energy blog, german feed-in tariffs 2014, 2014. URL www.germanenergyblog.de.
- [7] T. Thiringer. Grid-friendly connecting of constant-speed wind turbines using external resistors. *IEEE Transactions on Energy Conversion*, 2002.
- [8] S. A. Gomez and J. L. R. Amenedo. Grid synchronisation of doubly fed induction generators using direct torque control. *IEEE 2002 28th Annual Conference of the Industrial Electronics Society. IECON 02*, 2002.
- [9] A. D. Hansen and L. H. Hansen. Wind turbine concept market penetration over 10 years (1995 to 2004). pages 81 – 97, 2007.
- [10] E. Spooning and A.C. Williamson. Direct coupled, permanent magnet generators for wind turbine applications. *IEE Proc. A*, (to be published).
- [11] J. R. Bumby A. J. G. Westlake and E. Spooner. Damping the power-angle oscillations of a permanent-magnet synchronous generator with particular reference to wind turbine applications. *IEEE Proceedings Electric Power Applications*, 1996.
- [12] N. Celanovic S. Grabic and V. A. Katic. Permanent magnet synchronous generator cascade for wind turbine application. *IEEE Transactions on Power Electronics*, 2008.
- [13] Y. Kanamaru T. Fukami, K. Nakagawa and T. Miyamoto. A technique for the steady-state analysis of a grid-connected permanent magnet induction generator. *IEEE Transactions on Energy Conversion*, 2004.
- [14] J. H. Potgieter and M. J. Kamper. Design of new concept permanent magnet induction wind generator. *IEEE Energy Conversion Congress and Exposition (ECCE 2010), Atlanta, Georgia, USA*, 2010.
- [15] J. H. Potgieter. Optimal topology and critical evaluation of slip synchronous permanent magnet wind generator, 2014.
- [16] P.J. van Wyk. Design and evaluation of medium speed geared direct grid-connected wind generator drive train with specific focus on slip permanent magnetic coupling, 2015.
- [17] P.J. van Wyk and M. J. Kamper. Simplified analysis technique for double layer non-overlap multiphase slip permanent magnet couplings in wind energy applications. *IEEE International Electric Machines and Drives Conference*, 2015.
- [18] J. Ekanayake D. Sharpe and T. Burton. *Wind Energy Handbook*. Wiley, 2001.

- [19] G. M. Masters. *Renewable and Efficient Electric Power Systems*. Wiley, 2004.
- [20] C. Chellamuthu K. Rajambal, B. Umamaheswari. Electrical braking of large wind turbines. *Renewable Energy*, 2005.
- [21] P. Bouwer U. Hoffmann and M.J. Kamper. Direct grid connection of a slip-permanent magnet wind turbine generator. *Energy Conversion Congress and Exposition (ECCE), 2011 IEEE*, 2011.
- [22] S. J. Chapman. *Electric Machinery Fundamentals, 5th edition*. 2012.
- [23] S. J. Van Zyl. *Distribution Standard For The Interconnection Of Embedded Generation*, 2011.
- [24] N. Karnik S. Das and S. Santoso. Time-domain modeling of tower shadow and wind shear in wind turbines. *ISRN Renewable Energy*, 2011.
- [25] C. Su W. Hu and Z. Chen. Impact of wind shear and tower shadow effects on power system with large scale wind power penetration. *In Proceedings of the 37th Annual Conference of the IEEE Industrial Electronics Society, IECON*, pages 878–883, 2011.
- [26] D.J. Morrow D. McSwiggen, T. Litter and J. Kennedy. A study of tower shadow effect on fixed-speed wind turbines. *Universities Power Engineering Conference, 2008. UPEC 2008. 43rd International*, 2008.
- [27] G. Dawood. Design and evaluation of grid-connected permanent magnet synchronous generator. Master’s thesis, University of Stellenbosch, 2015. Final Year Project Report.
- [28] A. Emami-Naeini G. F. Franklin, J. D. Powell. *Feedback Control of Dynamic Systems*. Pearson, sixth edition edition, 2010.
- [29] O. Dwyer. Summary of pi and pid controller tuning rules for processes with time delay, part 1: Pi controller tuning rules. *Proceedings of PID 00: IFAC Workshop on Digital Control, Terrassa, Spain*, pages 175–180, 2000.
- [30] J. F. Smuts. *Process Control for Practitioners*. OptiControls Inc., 2011.
- [31] G. K. McMillan. So many tuning rules, so little time. . URL <https://www.controlglobal.com/assets/14WPpdf/141016-McMillanTunningRules.pdf>.
- [32] K. J. Astrom and B. Wittenmark. *Computer Controlled Systems - Theory and Design*. Prentice Hall, 1997.
- [33] F. Habring. Automatic tuning of gain scheduled controller. The MathWorks AB, Stockholm, Sweden.
- [34] Dr C. Carter-Brown. *GRID INTERCONNECTION OF EMBEDDED GENERATION*. Electricity Suppliers Liaison Committee, 1 Dr Lategan Road, Groenkloof, Pretoria, edition 1 edition. This document does not have the status of a South African National Standard.
- [35] J .L. Collins and R.K. Shaltens. Experience and assessment of the doe/nasa mod-1 200-kilowatt wind turbine at boone north carolina. Technical report, Nasa, April 1982.
- [36] D. Dolan and P. W. Lehn. Simulation model of wind turbine 3p torque oscillations due to wind shear and tower shadow. *IEEE TRANSACTIONS ON ENERGY CONVERSION*, 2006.
- [37] RSA Grid Code Secretariat. *GRID CONNECTION CODE FOR RENEWABLE POWER PLANTS (RPPs) CONNECTED TO THE ELECTRICITY TRANSMISSION SYSTEM (TS) OR THE DISTRIBUTION SYSTEM (DS) IN SOUTH AFRICA*. Eskom Transmission Division, P.O Box 103, Germiston 1400, 2.6 edition, November 2012.

List of Figures

1.1	Danish concept fixed-speed wind turbine.	3
1.2	Most common wind turbine drive-train layouts currently in use with (a) the variable speed doubly-fed induction generator (DFIG) with gearbox and partially rated converter, (b) the variable-speed doubly-fed induction generator (DFIG) with gearbox and full rated converter, (c) direct-drive wound rotor synchronous generator (WRSG) or permanent magnet synchronous generator (PMSG) and full rated power electronic converter. The gearbox is optional in (c).	4
1.3	Attempts to provide damping to a drivetrain including a PMSG with, (a) a spring and mechanical damper being used, (b) a PMSG with a partially rated star point converter and, (c) A direct-grid connected permanent magnet induction generator.	5
1.4	SS-PMG wind turbine drivetrain.	5
1.5	A wind turbine drivetrain concept based on the SS-PMG where the SS-PMG is separated into two distinct machines; with one being a S-PMC and the other a conventional PMSG.	6
1.6	CAD representation of the S-PMC assembly [17].	6
1.7	Line diagram of, (a) the resistive bank based speed control strategy and (b) the thyristor based single resistor strategy with optional resistor stages shown with dotted lines [21].	8
1.8	An oncoming generator (G_2) being connected to a power system [22].	8
2.1	A CAD representation of the downwind turbine drivetrain.	11
2.2	Figure showing the constructed PMSG rotor (a) and wound stator (b) [27].	12
2.3	The dynamic dq -equivalent circuits of the PMSG.	12
2.4	Figure showing the constructed S-PMC short-circuited rotor (a) and the PM rotor (b) [16].	13
2.5	S-PMC modelling with (a) the linear relationship between slip and torque for slip values between (0 - 5%)[16] and (b) the S-PMC gain block model.	13
2.6	Downwind turbine blades.	14
2.7	Wind power coefficient versus tip-speed-ratio curve for the 1.9 m blade set used for the downwind turbine [16].	14
2.8	Wind turbine power versus turbine speed curves (a)[16] and equivalent simulation block model (b).	14
2.9	GCC circuit diagram.	15
2.10	A block diagram representation of the open-circuited downwind turbine simulation model.	16
3.1	Block diagram model of the dynamic step-test performed on the downwind turbine drivetrain.	18
3.2	Simulated dynamic step-test results for a change in duty cycle (d_c) from 30% to 15 % for a constant input torque of 100 Nm, and a dumpload resistor value of 20 Ω	18
3.3	Block diagram model of the required PI-controlled speed controller.	19
3.4	Closed-loop speed controller block diagram.	22
3.5	Simulated results for the implemented PI-controller for different torque inputs where: $P = 27$, $I = 1$ and $I_{(limit)} = 15\%$	22
3.6	Simulated results for the implemented PI-controller for various torque inputs with adjusted controller gains: $P = 54$, $I = 1$ and $I_{(limit)} = 7\%$	23
3.7	Simulated results for the implemented PI-controller for different torque inputs using the proposed <i>Gain Scheduling</i> methodology, where: $P = 180$, $I = 1$ and $I_{(limit)} = 7\%$	24
4.1	Simplified line diagram showing the downwind turbine drivetrain and dumpload chopper circuit.	26
4.2	Flow diagram representation of the methodology used to determine whether or not the oncoming generator can be connected to the grid.	27
4.3	Simulated downwind turbine generator (V_{gen}) and grid (V_{grid}) phase voltage prior to and after grid connection where grid connection occurs at time $t = 3.215$ seconds	28

4.4	Simulated grid current response for varying voltage-phase-angle differences conditions prior to grid connection where in (a) $\Delta\phi \simeq 0^\circ$, (b) $\Delta\phi \simeq 43.2^\circ$ and (c) $\Delta\phi \simeq 68.4^\circ$	29
4.5	Simulated grid current response for varying difference-in-frequency conditions where (a) $\Delta f \simeq 0.5$ Hz, (b) $\Delta f \simeq 2.5$ Hz and (c) $\Delta f \simeq 5$ Hz. Grid connection is indicated by the arrow.	30
4.6	Block diagram representation of the grid connected downwind turbine.	31
4.7	Simulated turbine torque response (a) and current response (b) for a 0 to 1 p.u. step in turbine torque.	31
4.8	Simulated rotor speed response (generator side) (a) and power angle response (b) for a 0 to 1 p.u. step in turbine torque.	32
4.9	Simulated frequency response of τ_s/τ_t' for the 2.2 kW downwind turbine.	33
4.10	Simulated grid current response (a) for an input turbine torque with an 8 Hz frequency component and a peak-to-peak amplitude of 2.5 Nm which models the effect of tower shadow on turbine and generator torque (b).	33
4.11	Simulated grid current response (a) for an input turbine torque with an 2.5 Hz frequency component and a peak-to-peak amplitude of 0.5 Nm which models the effect of wind shear on turbine and generator torque (b).	33
4.12	Low voltage ride through (LVRT) specifications for wind turbines with a power rating of 0 - 13.8 kVA as per [37].	34
4.13	Simulated (a) Low voltage ride through (LVRT) condition as per [37] and (b) its effects on the grid current.	35
4.14	Simulated turbine and PM-rotor mechanical speeds (ω_t and ω_m) as a result of a 1.5 Hz per second change in grid frequency where the grid speed is given as $\omega_s = 2\pi f_s \times \frac{p}{2}$	35
5.1	Top level schematic of the downwind turbine drivetrain testing setup. The solid red lines indicate electrical connections and the dotted green connections represent mechanical connections.	37
5.2	Figure showing (a) a side view of the 2.2 kW downwind turbine drivetrain on test bench and (b) a front view of the 2.2 kW downwind turbine drivetrain which includes the dumpload and GCC.	37
5.3	Results of a test to identify the relation between duty cycle and drivetrain speed for a fixed input torque of (a) 20 Nm (p.u.) and (b) 50 Nm (0.34 p.u.).	38
5.4	Schematic of the practical implementation of the dynamic step-test from section 3.1.1 where the value of the dumpload resistor is 20 Ω	39
5.5	Dynamic step-test results of the downwind turbine drivetrain for a fixed 100 Nm torque input and a step in duty cycle from 30% to 15%.	39
5.6	Top level schematic of the laboratory setup used to conduct speed control tests on the downwind turbine drivetrain.	40
5.7	Closed-loop block diagram representation of Figure 5.6 where everything contained within the dotted lines are controlled within the GCC.	40
5.8	Measured speed control results for various torque inputs: (a) 50 Nm (0.34 p.u.), (b) 70 Nm (0.5 p.u.), (c) 100 Nm (0.7 p.u.), and (d) 145 Nm (1 p.u.). The dotted lines represent the suggested boundary restrictions as outlined in [37].	41
5.9	Measured results showing the PI-controller's disturbance rejection capabilities.	41
5.10	Figure showing: (a) drivetrain speed, (b) grid and PMSG phase voltages, and (c) generator current prior to and after grid connection for a torque input of 110 Nm (0.78 p.u.). Grid connection is indicated by the arrow.	43
5.11	Figure showing how the GCC connects the downwind drivetrain to the grid (solid arrows) and how and when the GCC disconnects the drivetrain from the grid (dotted arrows).	43
5.12	Schematic of the laboratory setup used to conduct the on-grid dynamic performance tests. The dotted arrows represent measurement points.	44
5.13	Figure showing: (a) step in torque input and (b) stator current response.	44
5.14	Downwind drivetrain's on-grid dynamic performance for (a) a rated torque input with a 2.5 Hz frequency component (resulting from the wind shear effect) and (b) a rated torque input with a 8 Hz frequency component (resulting from the tower shadow effect).	45
5.15	2.2 kW downwind turbine at the Stellenbosch University Mariendahl small wind turbine testing facility.	46
5.16	Average wind speed measurements recorded at the Mariendahl wind turbine testing facility over the weekend of 04 November 2017 to 06 November 2017.	46
A.1	Contents of the "Downwind Turbine and Chopper Circuit" block model of Figure 3.4	50

List of Tables

1.1	Parameter limits for synchronisation with the Eskom distribution network [23].	8
2.1	Downwind turbine simulation parameters.	16
4.1	Maximum disconnection times for Renewable Power Plants (RPPS) of Categories A1 [37].	34